INFORMATION TO USERS

NOTE TO USERS

This reproduction is the best copy avaiiable.

UMI

THE UNIVERSITY OF OKLAHOMA

GRADUATE COLLEGE

A FIXED BED CATALYTIC MICROREACTOR WITH REPETITIVE INJECTION

GAS CHROMATOGRAPHIC / MASS SPECTROMETRIC ANALYSIS.

A DISSERTATION

SUBMITTED TO THE GRADUATE FACULTY

in partial fulfillment of the requirements for the

degree of

DOCTOR OF PHILOSOPHY

By

EDOUARD BONNET

Norman, Oklahoma

2000

UMI Number: 9975806

UMI®

A FIXED BED CATALYTIC MICROREACTOR WITH REPETITIVE INJECTION

GAS CHROMATOGRAPHIC / MASS SPECTROMETRIC ANALYSIS.

A DISSERTATION APPROVED FOR THE

DEPARTMENT OF CHEMISTRY AND BIOCHEMISTRY

BY
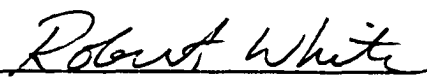
Dr. Robert L. White
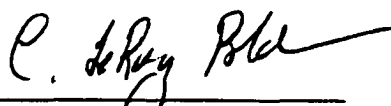
Dr. C. Leroy Blank
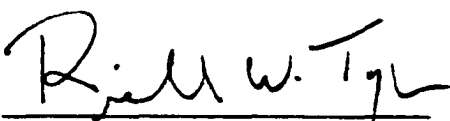
Dr. Richard W. Taylor
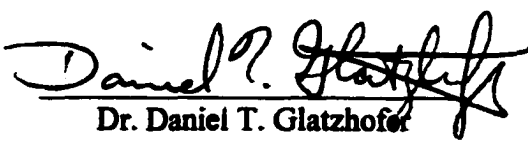
Dr. Daniel T. Glatzhofer
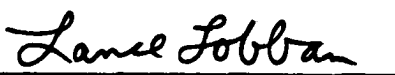
Dr. Lance L. Lobban

ACKNOWLEDGMENTS

The writing of this dissertation is the final step in the completion of my doctorate research. Although the pursuit of the Ph.D. degree took a lot of work on my part, a large number of people helped me along the way. I shall attempt to thank some of them and want to apologize to those I might forget.

First of all, I would like to express my gratitude to Dr. Robert L. White, my supervisor, for his advice and guidance throughout the entire course of my graduate studies at the University of Oklahoma. I am especially grateful for his dedication, availability, and encouraging support, not to mention his patience in editing my writing. My appreciation goes to Dr. C. Leroy Blank for the long discussion we had at times. I really enjoyed teaching the general chemistry laboratory under his supervision. My thanks to the other members of my advisory committee, Dr. Richard W. Taylor, and Dr. Lance L. Lobban for their interest in my research progress and to Dr. Glatzhofer for filling in on such a short notice.

My thanks to the past and present members of Dr. White's research group for the friendly atmosphere they created in the laboratory. I would especially like to thank Dr. Emmanuel Sikabwe, Dr. Rong Lin, Mr. Darrel Negelein, Ms. Mindy Phillips, Mr. Nathan Hesse, Mr. Jesse Copper III and Ms. Lihong Du for their helpful discussions.

TABLE OF CONTENTS

LIST OF TABLES

LIST OF FIGURES

x

CHAPTER 4 : NICKEL ALUMINATE OXIDATION STUDIES

ABSTRACT

Research projects in Dr. White's laboratory involve heterogeneous catalysis. Catalytic reaction studies include two types of analysis. First, surface analysis characterizes the reactant-catalyst interactions and may be able to identify the nature of intermediate species formed at the catalyst surface. Second, volatile product analysis allows for qualitative and quantitative determination of the catalytic reaction products. A variable temperature diffuse reflectance Fourier transform infrared spectrophotometer and a thermal analyzer coupled with gas chromatography and mass spectroscopy were developed in the past for surface and volatile product analysis respectively. Reactants were either coated or adsorbed onto the catalyst at the beginning of an experiment. These instruments gave us an insight to catalytic systems. However, our studies were limited because they did not readily allow for the use of flowing reactants.

The work presented here describes the development of a fixed bed catalytic microreactor capable of repetitive injection gas chromatographic analysis of microreactor effluent. The design of our fixed bed microreactor incorporates new features that overcome common limitations. Short, heated lines ensure quick transfer of reactor effluents to the GC/MS analyzer. The GC small size (8 in. x 6 in. x 6 in.) allows for rapid heating and cooling. Consequently, fast repetitive separations can be achieved even when using GC oven temperature ramps.

The microreactor-GC/MS system was characterized by applying it to studies of known catalytic systems. Consequently, flaws in the design became apparent and improvements were made. The microreactor system was then used to study nickel aluminate, $NiAl_2O_4$, a potential oxidation catalyst. Results indicated that nickel aluminate has some activity for the oxidation of cellulose and n-butane. However, kinetic studies showed that its activity was far less than that of 1% Pt-Alumina.

CHAPTER 1 : INTRODUCTION

In an article from Chemical & Engineering News, McCoy describes catalysts as "high-performance specialty chemicals that are critical to many industries."[1] It seems that almost no industrial process is functional without a catalyst to lower the reaction temperature or to favor the formation of a specific product. The catalyst market was worth $7.4 billion in sales in 1997 and has projected sales of $8.9 billion in 2003.[1] Developing and characterizing new industrial catalysts are today's catalytic chemist challenges. This task requires a better understanding of catalysts and how they work.

I. CATALYST DEFINITION

A catalyst is a "substance that increases the rate of a reaction without being consumed in the overall reaction".[2] The rate of a reaction depends on the reaction rate constant and often on the reactant concentration. For a given chemical reaction, the reaction rate constant depends on several parameters, as shown by the Arrhenius equation:

$$k = A \exp\left(-\frac{E_a}{RT}\right) \tag{1}$$

where k is the rate constant, A is the pre-exponential factor (also called frequency factor), E_a is the activation energy in Joules per mole, R is the gas constant with the value 8.314 J mol^{-1} K^{-1}, and T is the absolute temperature in Kelvin. The rate constant and the rate of a reaction can be increased by reducing the activation energy. A catalyst changes the mechanism of a reaction to provide a new reaction pathway that has a lower activation energy. This is graphically shown in Figure 1-1 for a hypothetical exothermic reaction.
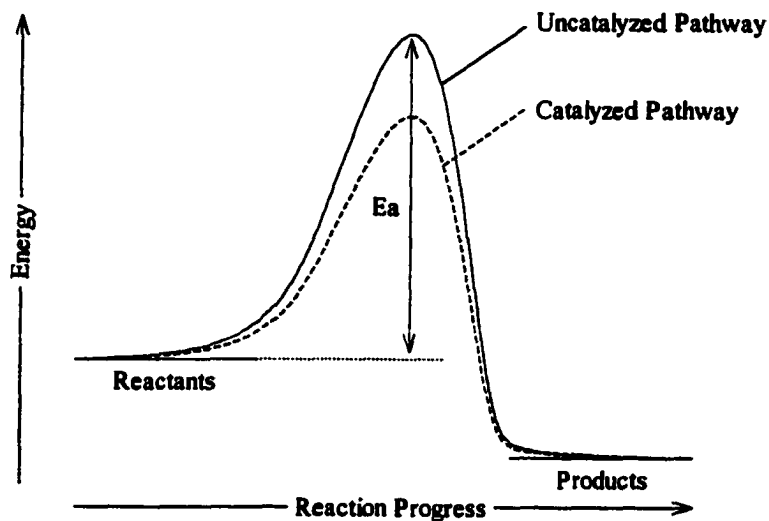
Figure 1-1 : Energy plots for catalyzed and uncatalyzed reaction pathways

Catalysts are often classified as homogeneous or heterogeneous, with the latter being the most commonly used in industry. A heterogeneous catalyst exists in a different phase from that of the reactant. Usually, the catalyst is a solid and the reactant is either a gas or a liquid. A typical heterogeneous catalysis reaction is illustrated in Figure 1-2. The reactant interacts with the catalyst to form an intermediate species at the catalyst surface. From this intermediate, products are generated and the unchanged catalyst is released. The question that remains is how to study a heterogeneous catalytic reaction?
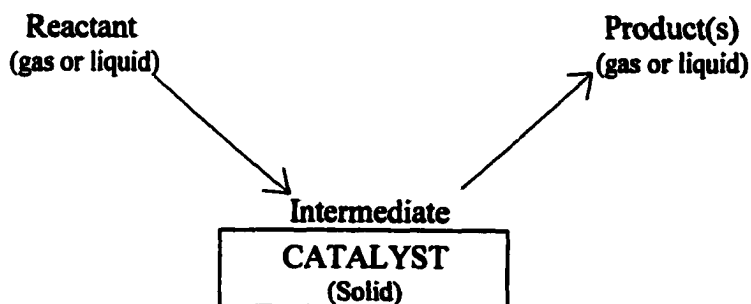
Figure 1-2 : Heterogeneous Catalysis Reaction Scheme

2

II. HETEROGENEOUS CATALYTIC REACTION STUDIES

In a heterogeneous catalytic reaction, the reactant is a known substance that is usually commercially available. The catalyst may need to be characterized if it is a specifically synthesized substance and not a well known commercial product. Analysis of the reaction products (often volatile products) provides information regarding the result of the reaction, whereas catalyst surface analysis provides information regarding reactant-catalyst interactions. Volatile product and surface analysis together can provide insight into the catalytic reaction mechanism.

Catalyst analyses attempt to characterize the solid catalyst bulk properties such as surface area, porosity, acidity, metal content, etc. These properties are important when comparing results from catalytic reactions because they characterize the number and strength of catalytic sites and how readily the reactant can reach them. Prior to the work described here, only catalyst acidity measurements could be done in Dr. White's laboratory. Catalyst samples had to be sent elsewhere for other analyses.

Heterogeneous catalytic reactions often yield a mixture of products. Structure-specific volatile product analysis permits identification and quantification of the individual mixture components. Depending on the instrumentation, product variations with time or another parameter (such as catalyst temperature) can be obtained from volatile product analysis. In Dr. White's laboratory, a Thermal Analysis-Gas Chromatography/Mass Spectrometry instrument (TA-GC/MS) was developed for analysis of volatile products evolved from mixtures of solid reactants and heterogeneous catalysts.[3-5]

In-situ structure-specific surface analysis can provide qualitative and quantitative information regarding species present at the catalyst surface and may be able to determine the

nature of the intermediate species. Like volatile product analysis, surface analysis can be used to monitor changes as a function of time or catalyst temperature. In Dr. White's laboratory, a Variable Temperature-Diffuse Reflectance Infrared Fourier Transform Spectroscopy (VT-DRIFTS) instrument was developed for analysis of catalyst surfaces during heterogeneous catalytic reactions.[6,7]

Although we were able to analyze volatile products and probe catalyst surfaces during heterogeneous catalytic reactions, our research studies were limited by our instrument capabilities. Volatile product analysis could only be performed for reactants that were mixed or coated on catalysts. We had no way of studying catalytic reactions involving flowing reactants. In order to extend our studies to such systems, it was necessary to develop a new research tool that was capable of accommodating reactant flows. Consequently, a microcatalytic reactor was constructed that would permit catalytic activity measurements and catalyst deactivation studies.

III. CATALYTIC REACTOR STUDIES

A wide range of catalytic reactors are used for heterogeneous catalytic reactions in industry.[8,9] They can be classified as fixed bed, fluidized bed, multitubular and batch reactors. The type of reactor used in a reaction depends on the properties of reactants and products. For example, fixed bed, fluidized bed, and multitubular reactors are used with vapor phase reactants and products whereas batch reactors accommodate liquids. Figure 1-3 shows schematic diagrams of each reactor type. In a fixed bed reactor (Fig. 1-3a), reactant gases flow over a catalyst bed, usually made of pellets. Products and excess reactant are collected at the end of the bed. Fixed bed reactors are used for high conversion reactions, for which there is usually little

a) Fixed Bed Reactor

Products/Reactants Out

Catalyst Bed

Reactants In

b) Fluidized Bed Reactor

Catalyst Fine Separation

Products /
Reactants Out

Catalyst Bed

Catalyst Screen

Reactants In

c) Multitubular Reactor

Products/Reactants Out

Tube Bundle

Heat Exchange
Fluid Out

Heat Exchange
Fluid In

Reactants In

d) Batch Reactor

Gas In →

→ Gas Out

Liquid In →

→ Liquid Out
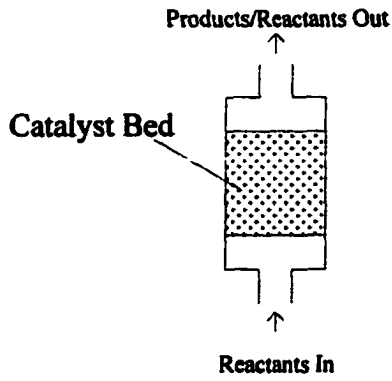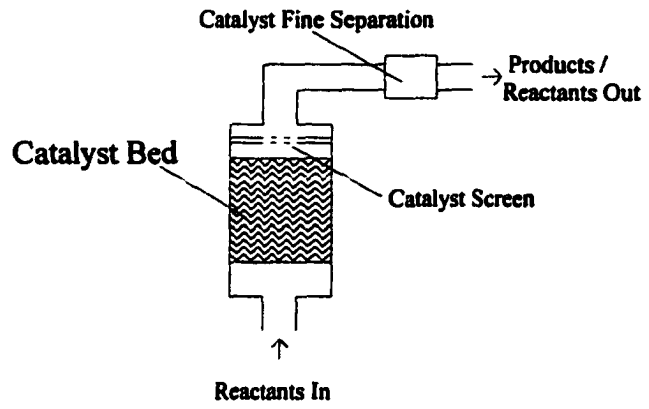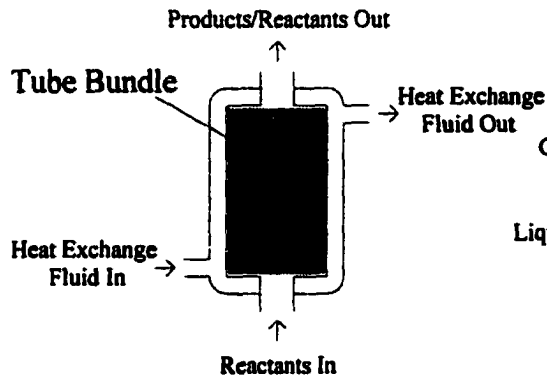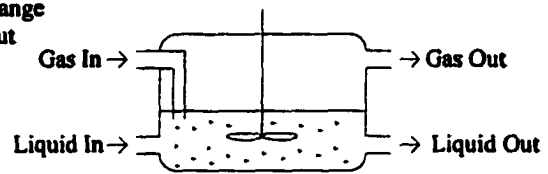
Figure 3-1 : Various Types of Reactor [9]

5

excess reactant. In a fluidized bed reactor (Fig. 1-3b), reactant gases are introduced at high velocity through a catalyst bed consisting of fine particles. The bed becomes a "turbulent fluid"[9] that facilitates transport of the reactants to the catalyst and transport of the products away from the catalyst, thus resolving possible diffusion limitations. Most catalyst particles are trapped in the reactor by a screen. Catalyst particles that pass through the screen are subsequently separated from the products and unreacted gases. Fluidized bed reactors are generally used when good mixing and good heat transfer with the reactor walls are required. Multitubular reactors (Fig. 1-3c) consist of many small diameter tubes in a bundle. Each tube is packed with catalyst and surrounded by a heat exchange fluid (liquid coolant or heating gas such as steam). This type of reactor is used when extremely good heat conduction between the fluid and the catalyst bed is required. Batch reactors (Fig. 1-3d) consist of a "stirred pot", also known as a continuously stirred tank reactor (CSTR). The reactant and catalyst are mixed and stirred in the reactor. Products are separated at desired time intervals, and high conversion is obtained.

Industrial reactors employ very large amounts of catalyst (several tons). This makes industrial reactors inflexible and consequently unsuitable for catalyst testing. Instead, scaled down reactors are used for catalyst testing. Different reactor sizes exist : pilot plants (100kg of catalyst), large-scale reactors (1kg of catalyst) and microreactors ($\leq$ 1g of catalyst). Catalyst development begins with microreactor studies. Potential new catalysts are further tested with increasing catalyst loadings using large-scale reactors and pilot plants. Microreactors of all reactor types (Fig. 1-3) can be made. However, fixed bed microreactors are the most commonly used in academia and industry for catalyst testing.

6

IV. RESEARCH FOCUS

The main objective of this research was to develop a fixed bed catalytic microreactor that incorporated the repetitive injection GC/MS apparatus that we built previously. The reactor was designed to be versatile so that it would allow for a wide variety of experiments, such as isothermal kinetic studies for catalytic activity determination and catalyst surface characterizations by temperature programmed desorption. In order to attain this goal, several features needed to be incorporated in the microreactor-GC/MS system:

- short transfer lines with small inside diameters to reduce dead volumes and analysis time.

- homogeneous heating of the transfer lines to avoid product condensation before detection.

- simultaneous detection with complementary detectors to provide qualitative and quantitative information regarding volatile products.

- minimal GC oven size to facilitate fast heating, fast cooling and cryogenic focusing in order to achieve short separation times and permit frequent repetitive injections.

- automatic injection and GC heating ramp control to facilitate reactor-GC/MS operation.

Once built, the instrument was characterized with well known catalytic systems and was then used to study nickel aluminate oxidation properties.

This dissertation is divided into four chapters. A general introduction to catalysts and reactor design is given in this chapter. Instruments other than the fixed bed catalytic reactor that were used for research are described in Chapter 2. Catalyst preparation methods are also given in Chapter 2. Chapter 3 describes the development and characterization of the fixed bed microreactor-GC/MS system. Finally, Chapter 4 describes the use of the microreactor system to characterize oxidation catalysts. The appendices contain descriptions of temperature controller electrical connections (Appendix A), the software used for data acquisition and treatment (Appendix B) and the details of kinetic experiments (Appendix C).

7

V. REFERENCES

1. M. McCoy, *Chem. Eng. News*, September 20 (1999) 17-25

    "Catalyst Makers Look for Growth"

2. D.D. Ebbing, *General Chemistry*, Third Edition, Houghton Mifflin Company: Princeton, NJ, 1990

3. E.C. Sikabwe, D.L. Neglein, R. Lin, and R.L. White, *Anal. Chem.*, 69 (1997) 2606-2609

    "A Thermogravimetry-Capillary Gas Chromatography/Mass Spectrometry Interface"

4. R.L. White, D.L. Neglein, E. Bonnet, and R. Lin, *Curr. Top. Anal. Chem.*, 1 (1998) 93-105

    "Repetitive Injection Gas Chromatography/Mass Spectrometry for Evolved Gas Analysis"

5. D.L. Neglein, E. Bonnet, and R.L. White, *J. Chromatogr. Sci.*, 37 (1999) 263-269

    "Effluent Monitoring by Repetitive injection Gas Chromatography-Mass Spectrometry"

6. R.L White, *J. Anal. Appl. Pyrolysis*, 18 (1991) 325-339

    "Thermal Analysis by Diffuse Reflectance Fourier Transform Infrared Spectroscopy / Mass Spectrometry"

7. R. Lin and R.L. White, *Instrum. Sci. & Tech.*, 24 (1996) 37-45

    "A Ceramic Sample Heater for Variable Temperature Diffuse Reflectance Fourier Transform Infrared Spectroscopy"

8. G.C. Bond, *Heterogeneous Catalysis - Principles and Applications*, Second Edition, Oxford Science Publications: London, England, 1987

9. M. Bowker, *The Basis and Applications of Heterogeneous Catalysis*, Oxford Chemistry Primers, Oxford Science Publications: London, England, 1998

CHAPTER 2 : EXPERIMENTAL

I.   INSTRUMENT OVERVIEW

In addition to the microreactor-GC/MS system described in Chapter 3, thermogravimetric analysis (TGA), thermal analysis - gas chromatography / mass spectrometry (TA-GC/MS), and variable temperature diffuse reflectance infrared Fourier transform spectroscopy (VT-DRIFTS) were employed in this work. The instrumentation used to perform these analyses are described in the following sections.

I.1   Thermogravimetric Analysis

Thermogravimetric analysis (TGA) is a technique known since the early 20th century in which sample mass changes are measured as a function of temperature.[1] A Dupont (Wilmington, DE) 951 thermogravimetric analyzer was used for studies described here. Figure 2-1 is a schematic of the thermogravimetric balance. It consists of an aluminum housing that contains the electronic balance meter movement. On one side of this housing is fitted a quartz tube enclosed in a 500 W furnace that contains the sample holder and a thermocouple. A glass enclosure attached to the other side contains tare weights and a photosensitive null detector. The TGA had a temperature range from ambient to 1200°C and accommodated sample sizes ranging from 0.020 to 400 mg. Catalyst samples were placed in 100 mg platinum sample pans and suspended on a horizontal quartz rod that was connected to the balance movement. Sample temperatures were measured by a thermocouple located next to the sample pan. Measurements made with empty sample pans revealed that detection limits were about 2.5 μg for mass loss

9

Electromagnetic
Balance

Tare Weights

FURNACE

← Gas Flow

Quartz Tube

Thermocouple

Sample Pan

Aluminum
Housing

Photosensitive
Null Detector

Figure 2-1 : Thermogravimetric Balance

10
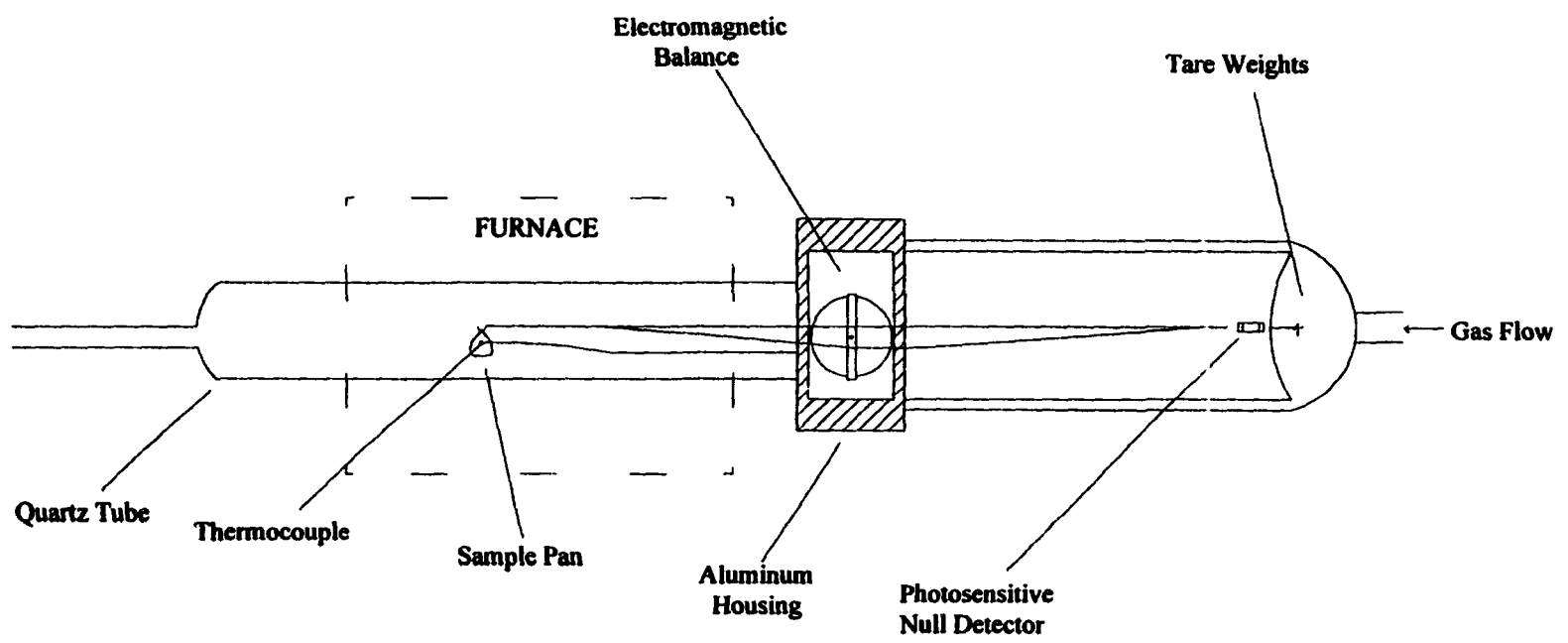
measurements.[2] Helium was used to purge evolved volatiles when samples were heated. The helium flow rate (typically 25mL/min) was controlled by an Edwards High Vacuum (Grand Island, NY) type 825 mass flow controller and a Model 1605 controller unit with digital display. The TGA instrument was controlled by a DuPont Thermal Analyst 2000 data system.

I.2   Thermal Analysis - Gas Chromatography / Mass Spectrometry

Thermal analysis (TA) techniques, such as TGA, are well established techniques and have been used to characterize solid-state material bulk properties for over thirty years. Bulk property information derived from thermal analysis techniques in which decomposition volatiles are removed from heated samples by a purge gas can be augmented by evolved gas analysis (EGA). Mass spectrometry provides structural information regarding volatiles generated during thermal analysis and is commonly employed as an evolved gas analyzer.[3-21] However, structural information provided by mass spectrometry EGA usually pertains to mixtures. To facilitate species-specific analysis when evolved gases contain many components, gas chromatographic separations have been combined with thermal analysis.[22-34] Gas chromatographic separations have typically been used to separate components that were cryogenically trapped from purge gas effluent during a thermal analysis. As a result, gas chromatographic peaks represent all species that evolved at the time of trapping during the thermal analysis measurement. Species-specific evolution profiles cannot be obtained by this method because information regarding species concentration as a function of time or sample temperature is not available. Meuzelaar et al.[32] described an EGA system that incorporates automated TA effluent sampling and a short chromatographic column to provide both satisfactory gas chromatographic separations and species-specific evolution profiles. Isothermal chromatographic separations could be repeated at one minute intervals during thermal analyses by using this system. Unfortunately, the system is limited to isothermal chromatographic separations, gas chromatographic column flow rates are

11

not easily varied, and sample injection is not readily adapted for retention time measurements of standards. We have developed an EGA system based on rapid gas chromatographic separation and mass spectrometric analysis that overcomes these problems and permits repetitive effluent mixture separations during a single thermal analysis. The thermal analysis - gas chromatography / mass spectrometry (TA-GC/MS) system, examples of data, and data treatment methods have been described in the literature.[35-37] Some improvements to our original design were made and Figure 2-2 is a schematic of the current TA-GC/MS system. It consists of a sample furnace connected to a Hewlett Packard (Palo Alto, CA) 5985 mass spectrometer via a heated interface and a small volume gas chromatograph. When mass loss information was not desired, a Carbolite (Watertown, WI) model MTF tube furnace was employed to heat samples. The 400W furnace could be heated up to 1000°C. However, the furnace temperature was not homogeneous.[38] In order to minimize temperature variations between experiments, temperatures were measured by using a thermocouple that was located in the center of the Vycor® tube inside the furnace cavity. Samples were placed in 100 mg platinum sample pans that were suspended from the tip of the thermocouple. The tube furnace temperature controller (Eurotherm 902) was either manually operated or connected to a computer and operated via software provided with the apparatus (IPSC version 2.04 from Eurotherm). The purge gas (e.g. helium) was introduced through a 1/8 in. o.d. copper tube connected to a Swagelok (Solon, OH) 1/8 in. -1/4 in. reducer attached to a Swagelok 1/4 in. tee union. A Swagelok 1/8 in. -1/4 in. reducer was mounted on the tee union, through which a 12 in. long, 1/8 in. o.d. exposed junction type K thermocouple was passed. The end of the thermocouple was placed near the middle of the tube furnace, where the temperature was found to be the most constant.[38] The other end of the union tee was connected to an 8 in. long, 3/4 in. o.d. Vycor® tube placed inside the tube furnace by a Swagelok 1/4 in. - 3/4 in. reducing union and a Cajon (Macedonia, OH) 3/4 in. quick connecting union.

12

Figure 2-2 : TA-GC/MS System

13
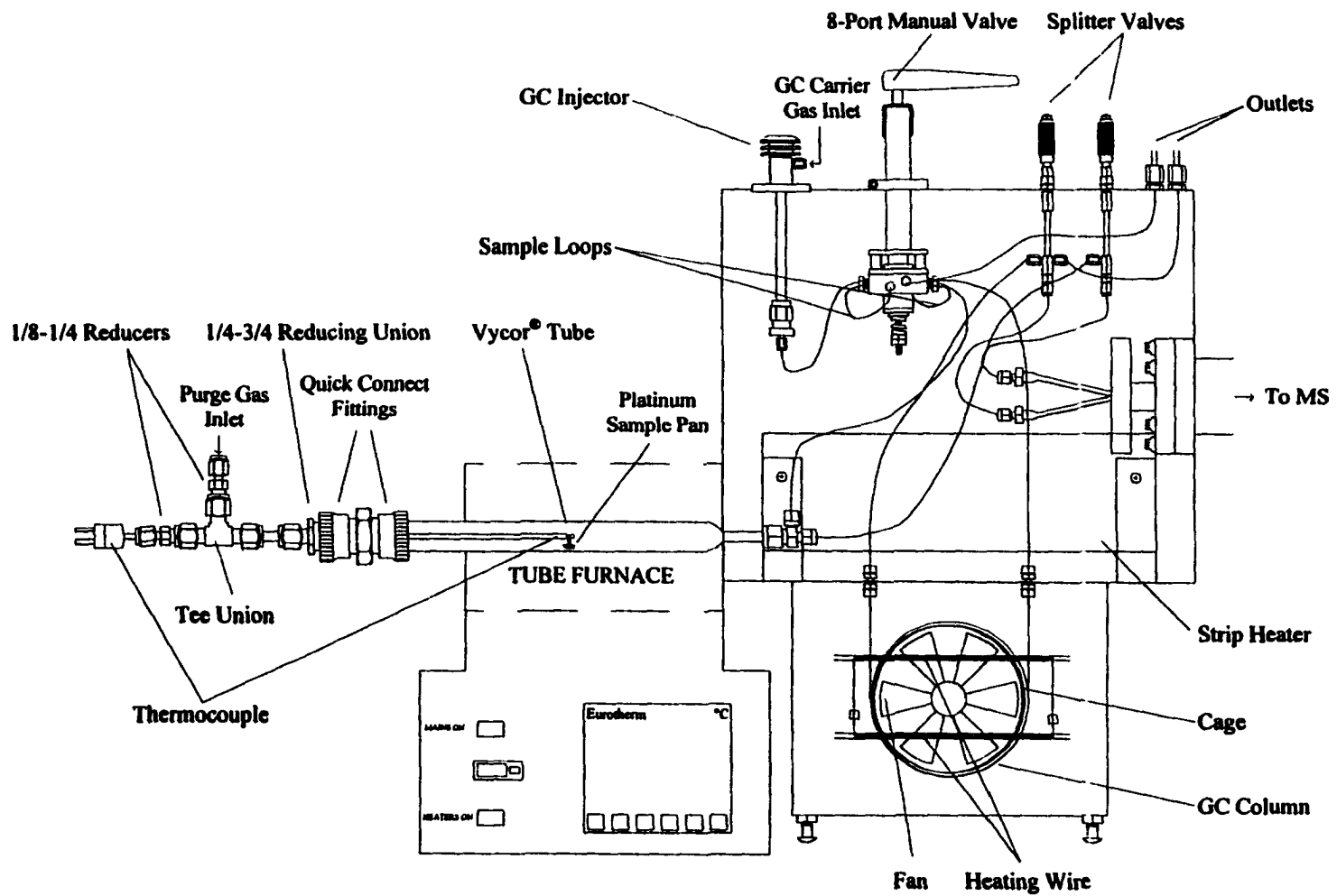
O-rings in the Cajon quick connect fittings were used without grease. A 1-½ in. long, 1/4 in. o.d. quartz tube terminated the Vycor® tube and served as the mass spectrometer interface connection. The interface was contained in a 12 in. × 10 in. × 6 in. aluminum oven that was used to heat a Valco Instruments, Inc. (Houston, TX) 4C8T eight-port two-position manual gas-switching valve, and two SGE (Austin, TX) splitter valves, model MCVT-1-50 and MCV-1-50, to prevent condensation of TA effluent. One-half in. thick ceramic insulator board from Cotronics (Brooklyn, NY) covered the interface inside walls. The interface oven could be heated to 300°C by two 3 in. × 10 in. 500W strip heaters (model 5-10-3-500W-120V from Thermal Corporation, Madison, AL) . The interface oven temperature was maintained by an Omega (Stamford, CT) CN76000 temperature controller. An SGE UNI-K10 on-column capillary gas chromatograph injector was mounted to the top of the interface oven and could be used to inject standards into the gas chromatograph column. All transfer lines were made from 0.332 mm o.d. uncoated fused silica. The front and back walls of the interface oven could be removed for access to the valves, heaters and GC injector.

TA effluent mixtures could be diverted to the mass spectrometer or injected into the capillary gas chromatograph. The capillary column was wrapped around a small cage and was contained in an 8 in. × 6 in. × 6 in. aluminum gas chromatograph oven placed beneath the interface oven. Ceramic blanket wrapped in insulation cloth was used to insulate the inside walls of the GC oven. The gas chromatograph incorporated a nichrome wire heating element and a fan. A Grainger (Oklahoma City, OK) liquid nitrogen solenoid valve (not shown in Figure 2-2) was mounted to the chromatograph front door. The solenoid valve was attached to a 25L liquid nitrogen dewar by insulated 1/4 in. o.d. copper tubing. The chromatograph oven temperature was maintained by using an Omega CN3202 heat/cool temperature controller, which varied the heating element current and energized the liquid nitrogen solenoid valve to heat/cool the oven to temperature setpoints.

The capillary gas chromatography / mass spectrometry interface flow diagram is illustrated in Figure 2-3. TA effluent can follow two different paths (at the point labeled "A") depending on whether chromatographic separation is employed. TA effluent can directly enter the mass spectrometer by opening the splitter valve L to facilitate TA-MS experiments. For TA-GC/MS experiments, TA effluent enters the eight-port injection valve at port #7, passes through one of the two 100 μl stainless steel sample loops (attached to valve ports #6 and #2), then exits the valve at port #3 to reach an outlet (mounted on the top of the interface oven). The GC helium carrier gas from the injector entered the eight-port injection valve at port #1, passed through the other 100 μl stainless steel sample loop (attached to valve ports #8 and #4), then exited the valve at port #5 to pass into the capillary column. The gas chromatograph capillary column exit was connected to the mass spectrometer through splitter valve T in the interface oven. GC/MS injections were obtained by manually rotating the eight-port valve. After rotation, the TA effluent trapped in one sample loop was swept into the GC column and TA effluent flowed into the other loop. The only difference between the two valve positions was which sample loop was loaded and which was injected.

I.3   Variable Temperature Diffuse Reflectance Infrared Fourier Transform Spectroscopy

Infrared spectroscopy is used in a wide range of applications for both qualitative and quantitative analysis. Initially, infrared spectroscopy was almost exclusively absorption spectroscopy, a technique in which the infrared beam passes through a sample and a transmission spectrum is recorded. By the late 1960s, when Fourier transform instruments with sensitive detectors were commercially introduced, techniques employing low energy throughput were possible. In 1978, Fuller and Griffiths[39,40] were the first to introduce diffuse reflectance
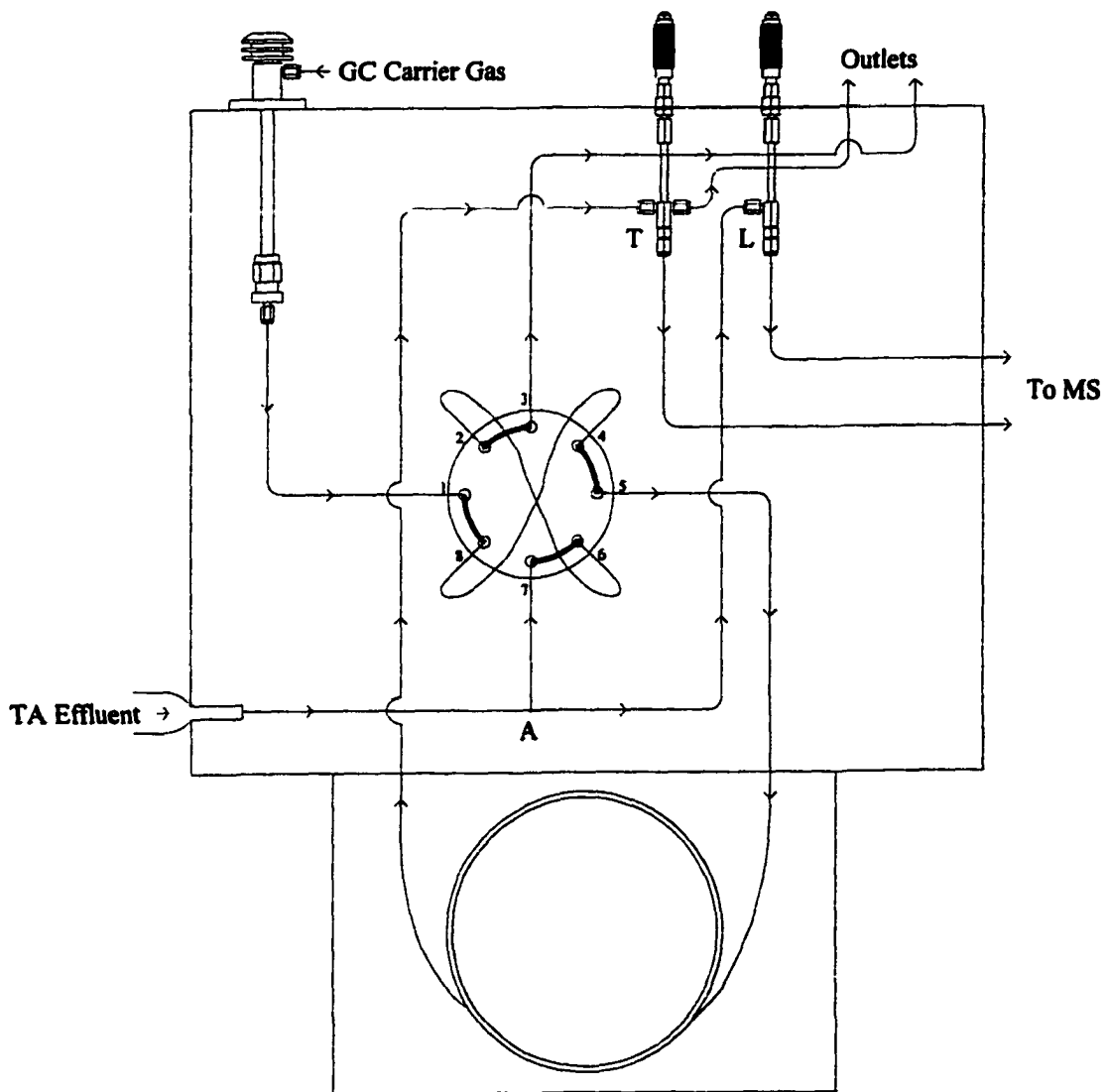
Figure 2-3 : TA-GC/MS System Flow Diagram

infrared Fourier transform spectroscopy (DRIFTS). In DRIFTS, the IR beam is scattered by irregular solid samples (generally powders). DRIFTS can be used for quantitative analyses,[41-43] based on the Kubelka-Munk (K-M) function, f:[44,45]

$$f(R_\infty) = \frac{(1 - R_\infty)^2}{2R_\infty} = \frac{k}{s} = \frac{2.303a}{s} \times c \tag{1}$$

where R_∞ is the sample absolute reflectance at infinite thickness, k the sample absorption coefficient, s the sample scattering coefficient, a the absorptivity of the absorbing species and c its concentration. When the scattering coefficient is constant, there is a linear relationship between the K-M function and concentration.

DRIFTS measurements depend on the sample powder properties. As a general rule, the intensity of the reflected beam increases when the particle size decreases.[46,47] Particles smaller than 20μm are recommended for quantitative analysis.[47] The reflected intensity is also influenced by the powder density. Intensity decreases with increasing powder density.[46,48] This effect is more pronounced for smaller particles.[46] This is due to the fact that the pressure applied when packing samples affects the scattering coefficient,[42,49] which is directly linked to the transmittance of a non-absorbing sample $T = e^{-sx}$, where x is the sample thickness.[50] As a result, grinding, sieving and sample packing are important steps in the preparation of samples and references.

In this study, variable temperature diffuse reflectance infrared Fourier transform (VT-DRIFT) spectra were acquired between 50 and 500°C and were converted to apparent absorbance format (log [1 / R_∞]).[51] Kubelka-Munk units were not used because spectra acquired at high temperatures exhibited temperature-dependent baseline artifacts that severely distorted Kubelka-Munk spectra.[52] Apparent absorbance is much less sensitive to temperature related offsets. Unlike the Kubelka-Munk function, apparent absorbance is not a linear function of

17

concentration. As a result, it was not possible to obtain quantitative information regarding catalyst surface adsorbed species. Instead, semi-quantitative IR band intensity variations are reported here.

A Mattson Instruments (Madison, WI) Sirius 100 FTIR spectrophotometer equipped with a water-cooled Globar infrared source and a liquid nitrogen-cooled mercury-cadmium-telluride photoconducting detector were used for infrared measurements. A Harrick Scientific Inc. (Ossining, NY) "praying mantis" diffuse reflectance accessory and a modified Harrick Scientific Inc. environmental chamber were used for diffuse reflectance measurements.[53] The original Harrick Scientific Inc. sample holder was replaced by a ceramic heater custom made by Hitachi Research Laboratory (Hitachi-shi, Japan). Figure 2-4 is a drawing of the ceramic sample heater and flange mount. A stainless steel cover was attached to the mounting flange and constituted the sample environmental chamber. Two zinc selenide windows mounted on this cover let the IR beam pass to and from the sample. A quartz viewport allows the operator to see the sample. The flange had two 1/8 in. Swagelok (Solon, OH) fittings and one 3/8 in. VCO (Cajon Co., Macedonia, OH) fitting. One of the Swagelok fittings served as an inlet for helium purge during VT-DRIFTS measurements. The VCO fitting was used to attach the environmental chamber to a vacuum system consisting of an E2 Edwards High Vacuum Inc. (Grand Island, NY) rough pump and a high vacuum diffusion pump. This vacuum feature was not used in this study and the VCO port served only as a purge outlet. The second Swagelok port was used to pass an Omega (Stamford, CT) CHAL-010 precision fine wire thermocouple into the environmental chamber. The thermocouple leads were sealed to prevent gas leakage by using epoxy cement. The tip of the ceramic heater had a small indentation that held approximately 15mg of catalyst sample. The thermocouple junction was placed in the powdered catalyst samples to measure temperatures. Sample temperatures were maintained by using a Eurotherm 818p Controls, Inc. (Reston, VA) temperature controller. Copper feedthroughs provided

18

ZnSe Windows

Quartz Viewport

Coolant In/ Out

2-3/4 in. Flange

Front Side

Insulating Ceramic

Conducting Ceramic

Silver Electrodes

Retaining Ring

Ceramic
Insulators

Heater

Electrical
Connections

2-3/4 in. Flange

Gas Purge In→

Thermocouple Leads

1/4 in. Swagelok Fittings

3/8 in. VCO Fitting

Copper Feedthroughs
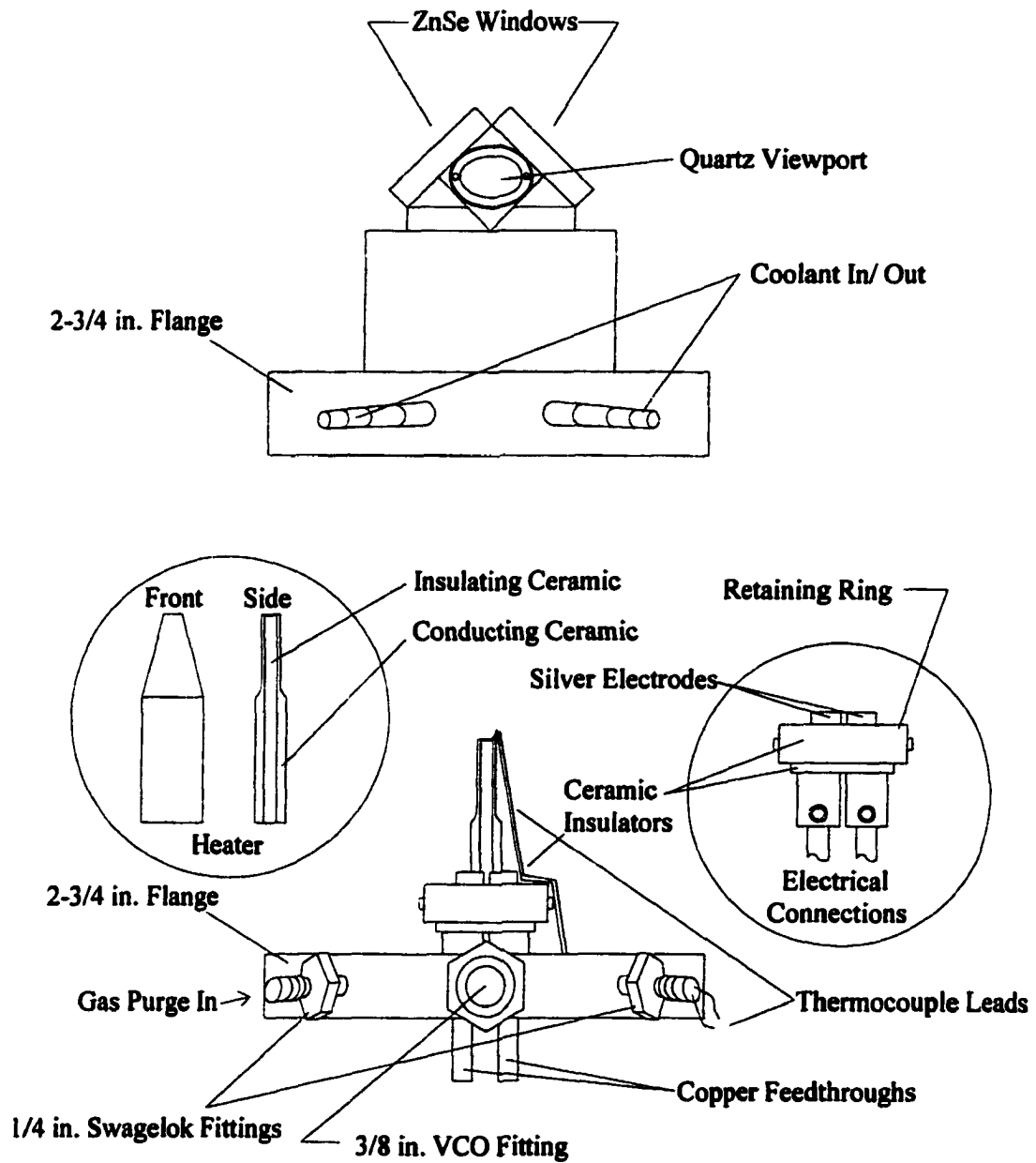
Figure 2-4 : Ceramic Sample Heater

electrical power and supported the ceramic heater. Silver electrodes connected the feedthroughs and the ceramic heater. These electrodes were customed made by the University Physics Shop.

During VT-DRIFTS measurements, the Eurotherm 818p temperature controller was programmed to heat catalyst samples at rates of $2°C/min$. Infrared interferograms were acquired at 8 cm^{-1} resolution and averaged for 2.5 minutes resulting in 4000-800 cm^{-1} infrared spectra at 5°C intervals.

I.4   Mass Spectrometer

A Hewlett Packard (Palo Alto, CA) 5988A gas chromatography / mass spectrometry (GC/MS) system was used to provide structural information regarding evolved species formed during initial microreactor system studies. The mass spectrometer was equipped with an electron impact / chemical ionization source, a hyperbolic quadrupole mass filter consisting of four 203mm long rods, an ion gauge pressure controller and a Galileo channeltron electron multiplier detector. The HP 5988 A mass spectrometer had a mass range from 10 to 1000 atomic mass units (amu), a mass stability of ±0.13 amu per 8 hours, and an accuracy of ±0.13 amu within the calibrated range. The ionization energy could be adjusted from 10 to 250 eV. The maximum scan speed was 2000 amu per second. The ion source temperature could be digitally controlled from 100 to 300°C at $\pm2°C$ steps. Two Edwards High Vacuum rough pumps and two Edwards High Vacuum diffusion pumps were used to attain background pressures as low as 5×10^{-8} Torr in the ion source. The mass spectrometer electronics employed linear amplification, providing a dynamic range of 2×10^{6}.

Sample ionization was obtained by operating the ion source at 200°C in the electron impact mode at 70 eV. The mass spectrometer was operated using GC/MS software provided by a Teknivent (St. Louis, MO) Vector/One™ data acquisition module (Revised version 3.01)

driven by an IBM compatible computer. The mass spectrometer was calibrated each morning by introducing perfluoro-tributylamine (PFTBA) into the ion source through a direct insertion probe. Selected ions in the PFTBA mass spectrum were checked for proper peak shape, width, and relative abundance. Mass spectral library searches employed a 38,000 spectra NBS library.

II. SAMPLE PREPARATION PROCEDURES

Sulfated zirconia, zeolites (ZSM-5 and Y), MCM-41, and nickel aluminate catalysts were synthesized in our laboratory. Silica Alumina (Siral 90) and 1% Platinum/Alumina were purchased from Condea (Hamburg, Germany) and Aldrich (Milwaukee, WI) respectively. Table 2-1 lists the chemicals needed to make the catalysts.

II.1 Unpromoted and 1% Fe Promoted Sulfated Zirconia

Sulfated zirconia (SZ) catalysts were synthesized from the zirconium hydroxide precursor obtained from Dr. Resasco's laboratory. It was prepared by precipitation from 0.5M zirconium tetrachloride solution by dropwise addition of conc. NH_4OH. Two methods can be used to add sulfate. In the "soak" method, described by Hino and coworkers,[54] zirconium hydroxide is mixed with a sulfate solution and then the solid is separated from the excess liquid. In the "incipient wetness" method, used by Hollstein et al.,[55] a predetermined amount of sulfate solution is used to "wet" the zirconium hydroxide. Excess water is removed by evaporation after thorough mixing. Promoted catalysts are prepared by adding metal promoters prior to the sulfation step. The incipient wetness method was used to prepare catalysts for this work because metal promoter loadings were easier to control.

21

Table 2-1: Chemical List

Name	Formula	Brand
Zirconium Hydroxide	$Zr(OH)_4$	obtained from DER*
Ammonium Sulfate	$(NH_4)_2SO_4$	Aldrich
Iron Nitrate Nonahydrate	$Fe(NO_3)_3 \bullet 9H_2O$	Aldrich
Tetrapropylammonium Bromide	$(C_3H_7)_4NBr$	Fluka
Sodium Hydroxide	$NaOH$	Mallinckrodt
Aluminum Sulfate Hydrated	$Al_2(SO_4)_3 \bullet 18H_2O$	Aldrich
LUDOX® LS colloidal silica (30% wt. in water)	SiO_2	Aldrich
Ammonium Nitrate	NH_4NO_3	Aldrich
CopperChloride Dihydrate	$CuCl_2 \bullet 2H_2O$	EM Science
Sodium Aluminum Oxide	$Al_2O_3 \bullet Na_2O$	Alfa Aesar
18-crown-6	$C_{12}H_{24}O_6$	Aldrich
Tetraethylammonium Hydroxide Pentahydrate	$(C_2H_5)_4NOH \bullet 5H_2O$	Aldrich
Dodecyltrimethylammonium Bromide	$C_{12}H_{25}N(CH_3)_3Br$	Aldrich
Silicon Oxide	SiO_2	obtained from Hitachi
Aluminum Oxide	Al_2O_3	Aldrich
Nickel Nitrate Hexahydrate	$Ni(NO_3)_2 \bullet 6H_2O$	Aldrich
Aluminum Nitrate Nonahydrate	$Al(NO_3)_3 \bullet 9H_2O$	Aldrich
Ammonium Hydroxide (>29% NH_3)	NH_4OH	Mallinckrodt

* DER - Professor Daniel E. Resasco, School of Chemical Engineering

Unpromoted sulfated zirconia catalyst was prepared by adding 2.5mL of a 1M $(NH_4)_2SO_4$ solution to 2.8g of dry $Zr(OH)_4$. The resulting paste was thoroughly mixed in a rotoevaporator and then dried at 110°C. This procedure yielded ca. 8% sulfate by weight prior to calcination. The solid was then calcined at 600°C for 4 hours. The 1% Fe promoted sulfated zirconia was prepared by mixing 5mL of a 0.1M $Fe(NO_3)_3$ solution with 2.8g of $Zr(OH)_4$. The mixture was stirred in a rotoevaporator for an hour and then dried at 110°C. Sulfation was then achieved as previously described for the unpromoted catalyst.

II.2 ZSM-5 Zeolite

ZSM-5 zeolite was synthesized by following the procedure from the Mobil Oil U.S. Patent.[56] Two solutions were prepared. The first solution was made by dissolving 31.2g of tetrapropylammonium bromide (TPA-Br) and 4.83g of sodium hydroxide in 200mL of distilled water. Aluminum sulfate, $Al_2(SO_4)_3$, (6.5g) and 1.56g of sodium hydroxide were dissolved in 20mL of distilled water to make the second solution. The two solutions were combined and mixed for about 5 minutes. After mixing, 38.2g of 30% colloidal SiO_2 solution was added and the solution was mixed for another 5 minutes. The mixture was autoclaved at 150°C for 6 days in a Parr 4842 pressure reactor. The resulting solid was filtered, rinsed with distilled water, dried at 110°C and then calcined at 630°C for 3.5 hours to eliminate the TPA-Br organic template. After calcination, the zeolite existed in the sodium form. HZSM-5 was obtained from the sodium form by exchanging sodium ions with ammonium ions. This was accomplished by flushing 1M NH_4NO_3 solution (about 1 liter) through the solid. The solid was then recalcined at 550°C for 3 hours. Ammonia was released when HZSM-5 was formed.

II.3 Y Zeolite

The method used to prepare the Y zeolite was slightly different from that described by Mostad and coworkers.[57] Sodium aluminum oxide (2.46g) and 4.40g of sodium hydroxide were dissolved in 30mL of distilled water. To this solution, 58.1g of 30% colloidal SiO_2 solution was slowly added while stirring vigorously for 1 minute. Next, 7.93g of 18-crown-6 was added and the solution was mixed well. The solution was then allowed to age for 24 hours and was then autoclaved at 100°C for 2 weeks. The mixture was then filtered and the solid was rinsed with

distilled water and dried at 110°C. The resulting Y zeolite was in the sodium form, NaY. Sodium ions were exchanged for ammonium ions by refluxing the NaY for 1 hour in 1M NH_4NO_3 solution. The solid sample was then dried at 110°C and calcined at 600°C for 4 hours to obtain HY.

II.4 MCM-41

The method used to synthesize MCM-41 was found in the literature.[58] Like the zeolite syntheses describe above, this method required the preparation of two solutions. The first solution was obtained my mixing 11.47g of 30% SiO_2 colloidal solution and 10g of tetraethylammonium hydroxide pentahydrate, in 16.4mL distilled water. The solution was aged for 2 days. Then, 20g of dodecyltrimethylammonium bromide and 0.296g of Al_2O_3 were added. The second solution was prepared by dissolving 1.29g of sodium hydroxide in 5.46mL distilled water and adding 2.5g of SiO_2. The two solutions were combined and the resulting mixture was autoclaved at 140°C for 4 days in a Parr 4842 pressure reactor. The resulting solid was filtered, rinsed with distilled water for an hour to remove excess Br^-, dried at 110°C and calcined at 600°C for 4 hours. The MCM-41 sodium form was ion-exchanged with 1M NH_4NO_3 and finally recalcined at 600°C for 4 hours to form MCM-41. The expected aluminum loading was 8%. However, analysis showed that there was only 5% aluminum because not all aluminum was incorporated during crystal formation.

II.5 Nickel Aluminate

Nickel aluminate, $NiAl_2O_4$, was prepared by coprecipitation of stochiometric amounts of nickel and aluminum nitrate salts. Nickel nitrate hexahydrate (8.26g) was dissolved in 15mL of distilled water. Then, 21.25g of aluminum nitrate nonahydrate was added and the green

solution was stirred until all solid was dissolved. Dropwise addition of 20mL of concentrated ammonium hydroxide while strirring resulted in the formation of a blue precipitate. The final product was a very viscous blue (and green) mixture. Although excess ammonium hydroxide was used, the remaining green color suggested that all of the nickel nitrate did not react. However, vigourous stirring during the ammonium hydroxide addition reduced the residual green color. The viscous mixture was dried at 105-110°C overnight resulting in a green brittle crystalline solid. Calcination at 1200°C for one hour yielded a blue crystalline solid.

Aluminum nitrate nonahydrate is very hygroscopic. Consequently, stoichiometric amounts were difficult to obtain by weight, resulting in excess nickel and the formation of nickel oxide, NiO, which was responsible for some of the green color of the final product.

III. REFERENCES

1. C.M. Earnest, *Anal. Chem.*, **56** (1984) 1471A-1486A

   "Modern Thermogravimetry - A brief review"

2. E.C. Sikabwe, "Investigations of the Effects of Iron, Manganese, amd Nickel on the Properties of Sulfated Zirconia Catalysts", Ph.D. dissertation, University of Oklahoma, 1997

3. F. Zitomer, *Anal. Chem.*, **40** (1968) 1091-1095

   "Thermogravimetric - Mass Spectrometric Analysis"

4. E.K. Gibson, and S.M. Jonhson, *Thermochim. Acta*, **4** (1972) 49-56

   "Thermogravimetric-Quadrupole Mass-Spectrometric Analysis of Geochemical Samples"

5. J. Mitchell, J. Chiu, *Anal. Chem.*, **45** (1973) 273R-332R

   "Analysis of High Polymers"

6. E. Baumgartner, and E. Nachbaur, *Thermochim. Acta*, **19** (1977) 3-12

   "Thermogravimetry Combined with Chemical Ionization Mass Spectrometry A new Technique in Thermal Analysis"

7.   J. Chiu, and A. Beattie, *Thermchim. Acta*, **40** (198) 251-259

      "Techniques for Coupling Mass Spectrometry to Thermogravimetry"

8.   H.K. Yuen,G.W. Mappes, and W.A. Grote, *Thermochim. Acta*, **52** (1982) 143-153

      "An Automated System for Simultaneous Thermal Analysis and Mass Spectrometry Part 1."

9.   S.M. Dysel, *Thermochim. Acta*, **61** (1983) 169-183

      "Thermogravimetry Coupled with Atmospheric Pressure Ionization Mass Spectrometry. A New

      Combined Technique"

10.   D. Dollimore, G.A. Gamlen, and T.J. Taylor, *Thermochim. Acta*, **75** (1984) 59-69

      "Mass Spectrometric Evolved Gas Analysis - An Overview"

11.   M.R. Holdiness, *Thermochim. Acta*, **75** (1984) 361-399

      "Evolved Gas Analysis by Mass Spectrometry - A Review"

12.   K.H. Ohrbach, W. Klusmeier, and A. Kettrup, *Thermochim. Acta*, **72** (1984) 165-169

      "Simultaneous Thermoanalytical and Mass Spectrometric Investigation of a Gas Flame Coal"

13.   E. Kaisersberger, and W.D. Ammerich, *Thermochim. Acta*, **85** (1985) 275-278

      "New TA-MS Coupling System with Increased Sensitivity for Low Volatile Material"

14.   E.L. Charsley, N.J. Manning, and S.B. Warrington, *Thermochim. Acta*, **114** (1987) 47-52

      "A New Integrated System for Simultaneous TG-DTA-Mass Spectrometry"

15.   R. Behrens, *Rev. Sci. Instrum.*, **58** (1987) 451-461

      "New Simultaneous Thermogravimetry and Modulated Molecular Beam Mass Spectrometry

      Apparatus for Quantitative Thermal Decomposition Studies"

16.   J.C. May, A. Del Grosso, and R. Wheeler, *Thermochim. Acta*, **115** (1987) 289-295

      "TG/MS Interface: Applications to the Determination of Moisture in Polysaccharides and Freeze-

      dried Biological Products"

17.   W. Schwanebeck, and H.W. Wenz, *Fresenius' J. Anal. Chem.*, **331** (1988) 61-64

      "Simultaneous Thermogravimetry / Mass Spectrometry: A New TG-MS Interface for Forensic

      Science Applications"

18.   Y. Yun, and H.L.C. Meuzelaar, *Energy Fuels*, **5** (1991) 22-29

"Vacuum Pyrolysis Mass Spectrometry of Pitsburgh N°8 Coal: Comparison of Three Different Time-Resolved Techniques"

19.   L.C. Wei, X.T. Geng, Y.X. Hua, C.Y. Xian, D.X. Ming, S.D. Kun, L.W. Sheng, and Z.S. Gui, *Thermochim. Acta*, **260** (1995) 137-145

"Experimental Studies on the Transition from Xerogels to Glasses for the System SiO_2-PbO-B_2O_3 with Added DMSO using Thermal-Mass Spectroscopy Coupled Technique"

20.   G. Matuschek, *Thermochim. Acta*, **263** (1995) 59-71

"Thermal Degradation of Different Fire Retardant Polyurethane Foam"

21.   T. Tsuchida, and T. Hasegawa, *Thermochim. Acta*, **276** (1996) 123-129

"TG-DTA-MS Study of Self-Ignition in Self-Propagating High-Temperature Synthesis of Mechanically Activated Al-C Powder Mixtures"

22.   J. Chiu, *Anal. Chem.*, **40** (1968) 1516-1520

"Polymer Characterization by Coupled Thermogravimetry-Gas Chromatography"

23.   G. Blandenet, *Chromatographia*, **5** (1969) 184-191

"Simultaneous Thermogravimetry and Gas Chromatography"

24.   J. Chiu, *Thermochim. Acta*, **1** (1970) 231-238

"Coupler for Thermogravimetry - Gas Chromatography"

25.   T. Chang, and T.E. Mead, *Anal. Chem.*, **43** (1971) 534-538

"Tandem Thermogravimetric Analyzer-Gas Chromatograph-High Resolution Mass Spectrometry"

26.   C.G. Sceney, J.F. Smith, J.O. Hill, and R.J. Magee, *J. Therm. Anal.*, **9** (1976) 415-421

"On-line Thermogravimetry / Gas Chromatography / Mass Spectrometry"

27.   H.K. Yuen, and G.W. Mappes, *Thermochim. Acta*, **70** (1983) 269-281

"An Automated System for Simultaneous Thermal Analysis and Mass Spectrometry Part2. Combination with Gas Chromatography/Mass Spectrometry"

28.   L.F. Whiting, P.W. Langvardt, *Anal. Chem.*, **56** (1984) 1755-1758

"On-Column Sampling Device for Thermogravimetry / Capillary Gas Chromatography / Mass Spectrometry"

29.   J. Chiu, *Anal. Calorim.*, 5 (1984) 197-207

"A Combined TG-GC-MS System for Materials Characterization"

30.   A.E. Pavlath, K.S. Gregorski, and R. Young, *Thermochim. Acta*, 92 (1985) 383-384

"Coupling a Thermogravimetric Analyzer with Mass Spectrometer"

31.   H.L. Chung, and J.C. Aldridge, *Anal. Instrum.*, 20 (1992) 123-135

"On-line Thermogravimetry / Gas Chromatography / Mass Spectrometry"

32.   W.H. McClennen, R.M. Buchanan, N.S. Arnold, J.P. Dworzanski, and H.L.C. Meuzelaar, *Anal. Chem.*, 65 (1993) 2819-2823

"Thermogravimetry/Gas Chromatography/Mass Spectrometry and Thermogravimetry/Gas Chromatography/ Fourier Transform Infrared Spectroscopy: Novel Hyphenated Methods in Thermal Analysis"

33.   E. Jakab, K. Liu, H.L.C. Meuzelaar, *Ind. Eng. Chem. Res.*, 36 (1997) 2086-2095

"Thermal Decomposition of Wood and Cellulose in the Presence of Solvent Vapor"

34.   T. Arii, T. Senda, and N. Fujii, *Thermochim. Acta*, 267 (1995) 209-221

"A Combined Thermogravimetric-Gas Chromatographic/Mass Spectrometric Analysis (TG-GC/MS) using High Resolution TG Technique"

35.   E.C. Sikabwe, D.L. Neglein, R. Lin, and R.L. White, *Anal. Chem.*, 69 (1997) 2606-2609

"A Thermogravimetry-Capillary Gas Chromatography/Mass Spectrometry Interface"

36.   R.L. White, D.L. Neglein, E. Bonnet, and R. Lin, *Curr. Top. Anal. Chem.*, 1 (1998) 93-105

"Repetitive Injection Gas Chromatography/Mass Spectrometry for Evolved Gas Analysis"

37.   D.L. Neglein, E. Bonnet, and R.L. White, *J. Chromatogr. Sci.*, 37 (1999) 263-269

"Effluent Monitoring by Repetitive injection Gas Chromatography-Mass Spectrometry"

38.   E. Bonnet, "Effects of Water Vapor on the Thermal Decomposition Mechanisms of Poly(Vinyl Butyral) Coated on Silica, Mullite, α-Alumina, and γ-Alumina", M.S. Thesis, University of Oklahoma, 1997

39.   M.P. Fuller and P.R. Griffiths, *Anal. Chem.*, 50 (1978) 1906-1910

"Diffuse Reflectance Measurements by Infrared Fourier Transform Spectrometry"

40   M.P. Fuller and P.R. Griffiths, *Appl. Spectrosc.*, **34** (1980) 533-539

"Infrared Microsampling by Diffuse Reflectance Fourier Transform Spectrometry"

41.   A. Tsuge, Y. Uwamino, T. Ishizuka and K. Suzuki, *Appl. Spectrosc.*, **45** (1991) 1377-1380

"Quantitative Analysis of Powdery Sample by Diffuse Reflectance Infrared Fourier Transform Spectrometry: Determination of the α-Component in Silicon Nitride"

42.   F. Boroumand, H. van den Bergh and J.E. Moser, *Anal. Chem.*, **66** (1994) 2260-2266

"Quantitative Diffuse Reflectance and Diffuse Transmittance Infrared Spectroscopy of Surface-Derivatized Silica Powders"

43.   Z. Krivacsy and J. Hlavay, *J. Mol. Struct.*, **349** (1995) 289-292

"Method for the Reliable Quantitative Analysis by Diffuse Reflectance Infrared Spectroscopy"

44.   P. Kubelka and F. Munk, *Z. Tech. Phys.*, **12** (1931) 593-601

"Ein Beitrag zur Optik der Farbanstriche"

45.   P. Kubelka, *J. Opt. Soc. Am.*, **38** (1948) 448-457

"New Contributions to the Optics of Intensely Light Scattering Materials. Part I"

46.   K. Moradi, C. Depecker and J. Corset, *Appl. Spectrosc.*, **48** (1994) 1491-1497

"Diffuse Reflectance Infrared Spectroscopy: Experimental Study of Nonabsorbing Materials and Comparison Theories"

47.   A.A. Christy, Y-Z. Liang, C. Hui and O.M. Kvalheim, *Vib. Spectrosc.*, **5** (1993) 233-244

"Effect of Particle Size on Diffuse Reflectance Infrared Spectra of Polystyrene Spheres"

48.   Z. Krivacsy and J. Hlavay, *Talanta*, **41** (1994) 1143-1149

"Effect of Sample Packing on the Scattering Properties of the Reference Material in Diffuse Reflectance Infrared Spectrometry"

49.   M.L.E. Tevrucht and P.R. Griffiths, *Appl. Spectrosc.*, **43** (1989) 1492-1494

"A Simple Packing Accessory for Diffuse Reflectance Infrared Spectrometry"

50.   D.J.J. Frasier and P.R. Griffiths, *Appl. Spectrosc.*, **44** (1990) 193-199

"A Simple Packing Accessory for Diffuse Reflectance Infrared Spectrometry"

51.   S. Dai, J.P. Young and G. Mamantov, *Appl. Spectrosc.*, **45** (1991) 1056-1058

"A New Cell for Diffuse Reflectance Infrared Spectroscopy of Air-Sensitive Solid Samples"

52.   R.L White, *J. Anal. Appl. Pyrolysis*, 18 (1991) 325-339

"Thermal Analysis by Diffuse Reflectance Fourier Transform Infrared Spectroscopy / Mass

Spectrometry"

53.   R. Lin and R.L. White, *Instrum. Sci. & Tech.*, 24 (1996) 37-45

"A Ceramic Sample Heater for Variable Temperature Diffuse Reflectance Fourier Transform

Infrared Spectroscopy"

54.   M. Hino, K. Arata, *J. Chem. Soc., Chem. Commun.*, (1980) 851-852

"Synthesis of Solid Superacid Catalyst With Acid Strength $H_0 \leq -16.04$"

55.   E.J. Hollstein, J.T. Wei and C.Y. Hsu, *US Pat. 4,956,519*, (1990)

"Catalyst for Hydrocarbon Conversion and Conversion Process Utilizing the Same"

56.   R.J. Argauer and G.R. Landlot, *U.S. Patent 3702886*, (1972)

"Crystalline Zeolite ZSM-5 and Method of Preparing the Same"

57.   H.B. Mostad, *Appl. Catal. A*, 144 (1996) 305-316

"Comparison of the Isostructural H-SAPO-37 and H-faujasite as Catalysts for the Isobutane /

2-Butene Alkylation"

58.   R. Schmidt, D. Akporiaye, M. Stocker and O.H. Ellestad, *J. Chem. Soc., Chem. Commun.*, (1994)

1493-1494

"Synthesis of Mesoporous MCM-41 Material With High Levels of Tetrahedral Aluminum"

CHAPTER 3 : REACTOR DESIGN

I. INTRODUCTION

Our research laboratory was previously involved in the study of the effects of metal promoters on the catalytic activities of sulfated zirconias.[1,2] This research was conducted in cooperation with Professor Daniel E. Resasco, Chemical Engineering Department, School of Engineering at the University of Oklahoma. Catalyst characterization experiments, such as temperature programmed desorption (TPD), thermogravimetry-capillary gas chromatography / mass spectrometry (TG-GC/MS) studies and variable temperature diffuse reflectance Fourier transform infrared spectroscopy (VT-DRIFTS) measurements were performed in our laboratory. Catalyst activities were determined by catalytic reactor studies of the isomerization of n-butane to iso-butane in Dr. Resasco's laboratory. In order to expand our catalysis research to new systems, it was necessary to build our own fixed bed catalytic reactor so that we could independently conduct catalytic activity measurements.

Catalytic activity studies often include attempts to obtain kinetic information regarding specific reactions. Under typical operating conditions, reactant concentrations decrease and product concentrations increase with increasing penetration into the catalyst bed. These concentration variations result in changes in reaction rates throughout the bed, which makes reaction kinetics difficult to study. To minimize this problem, reactant concentrations must be kept nearly constant throughout the catalyst bed. This can only be achieved under low conversion reactor conditions.[3] Furthermore, catalyst temperature must not vary significantly.

31

This is best achieved by placing catalysts into small diameter tubes ($\leq$ 1/4 in. o.d. or less[4]) which permits good heat transfer. Mass transfer (the physical process that transports reactants and products to and from catalyst active sites) is also aided by the use of small reactor tubes and small catalyst particle sizes.

Figure 3-1 shows a typical layout of a fixed bed microreactor. The points labeled A, B, C, and D on this figure represent bi-directional valves where gas flow can be switched between two paths. At least two gases are used in typical microreactor studies: a reactant and an inert gas (nitrogen or helium). The inert gas is used to vary the reactant concentration without changing the flow space velocity (i.e. the contact time between the reactant and the catalyst). Reactant and inert gas flows are controlled independently. Flow rates are measured by diverting the gas stream to a flow meter. This can be done before and after the reactor by using valves A and D respectively. The reactant mixture (reactant + inert gas) can either flow through the catalyst bed in the microreactor or bypass it depending on the positions of valves B and C. The reactor bypass is used to analyze the reactant mixture to assure that reactant concentrations are correct and stable prior to microreactor studies. Reactor effluent is separated by gas chromatography. Separated components are usually detected by a flame ionization detector. Other detection methods, such as mass spectrometry, have also been used.

One drawback of the fixed bed microreactor shown in Figure 3-1 is that the transfer line between the microreactor and effluent analysis is often long and unheated. Consequently, only products that are volatile at room temperature are detected. The transfer line often has a large inside volume because the tubing commonly employed is several feet long and has a diameter of at least 1/8 in. This dead volume results in a time delay between when effluents leave the microreactor and when they are detected. The dead volume must be minimized to permit monitoring microreactor effluent composition variations with time. In some cases, an inert gas flow is added to the microreactor effluent to increase the overall flow rate and more quickly

32
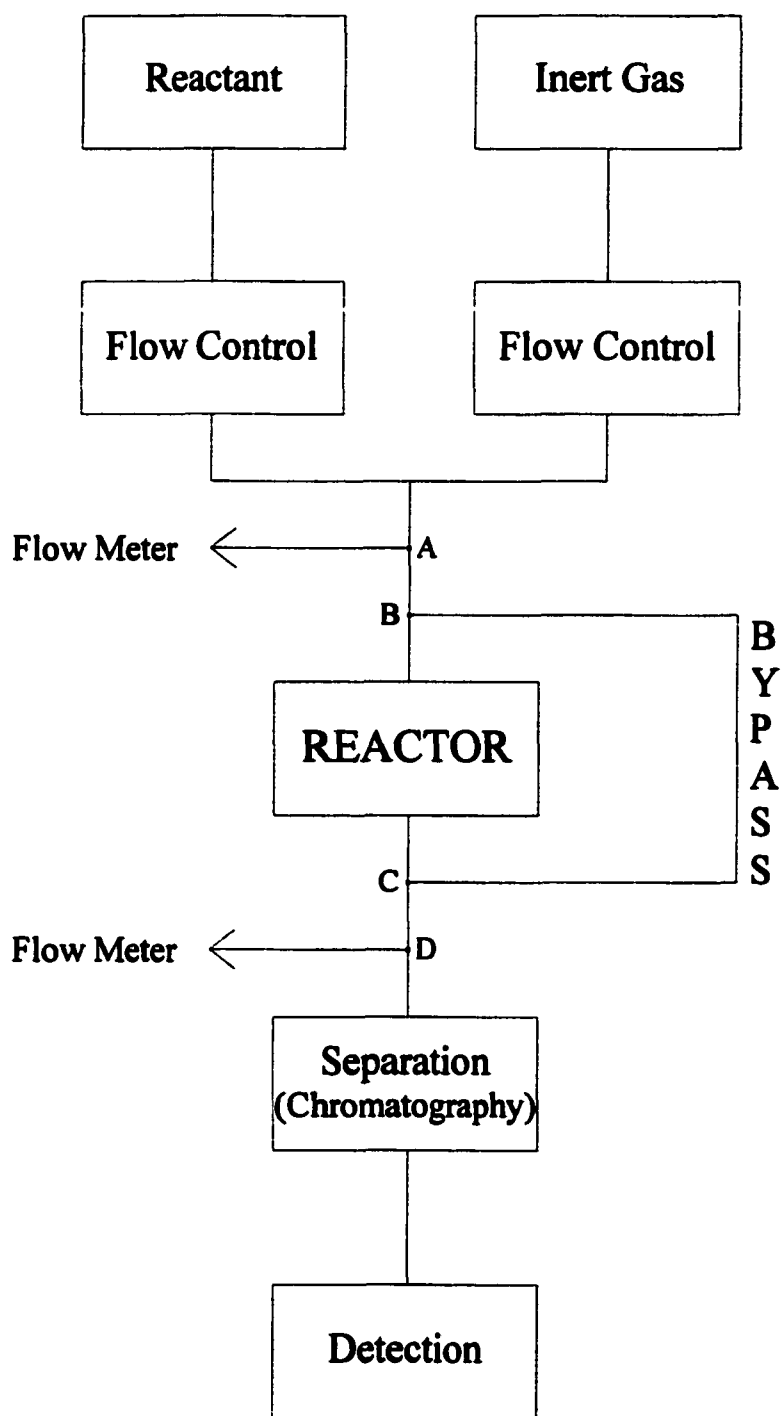
Figure 3-1 : Typical Fixed Bed Microreactor Layout

transfer species to the analyzer. However, this also dilutes microreactor effluent, which increases detection limits.

Microreactors are commonly limited to isothermal conditions. Because most catalytic applications employ isothermal conditions, microreactors are generally not designed to allow for heating ramps and microreactor temperature controllers may not permit heating ramp programs. Furthermore, the microreactor furnace may not be capable of generating reproducible catalyst temperature ramps. As a result, the range of possible microreactor applications is restricted. For example, studies of probe reactant-catalyst interactions as a function of catalyst temperature (e.g. ammonia temperature programmed desorption), cannot be carried out with typical fixed bed microreactors and require additional instrumentation.

The design of our general purpose fixed bed microreactor is similar to those commonly employed for catalyst testing, but incorporates new features to overcome some of the common limitations :

- short transfer lines with relatively small diameters (1/16 in. o.d. tubing) were used to minimize dead volume and the time required for reaction products to reach the detectors.

- the microreactor furnace and transfer lines were contained within a temperature controlled environment to eliminate cold spots before gas analysis.

One goal for the system design was to make it versatile, so that it could be used for isothermal catalytic activity determinations and temperature programmed catalyst characterization measurements. GC injections were automated to simplify operation of the system. To facilitate different experiments, connections to the reactor and gas chromatograph were incorporated that permitted them to be selectively bypassed. Thus, unnecessary separations could be avoided when microreactor effluent consisted of a single species.

34

II. REACTOR DEVELOPMENT

A fixed bed microreactor was built in our laboratory to characterize solid acid catalysts. However, flaws in the initial design were apparent after a series of experimental tests and improvements were subsequently made. In this section, first the initial reactor design and then the improvements will be described.

II.1 Initial Reactor Design

Figure 3-2 is a drawing of our initial microreactor system. The GC/MS analyzer was a Hewlett Packard 5988A GC/MS system that included a 5890 series II gas chromatograph. Table 3-1 lists the components of the initial reactor system.

The main reactor components are labeled in Figure 3-2, but the connections between them have been excluded for clarity. Instead, numbers are used to indicate which fittings are connected. The numbering starts with the manual valve ports and then continues with the automatic valve ports. All transfer lines were made from 1/16 in. o.d. stainless steel tubing.

The catalyst sample was contained within a Vycor® tube that was placed inside a tube furnace. A six-port manual switching valve diverted gas flows so that reactants could be passed through the catalyst or bypass it. Reactor effluent flowed through a sample loop that was attached to a second six-port gas switching valve. GC/MS injections were made by automatically rotating this valve. Valve rotations were controlled by a timer, which was used to sample reactor effluent at predetermined time intervals.
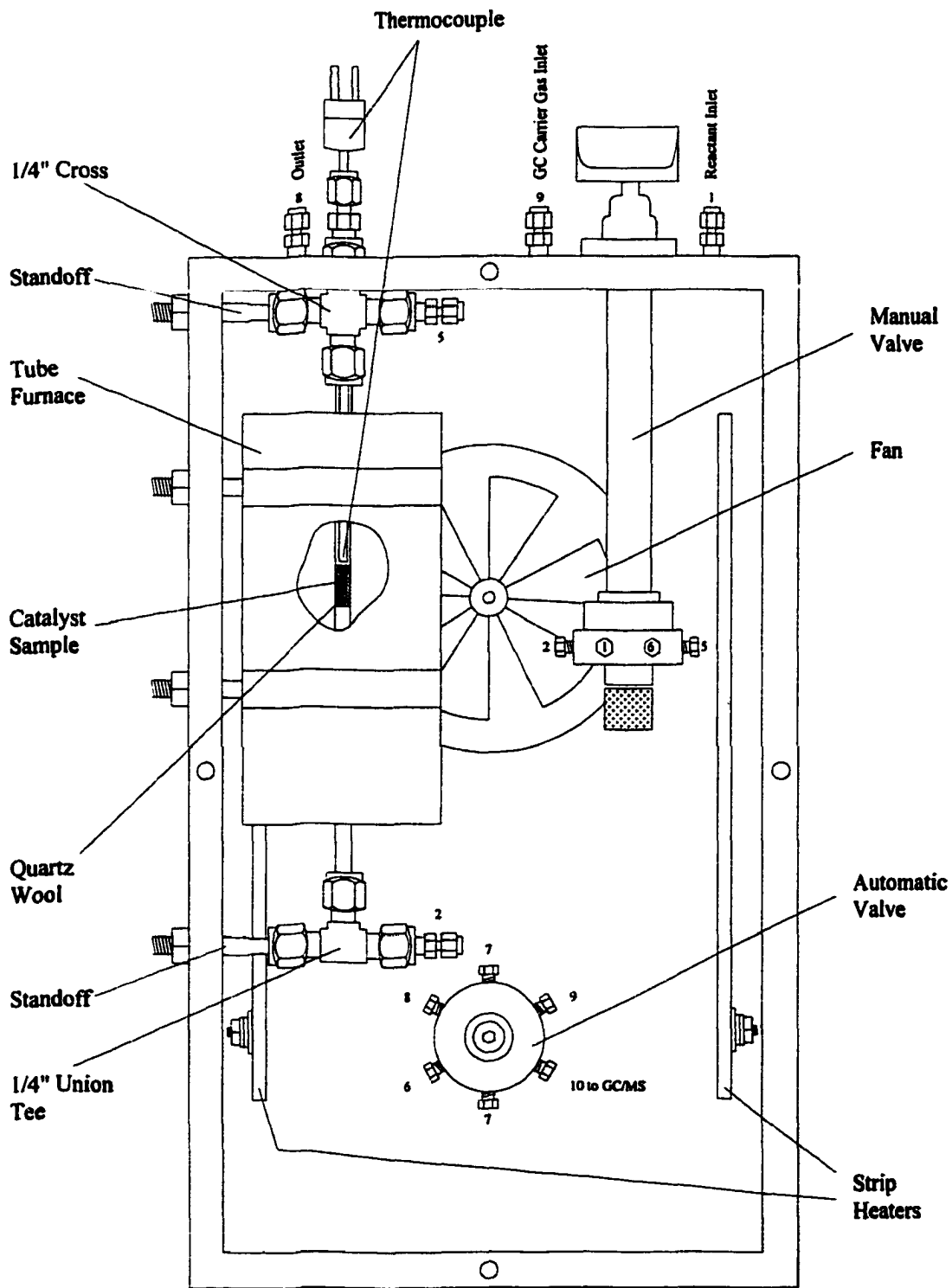
Figure 3-2 : Initial Microreactor System Design

Table 3-1 : Initial Reactor System Part List :

Part	Manufacturer	Part Number
15"×9"×9" Stainless Steel Box	Customed made (University Machine Shop)	
1/4" o.d. Vycor® Tube	Thomas Scientific (Swedesboro, NJ)	5694-G16
Tubular Ceramic Radiant Heater	Omega (Stamford, CT)	CRFC-756-60-A
Two Position 6-Port Valve	Valco Instruments Co. (Houston,TX)	6C6UWT
Two Position 6-Port Valve	Valco Instruments Co. (Houston,TX)	6C6UWE
2 × 1/16" Plugs	Valco Instruments Co. (Houston,TX)	ZP1
Micro-Electric Actuator	Valco Instruments Co. (Houston,TX)	ETMA
Actuator Control Module	Valco Instruments Co. (Houston,TX)	ETCA
Digital Sequence Programmer	Valco Instruments Co. (Houston,TX)	DVSP2
2 × Strip Heaters	Thermal Corporation (Madison, AL)	5-10-3-500W-120V
Sample Loop (15μL)	Alltech (Deerfield, IL)	91056
Sample Loop (~ 80μL)	Laboratory made	
Ceramic Blanket	Cotronics (Brooklyn, NY)	370-1
Insulation Cloth	Wale Apparatus (Hellertown, PA)	15-1420
Fan Motor	Grainger (Oklahoma City, OK)	4M070
Fan Blade	Grainger (Oklahoma City, OK)	2C953
Dual Input Temp. Controller	Omega (Stamford, CT)	CN3240
Solid State Relay	Omega (Stamford, CT)	SSR240DC10
Heat Sink	Omega (Stamford, CT)	FHS-2
Mechanical Relay	Grainger (Oklahoma City, OK)	K10P-11A15-120
3 × 1/16" Steel Bulkhead Unions	Swagelok (Solon, OH)	SS-100-61
2 × 1/16" to 1/4" Reducers	Swagelok (Solon, OH)	SS-100-R-4
1/4" Union Tee	Swagelok (Solon, OH)	SS-400-3
Quartz Wool	Alltech (Deerfield, IL)	4033
2 μm Removable 1/4" o.d. Frits	Alltech (Deerfield, IL)	716505
Thermocouple	Omega (Stamford, CT)	KMQSS-125U-6
1/4" Cross	Swagelok (Solon, OH)	SS-400-4
1/8" to 1/4" Reducer	Swagelok (Solon, OH)	SS-200-R-4

The catalyst sample (~0.2g capacity) was packed between two pieces of quartz wool inside a 1/4 in. o.d. × 9 in. long Vycor® quartz tube. The catalyst sample tube, the tube furnace, the two switching valves and the transfer lines were contained within a 15 in. × 8 in. × 9 in. stainless steel oven. This oven could be uniformly heated to 225°C by two 10 in. × 3 in. 500W strip heaters. Ceramic blanket wrapped in insulation cloth was used to insulate the inside walls of the reactor oven. A fan circulated the heated air to prevent temperature gradients within the reactor oven. The tube furnace provided catalyst temperatures in excess of 700°C. The tube

furnace and the reactor oven temperatures were controlled by an Omega CN3240 dual input temperature controller. The electrical connections for this temperature controller are depicted in Appendix A.

The reactant gas inlet was a 1/16 in. Swagelok bulkhead union mounted on top of the microreactor system oven and connected to port #1 of the six-port manual gas switching valve. Ports #3 and #4 (not shown in Fig. 3-2) of this manual valve were unused and sealed with 1/16 in. plugs. Port #2 was connected to the catalyst sample tube via a 1/16 in. to 1/4 in. Swagelok reducer attached to a 1/4 in. Swagelok union tee. A 1/4 in. o.d. 2μm frit was placed between the union tee and the reducer to prevent sample catalyst particles from reaching and damaging the manual valve. A stainless steel standoff was inserted into the union tee so that it could be attached to the reactor oven wall. The other end of catalyst sample tube was attached to a 1/4 in. Swagelok cross. Another standoff was used to attach the cross to the reactor oven wall. A 1/8 in. o.d. × 6 in. long thermocouple was inserted into the sample tube through the cross via a 1/8 in. to 1/4 in. Swagelok reducer. A 1/16 in. to 1/4 in. reducer was attached to the remaining arm of the cross to facilitate connection to port #5 of the manual valve. A 1/4 in. o.d. 2μm frit was placed between the cross and the reducer to protect the manual valve from damage due to catalyst particles. Port #6 of the manual valve was connected to the six-port automatic gas switching valve. This automatic valve was equipped with a sample loop that was attached to the ports labeled #7 in Figure 3-2. Port #8 was connected to a 1/16 in. Swagelok bulkhead union mounted on top of the microreactor system oven that served as the reactor outlet. The GC carrier gas (helium) inlet was a 1/16 in. Swagelok bulkhead union mounted on top of the microreactor system oven and connected to port #9 of the automatic valve. The GC column was attached to port #10 of the automatic valve.

The initial microreactor system flow paths and valve positions are illustrated in Figures 3-3 and 3-4 respectively. The numbering schemes in both figures are the same as that used in Figure 3-2. The dashed rectangle in Figure 3-3 represents the microreactor system oven walls. The three connections on top of this oven correspond to the reactant inlet (labeled #1), GC carrier gas inlet (#9) and outlet line (#8). A maximum of three gases could be combined for the reactant flow. These were: an inert gas (helium), an oxidizing gas (air), and a reactant that depended on the experiment. All three lines were equipped with a desiccant trap, labeled "dryer" on Figure 3-3, to remove water vapor. Each flow could be independently regulated. The air and helium flows were maintained by using Edwards (Wilmington, MA) 825 mass flow controllers connected to an Edwards (Wilmington, MA) 1605 control unit. The desired flow rates were set by the control unit and were supplied by the controller regardless of upstream or downstream pressure changes. The helium GC carrier gas flow was also set and maintained by using an Edwards (Wilmington, MA) 825 mass flow controller. The reactant flow was adjusted by using a Swagelok (Solon, OH) SS-SS2 metering valve and an SS-2P4T ON/OFF valve because some reactants could damage mass flow controller sensors. Another desiccant trap was added before the reactant inlet and a 2 μm removable frit was inserted to prevent damage to the manual valve (M) by desiccant particles. This manual valve was used to direct reactants through the reactor or to the bypass. In the "Reactor Mode" (Fig. 3-4), port #1 was connected to port #2 and reactant gas flowed through the reactor. Reactor effluent returned to the manual valve at port #5 and was directed to the automatic valve (A) through port #6. In the "Bypass Mode", manual valve port #1 was connected to port #6. Consequently, the reactant gas flowed directly to the automatic valve, bypassing the reactor. In this valve position, gas was trapped in the reactor because ports #3 and #4 of the manual valve were plugged. The automatic valve permitted injection of reactor effluent into the GC/MS analyzer. In the "Load Mode", port #6 of the automatic valve was connected to port #8 through the sample loop (ports #7). The GC carrier

Figure 3-3 : Initial Microreactor System Flow Diagram

MANUAL VALVE

Reactor Mode :

4
×
from Reactor 5
M
to Automatic
Valve   6   2 to Reactor
3
1
Reactant Inlet

Bypass Mode :

4
×
from Reactor 5
M
to Automatic
Valve   6   2 to Reactor
3
1
Reactant Inlet

AUTOMATIC VALVE

Load Mode :

7
to Outlet   8   9 GC Carrier Gas
A
from Manual
Valve   6   10 to GC/MS
7

Inject Mode :

7
to Outlet   8   9 GC Carrier Gas
A
from Manual
Valve   6   10 to GC/MS
7
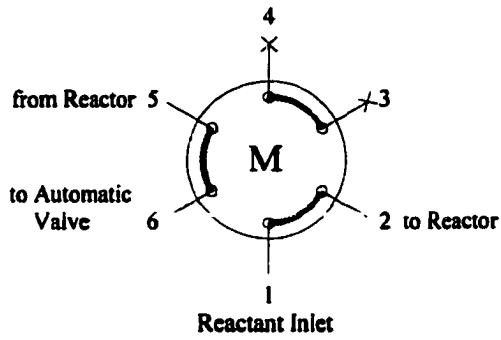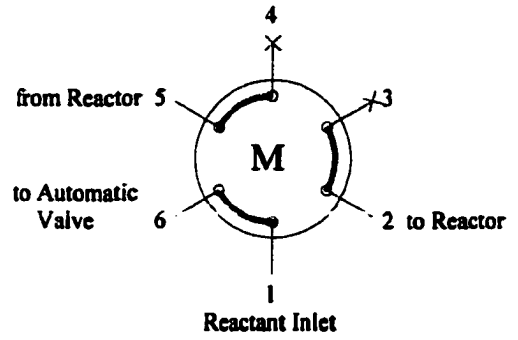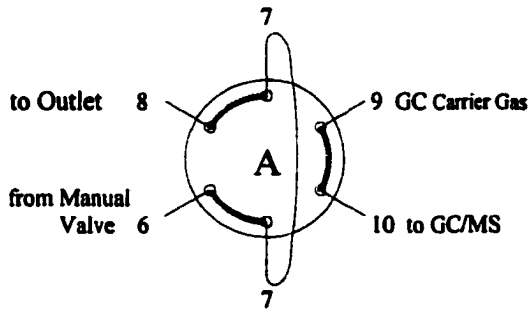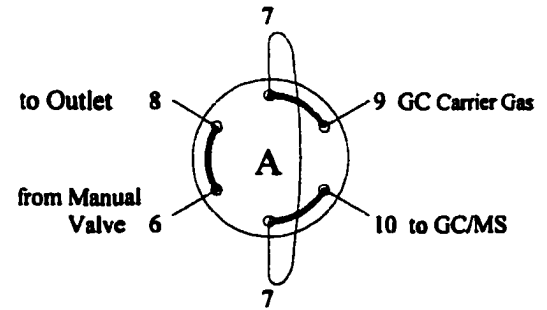
Figure 3-4 : Initial Valve Positions

gas port #9 was connected to the GC/MS column port #10. In the "Inject Mode", ports #6 and #8 were connected and the GC carrier gas (port #9) swept the reactor effluent trapped in the sample loop into the GC column (port #10).

II.2 Improvements to the Initial Design

After a series of experimental tests, flaws in the initial reactor design became apparent and improvements were made. Figure 3-5 is a drawing of the current version of the microreactor system, with modifications to the initial design labeled. Like Figure 3-2, connections are excluded for clarity and numbers indicate which components are connected. Note that due to the improvements, the numbering scheme was slightly altered.

Two gas inlets were added on top of the microreactor oven, namely a reactor purge (#3) and a make up gas (#11). Connecting the make up gas line inside the microreactor system oven required a 1/16 in. union tee. Indentations were made in the sample tube to improve catalyst positioning and a Vycor® protective tube was inserted inside the tube furnace cavity around the sample tube. The thermocouple located inside the sample tube was replaced by a fine wire thermocouple and another fine wire thermocouple was mounted on the surface of the protective tube. Ceramic blanket was used to fill the tube furnace cavity to minimize convection. The modified reactor flow path is shown in Figure 3-6. The two additional helium flows (inlets labeled #3 and #11) were adjusted by using mass flow controllers. Table 3-2 lists the parts that were necessary to make the modifications.
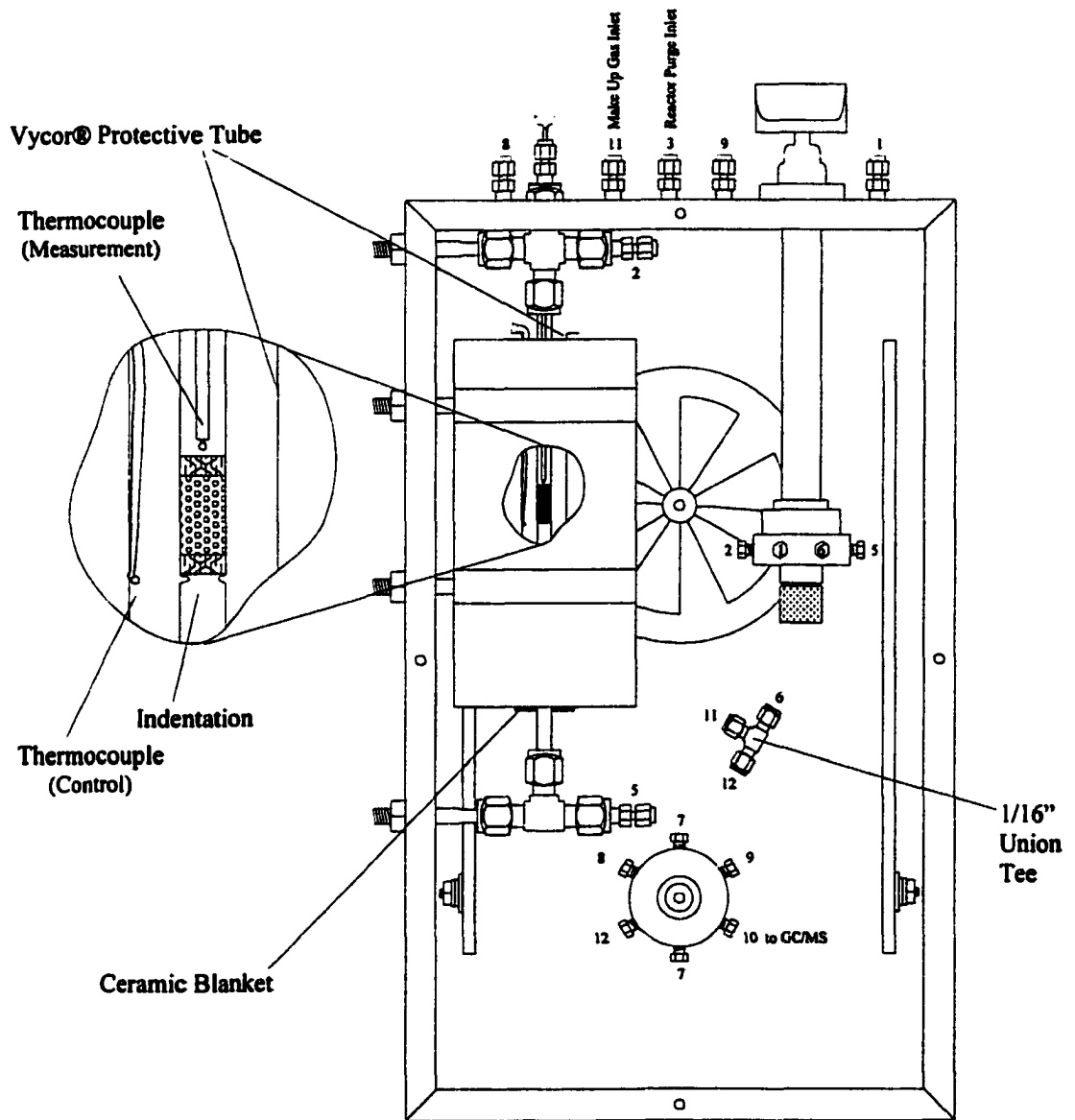
Figure 3-5 : Current Microreactor System Design

Reactant ─[Dryer]─ ⌀ ⊗

Air ─[Dryer]─ [Mass Flow] [Dryer] [f]

[Mass Flow]

[Mass Flow] GC Carrier Gas

Helium ─[Dryer]─ [Mass Flow] Reactor Purge

[Mass Flow] Make Up

Outlet

Reactant Inlet

8   11   3   9   1

[f]

2
R
E
A
C
T
O
R
5

Outlet

4
5   3
M
6   2
1

11

7
8   9
A
12   10
7

→ to GC/MS

Microreactor System Oven
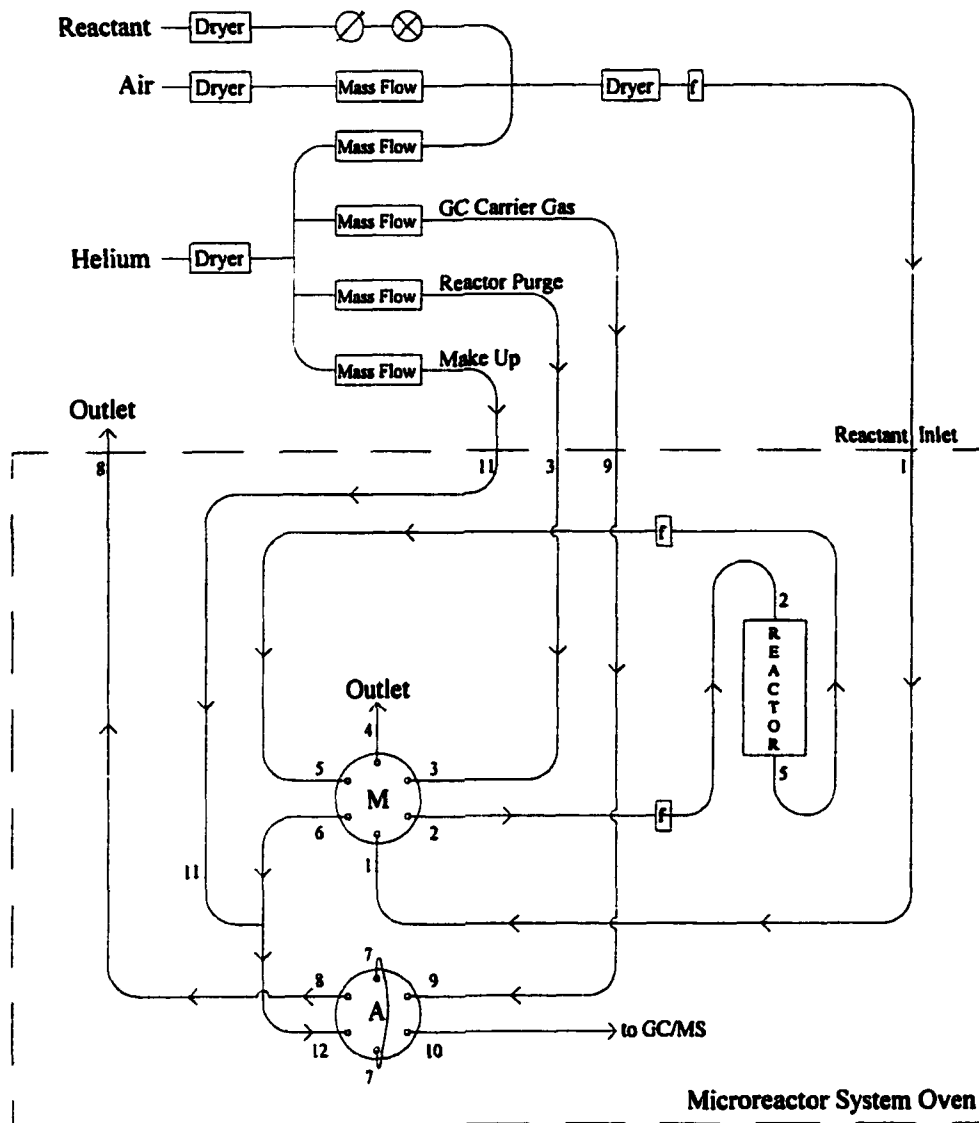
[f] Frit

⌀ Metering Valve

⊗ ON/OFF Valve

Figure 3-6 : Current Microreactor System Flow Diagram

44

Table 3-2 : Reactor System Modification Part List :

Part	Manufacturer	Part Number
5/8" o.d. Vycor® Tube	Thomas Scientific (Swedesboro, NJ)	
2 × Fine Wire Thermocouples	Omega (Stamford, CT)	CHAL-010
Temperature Controller	Omega (Stamford, CT)	CN2011-K-D3
1/16" Steel Bulkhead Union	Swagelok (Solon, OH)	SS-100-61
2 Hole Round Insulator	Omega (Stamford, CT)	TRM164116
1/16" to 1/4" Reducer	Swagelok (Solon, OH)	SS-100-R-4
Two Position 8-Port Valve	Valco Instruments Co. (Houston,TX)	6C8UWT
2 × Sample Loop (15µL)	Valco Instruments Co. (Houston,TX)	SL15CUW

In most experiments, the catalyst must first be calcined in-situ in air, cooled to the reaction temperature, and finally flushed with helium. The manual valve is first placed in the "Bypass Mode" so that the reactant concentrations can be measured and adjusted. With the previous reactor design, helium would be trapped in the reactor when the manual valve was in the "Bypass Mode" position. If a leak was present, this helium could escape and contaminants such as water vapor could enter the catalyst sample tube. This was not acceptable because such contamination would affect the catalyst properties. To solve this problem, a reactor purge line was added so that helium continued to flow through the reactor when the manual valve was in the "Bypass Mode" position. The reactor purge gas inlet consisted of a 1/16 in. Swagelok bulkhead union mounted on top of the microreactor system oven and connected to port #3 (not shown in Fig. 3-5) of the manual valve. The modified reactor valve positions are shown in Figure 3-7. In the "Reactor Mode", port #3 is connected to port #4, which is connected to an outlet. In the "Bypass Mode", port #3 connects to port #2 and reactor purge gas flows through the reactor and returns to the manual valve at port #5, which is connected to the outlet port #4.

MANUAL VALVE

Reactor Mode :

Outlet
4

from Reactor 5

3 Reactor Purge

M

to Automatic
Valve   6

2 to Reactor

1

Reactant Inlet

Bypass Mode :

Outlet
4

from Reactor 5

3 Reactor Purge

M

to Automatic
Valve   6

2 to Reactor

1

Reactant Inlet

AUTOMATIC VALVE

Load Mode :

7

to Outlet   8

9 GC Carrier Gas

A

from Manual
Valve   12

10 to GC/MS

7

Inject Mode :

7

to Outlet   8

9 GC Carrier Gas

A

from Manual
Valve 12

10 to GC/MS

7
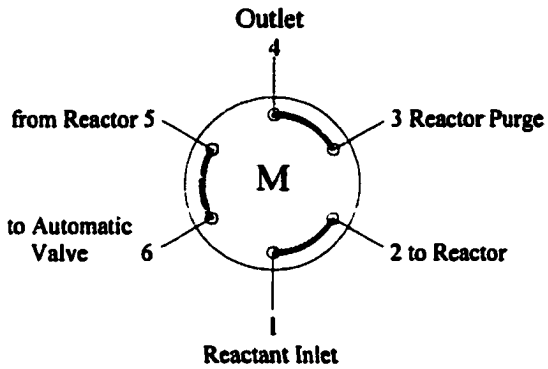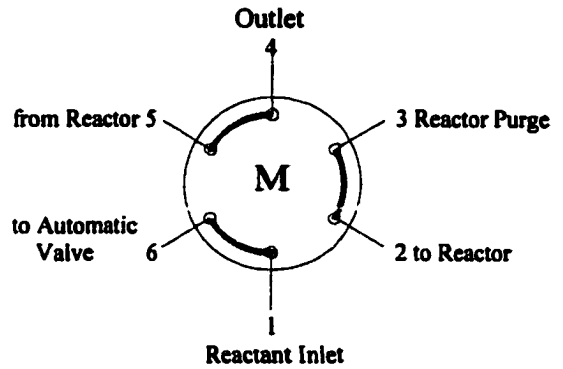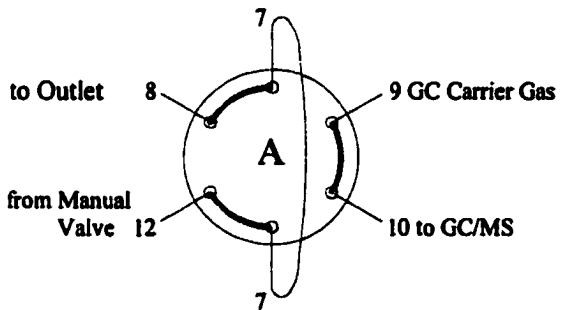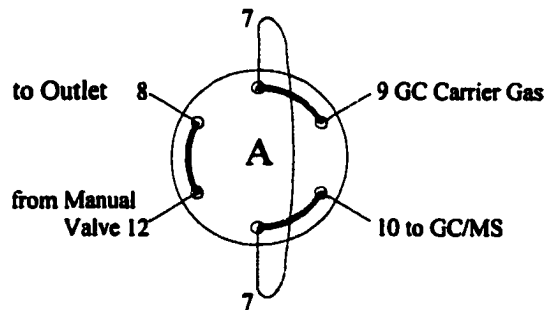
Figure 3-7 : Current Valve Positions

Results from n-hexane cracking by 100mg of HZSM-5 zeolite showed that automatic injection into the GC was not reproducible with the initial reactor system. Figure 3-8 shows the successive chromatograms obtained during n-hexane cracking plotted versus catalyst temperature over the 450-600°C range. The y-axis denotes the mass spectrometer total ion current (TIC). Injections below 575°C resulted in two peaks corresponding to propene and hexane. The highly variable signal obtained during this experiment did not result from MS ion source variations. By monitoring the reactor outlet (#8 in Figs. 3-5 and 3-6), it was determined that the flow through the reactor was not constant. Flow through the reactor stopped when the automatic valve rotated between the "Load" and "Inject" positions and then resumed after the "Inject" position was reached. Furthermore, the equilibrium flow rate measured when the automatic valve was in the "Inject" position was more than when it was in the "Load" position. This was explained by the fact that the sample loop restricted the flow and also caused a pressure increase in the reactor. The change in pressure not only affected the hexane conversion but also the amount of reactor effluent injected (constant volume but different pressure) into the GC/MS analyzer. This resulted in irreproducible injection quantities. To reduce pressure changes in the reactor when the automatic valve rotated, a helium make up gas flow was added at the reactor exit. Consequently, reactor effluent was diluted and larger sample loops (~80μL) that provided less restriction could be used. The make up gas inlet (labeled #11 in Fig. 3-5) consisted of a 1/16 in. Swagelok bulkhead union connected to a 1/16 in. Swagelok union tee. The other ends of the tee were connected to port #6 of the manual valve and to port # 12 of the automatic valve. The reactant gas that passed through or bypassed the reactor came from the manual valve, was diluted with make up helium, and was directed to the automatic valve for GC analysis. The 1/16 in. stainless steel tubing used to connect the tee and the manual valve had an inner diameter that was about 10 times smaller than the other transfer lines to ensure that the path of least resistance was through the automatic valve and that the make up helium did not
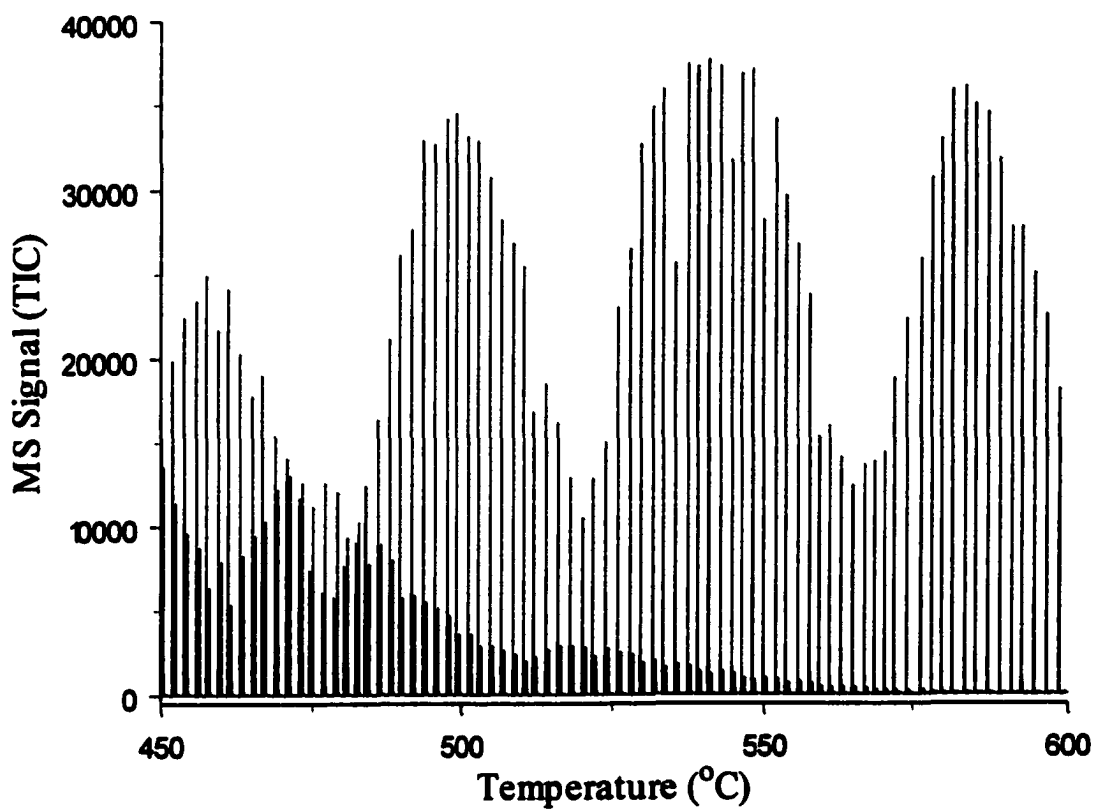
Figure 3-8 : Irreproducible GC Injections during n-Hexane Cracking

enter the reactor. Consequently, reactor effluent encountered different flow resistances when directed to the automatic valve ("Reactor Mode", port #6 in Fig. 3-7) and the outlet ("Bypass Mode", port #4). To solve this problem, a similar length piece of the same tubing used to connect port #6 of the manual valve to the tee union was employed to connect the outlet to port #4.

Between experiments, the catalyst sample tube must be removed and replaced. To do this, the thermocouple must be removed first, then the nuts that secure the Vycor® tube to the union tee and cross must be loosened. The tube could then be pushed up through the top of the microreactor system oven. The tube furnace cavity was large enough (0.75 in. i.d.) for a Swagelok 1/4 in. nut (~0.65 in.) to pass through. This was unacceptable because the nut could damage the heating element or become stuck in the furnace. To avoid potential problems, a 5/8 in. o.d. × 9 in. long Vycor® tube with one end flattened out to make a ca. 1 in. diameter ring, was inserted into the top of the furnace. This tube not only prevented the nut from getting inside the furnace, but also protected the heating element. Because the tube shielded catalyst samples from the heating source, the temperature controller had to be retuned after the tube was installed.

As mentioned previously, in the initial reactor design, the thermocouple had to be removed to replace the sample tube. A black deposit was often observed on the thermocouple surface after experiments. The presence of the deposit suggested that reactions may have occurred on the thermocouple surface. Furthermore, incorrect sample temperature measurements can result when reactions are endo- or exothermic and the thermocouple is placed downstream from the sample. To prevent these problems, the thermocouple was moved so that it was placed upstream from the sample. This was accomplished by switching the reactor inlet and outlet at

the manual valve (Fig. 3-6). These changes made the fixed bed reactor a downflow reactor, because the reactant gases flowed through the reactor from top to bottom.

The bulky 1/8 in. o.d. thermocouple was replaced with a fine wire thermocouple. Compared to the 1/8 in. o.d. thermocouple, the decreased thermocouple wire diameter resulted in a faster thermocouple response. This was important for temperature programmed measurements. The leads of this thermocouple were supported by a 1/16 in. o.d. × 6 in. long 2 hole ceramic insulator. The new thermocouple was inserted through the 1/4 in. cross via a 1/16 in. to 1/4 in. reducer. The holes in the ceramic insulator through which the thermocouple wires passed were sealed with epoxy cement to prevent gas leakage. A second fine wire thermocouple was added to the reactor system to measure the furnace temperature. These two thermocouples will be referred to as "measurement" and "control" thermocouples respectively. The "measurement" thermocouple was placed inside the quartz tube near the catalyst sample to measure its temperature. The position of the "measurement" thermocouple inside the catalyst sample tube could be adjusted so that it was in contact with the quartz wool that held the catalyst in place. Indentations were added to the quartz sample tubes to ensure that catalyst samples were repeatedly placed in the same position within the reactor furnace. The "measurement" thermocouple was connected to an Omega CN2011-K-D3 temperature controller, which was equipped with an RS232 port so that sample temperatures could be read and stored by a computer. The measured catalyst temperature could be used to trigger the automatic injection valve rotation. As a result, GC injections could be programmed based on elapsed time or catalyst temperature. The "control" thermocouple was held in place inside the furnace by passing it through two holes made in the Vycor® protective tube. Between the two holes, the thermocouple lead could touch the heating coil. As a result, the Vycor® tube was purposely distorted to ensure that the thermocouple leads did not short to the heater coil. The "control" thermocouple was connected to an Omega CN3240 dual input temperature controller,

which was used to maintain the furnace temperatures. Wiring schematics for both temperature controllers are given in Appendix A.

II.3 Temperature Characterization

The microreactor system has two different temperature zones : the reactor furnace and the reactor system oven. The temperatures of these two zones can be independently controlled. The oven could be heated to temperatures as high as 225°C. The reactor system oven temperature must be maintained at or below 225°C to prevent damage to the manual 6-port valve rotor material. The reactor furnace could be heated to temperatures in excess of 700°C. However, furnace temperature varies within the catalyst sample tube. To minimize temperature variations, indentations in the quartz tubes permitted samples to be loaded into the tubes at the same location. Consequently, catalysts could be reproducibly positioned at the same location in the furnace. Isothermal reactor furnace temperature profiles were characterized and reactor furnace heating ramps were tested.

II.3.a Isothermal Temperature Profiles

Figures 3-9a and 3-9b show temperature profiles measured by moving a thermocouple inside the quartz sample tube when the furnace was set to 100°C and 500°C respectively while 25mL/min helium was flowing through the tube. The x-axes in Figure 3-9 denotes the measured temperatures. The y-axes are the same in both plots and denote the distance between the "measurement" thermocouple and the bottom of the furnace (y=0). The hatched rectangles denote the sample location in the tube. The height of the rectangle corresponds to the maximum tube length necessary to accommodate ~200mg of catalyst sample and was estimated to be ca.
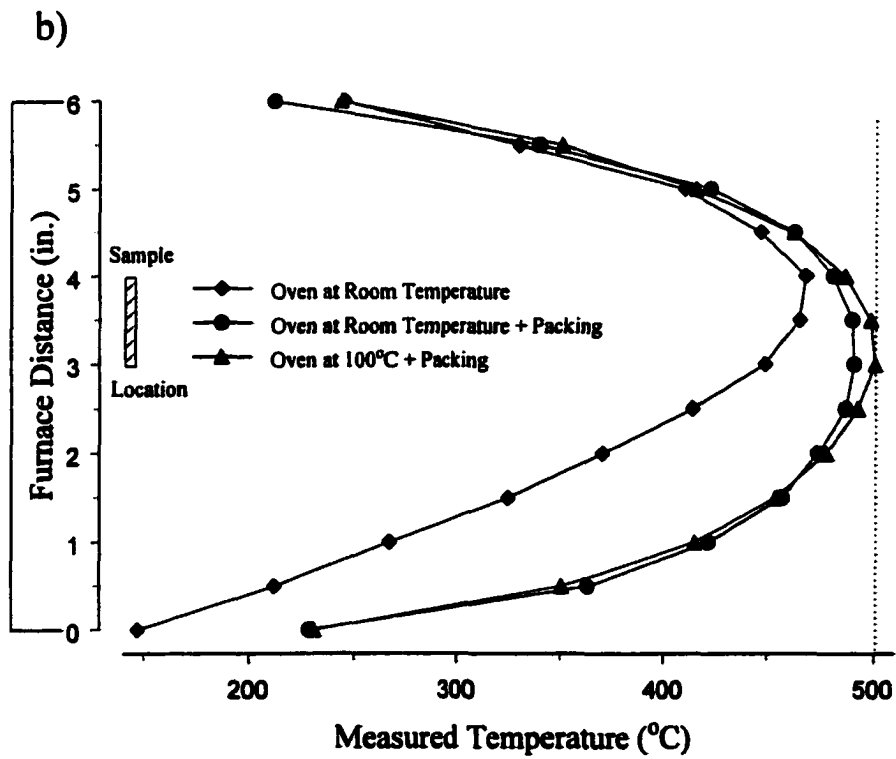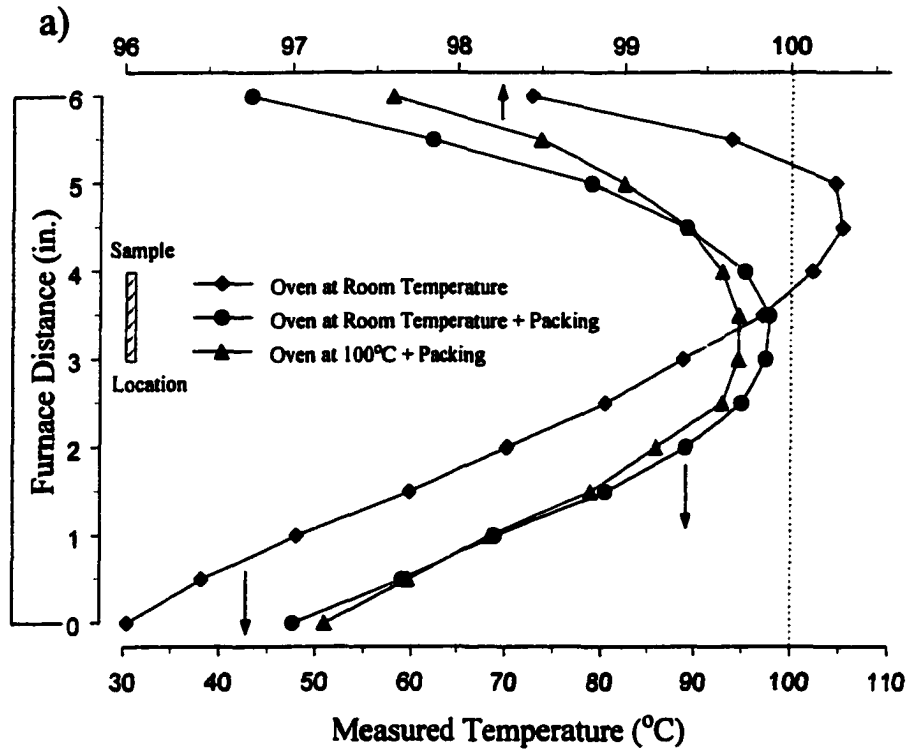
Figure 3-9 : Temperature Profiles in the Ceramic Radiant Tube Furnace. Furnace set point at a) 100°C and b) 500°C

52

1 in. The actual catalyst location depends on the catalyst density and amount loaded. The vertical dotted line in each figure denotes the setpoint temperature. The ◆ symbols correspond to sample tube temperatures obtained when the microreactor system oven was not heated. Note that heating the reactor furnace to 100°C and to 500°C (setpoint based on the "control" thermocouple) also heated the reactor system oven. The oven temperature rose to 36°C and to 63°C respectively. At both setpoints, the maximum temperature was not found at the tube furnace center (y=3), but slightly above it. This may be explained by convective heat rising. However, the maximum temperature was found at a different furnace position at each setpoint. The maximum temperature was found at a furnace position near 4.5-5 in. when the reactor furnace was heated to 100°C and near 3.5-4 in. at 500°C. It is also interesting to note that the maximum temperature exceeded the setpoint when the reactor furnace was heated to 100°C (T_{max}=105°C) but was far below the setpoint when the reactor furnace was heated to 500°C (T_{max}=468°C). The differences in the maximum temperature locations and deviations from the setpoints may be explained by the effects of the colder reactor system oven air. The larger deviation from the setpoint at 500°C can be explained by a greater cooling effect on the sample tube temperature. To test this hypothesis, ceramic insulation was used to plug both ends of the furnace to prevent reactor system oven air from passing through the furnace cavity. The ● symbols correspond to sample tube temperatures measured under these conditions. At both setpoints, the maximum temperature was found near the center of the furnace (y=3) and the temperature profile was much more symmetric. However, the maximum temperatures (98°C and 491°C) were still below the setpoints. This can be explained by the fact that the "control" thermocouple was closer to the heating element than the "measurement" thermocouple.

Because the reactor system oven must be heated for many studies, the effect of the oven temperature on the catalyst temperature was assessed. The ▲ symbols in Figure 3-9 represent sample tube temperatures measured when the oven was maintained at 100°C. Under these

conditions, the temperature at the sample location was virtually constant when the reactor

setpoint was 100°C (ranged between 99.6°C and 99.7°C). When the setpoint was 500°C, the

temperature profile was less affected as the temperature span remained large (between 487°C

and 500°C at the sample location). However, the maximum temperature rose to the set point

when the oven was heated (Fig. 3-9).

This study has shown that isothermal furnace temperature can be obtained. However,

"control" temperature setpoints must be manually adjusted to achieve the desired catalyst

temperature at the "measurement" thermocouple.

II.3.b Temperature Ramps

Temperature programmed desorption (TPD) measurements can be made by ramping the

reactor furnace temperature. Although other heating rates are possible, 10°C/min was chosen for

studies described here because it is the most commonly used heating rate employed in TPD

experiments. The temperature ramp was programmed by the Omega CN3240 temperature

controller used to maintain the reactor furnace temperature. The accuracy and reproducibility of

heating the furnace at 10°C/min are illustrated in Figures 3-10 and 3-11 respectively. Furnace

temperatures were recorded at 10 second intervals. The solid lines in Figure 3-10 denote the

temperature inside the sample tube plotted versus the programmed temperature (lower x-axis)

and time (upper x-axis) when the furnace temperature was raised from 100°C to 650°C at

10°C/min. The dotted lines denote the programmed heating ramp. During most of the furnace

heating period, the furnace temperature was below the programmed value. After about 46

minutes, the furnace temperature reached the programmed value (~560°C) and then became

slightly higher than the programmed value. The first five minutes of the heating ramp,

corresponding to programmed temperatures of 100°C to 150°C, are expanded in Figure 3-10b.
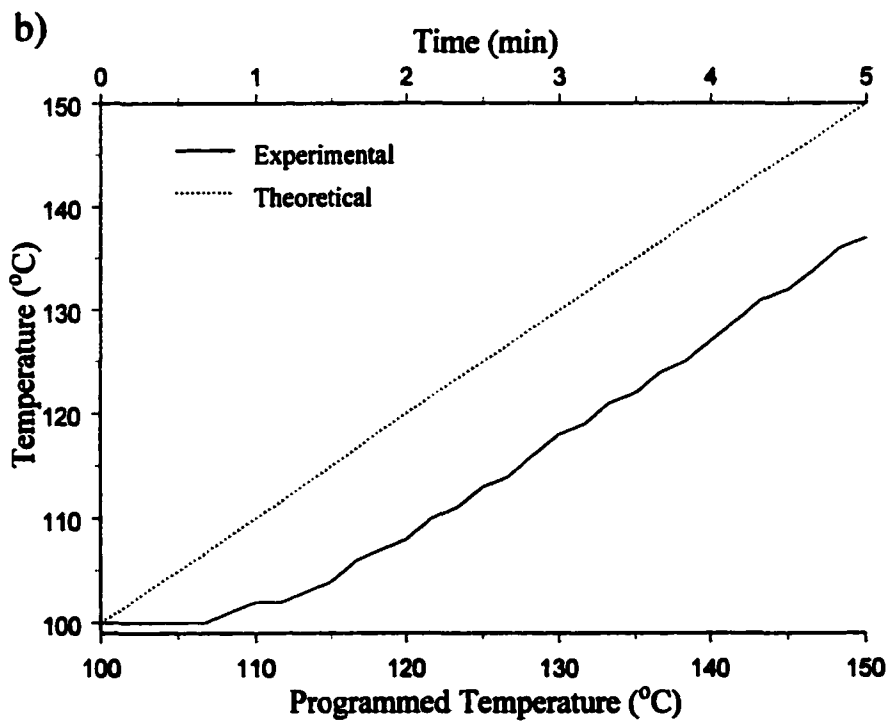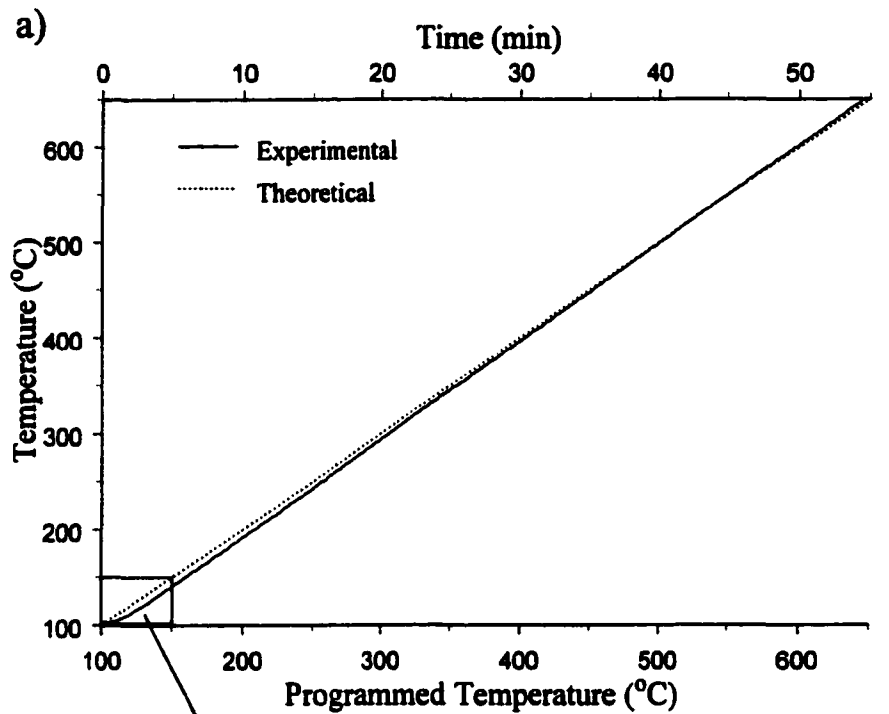
Figure 3-10 : Temperature Ramp (10°C/min) Accuracy
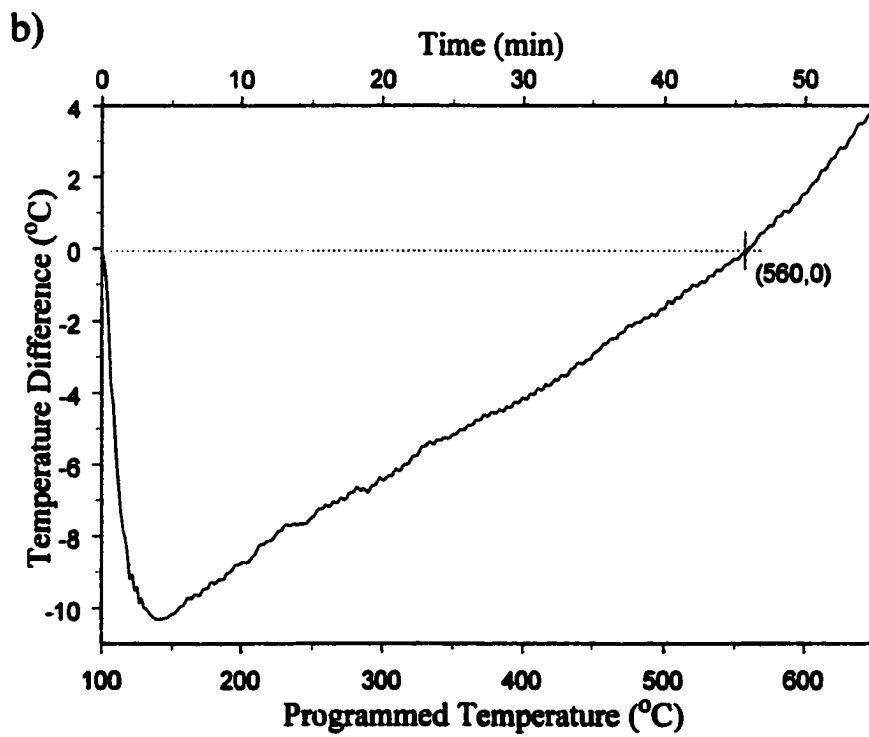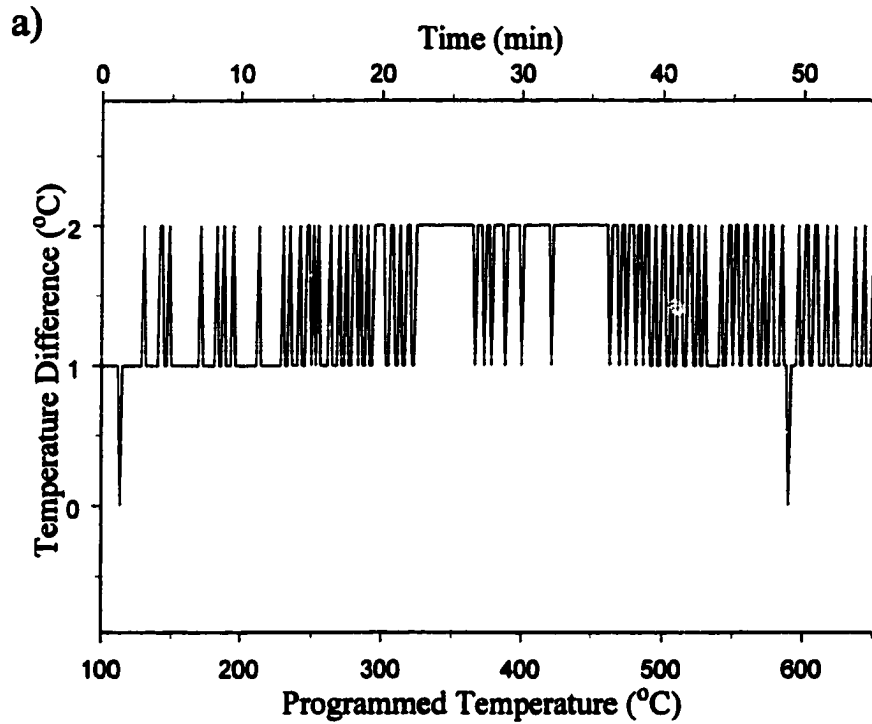
Figure 3-11 : Temperature Ramp (10°C/min) Reproductibility

For about 30 seconds, the furnace temperature (solid line) did not increase. This was likely due to the different locations of the "control" and "measurement" thermocouples. The temperature controller maintained the programmed temperature based on the "control" thermocouple. The "measurement" thermocouple was further away from the heating element and was shielded by the Vycor® protective tube and sample tube. As a result, a delay was observed before the temperature measured inside the sample tube rose. For the same reason, it took about 3 minutes for the furnace heating rate to match the programmed $10°C/min$ rate. After 3 minutes, the temperature increased linearly to $650°C$. However, the heating rate was not exactly $10°C/min$. Least-squares regression for tube temperatures measured between 5min and 55min yielded a sample heating rate of $10.26°C/min$. The slight difference between the furnace heating rate and the programmed rate is not a problem for TPD studies as long as the temperature ramp is reproducible.

The reproducibility of the ramp was tested by repeating the heating process 6 times for both empty tubes and tubes loaded with approximately 100mg of silica. No significant change in the temperature ramp was observed when the silica was present. Figure 3-11a shows differences in measured temperatures during repeated heating ramps plotted versus the programmed temperature and time. The solid line represents the absolute value of the largest difference between all six ramps. This value ranges from 0 to $2°C$ over the $100-650°C$ temperature range and clearly shows that the temperature ramp was reproducible to $\pm2°C$. Figure 3-11b illustrates the difference between experimental and programmed temperature ramps. The solid line in Figure 3-11b represents the difference between the average temperature obtained for the six heating ramps and the programmed temperature. This difference increased to ca $-10°C$ at $140°C$ during the first 4 minutes of the ramp due to the delay in heating the "measurement" thermocouple. After this delay, the temperature difference decreased as the average temperature

57

approached the programmed temperature. As expected from Figure 3-10a, this increase was linear from 150 to about 560°C. The average temperature was below the setpoint during most of the heating process. At 560°C, the temperature difference was negligible. Above 560°C, the temperature difference was positive because the average temperature was higher than the programmed temperature.

Although the ramp heating rate was not exactly 10°C/min, the ±2°C reproducibility of the furnace temperature ramp was sufficient for TPD experiments. However, the measured temperature did not vary linearly over the entire temperature range. By measuring elapsed times along with temperatures and detector signals, catalyst temperatures at which each detector signals were measured could be correlated. The program TIC.EXE in Appendix B was used to combine detector signals, catalyst temperatures and elapsed times into a single data file.

II.4 Development of the GC and GC/MS Interface

The bulky commercial GC was replaced with a laboratory made GC that permitted fast repetitive injections and an interface that connected it to the Hewlett Packard Mass Spectrometer. Table 3-3 lists the parts that were needed to construct the GC and interface.

Figure 3-12 is a drawing of the GC and GC/MS interface. The GC consisted of a 6 in. × 6 in. × 8 in. aluminum oven. The capillary column was wrapped around a 4.75 in. diameter cage constructed from two copper vacuum gaskets. One-half in. thick ceramic insulator board wrapped by insulating cloth covered the inside walls of the GC oven. The front and back walls of the oven could be removed for access to the column, heaters, and fan. The heating element, fan and thermocouple were mounted on the back wall. The thermocouple (not shown in Fig. 3-12) was placed right behind the fan. The heating element consisted of two 26 gauge nichrome wire coils connected in parallel. Each wire coil was wrapped around a 1/8 in. o.d., 6 in. long

Reactor-MS Splitter Valve

Reactor-GC/MS Splitter Valve

Bulkhead
Unions

to Automatic
Valve

Outlets

to Manual
Valve (Port #4)

to MS ←

Strip Heater   Heating Wires   Cage   Fan   GC Column
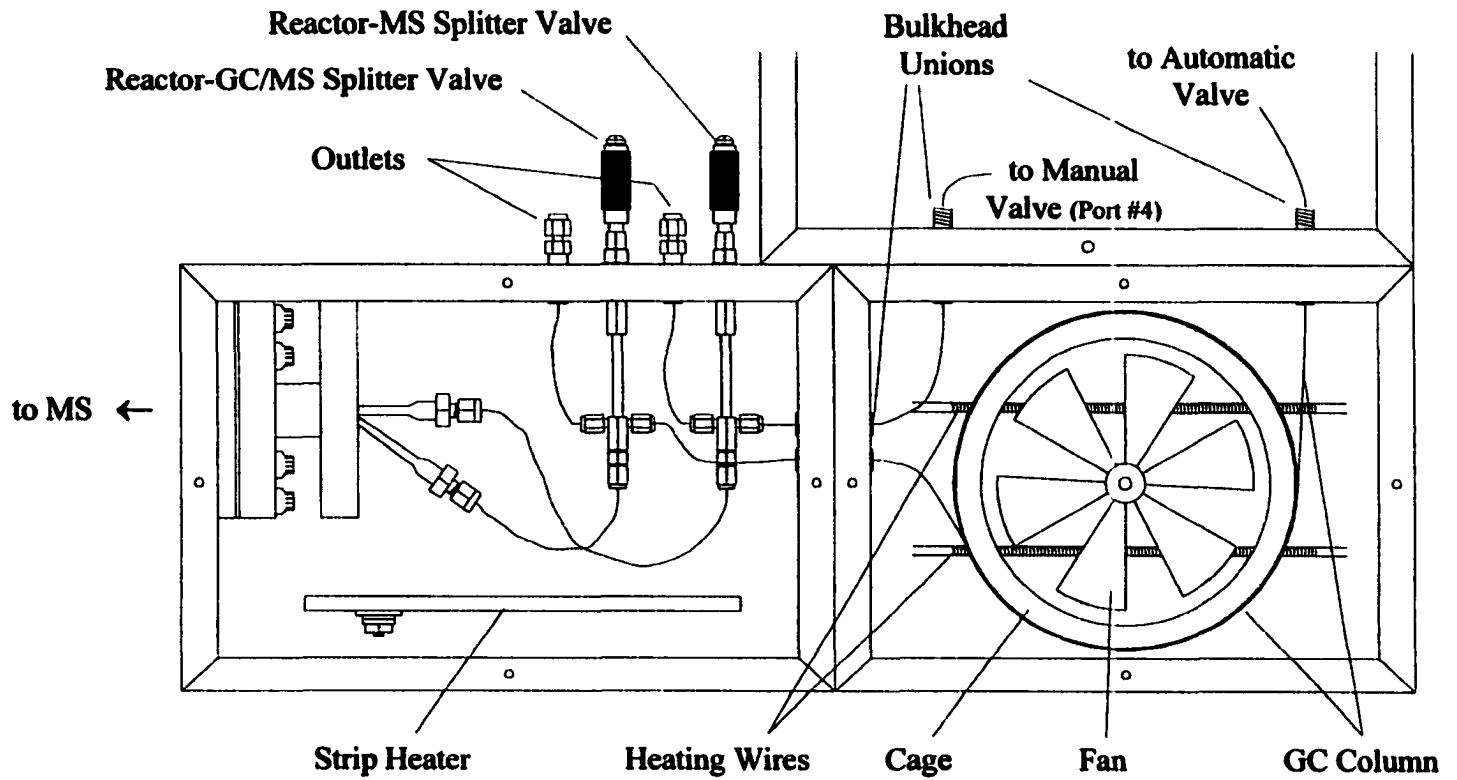
Figure 3-12 : GC and GC/MS Interface Design

59

Table 3-3 : GC and GC/MS Interface Part List

	Manufacturer	Part Number
GC Parts		
Fan Motor	Grainger (Oklahoma City, OK)	4M078
Fan Blade	Grainger (Oklahoma City, OK)	2C953
6 in Ceramic Tubes (1/8"od)	Omega A-85	ORX11618
Heating Wire (Ni-Cr Alloy)	Omega H-13	
Heater Hook up Wire	Omega H-45 / 51	
1/16" bulkhead union	Swagelok (Solon, OH)	SS-100-61
2 holes ceramic tubes	Omega (Stamford, CT)	TRM164116
Valves : Solenoids coils	Grainger (Oklahoma City, OK)	6X543
Insulation Cloth	Wale Apparatus (Hellertown, PA)	15-1420
Insulation Board	Cotronics (Brooklyn, NY)	360-2
Temperature Controller	Omega (Stamford, CT)	CN3202TC1-F1-8
Pulse Control Module	Omega (Stamford, CT)	PCM1
Solid State Relay	Omega (Stamford, CT)	SSR240DC25
Heat Sink	Omega (Stamford, CT)	FHS-2
2 × Bulkhead Union (1/16")	Swagelok (Solon, OH)	SS-100-61
GC/MS Interface Parts		
Insulation Cloth	Wale Apparatus (Hellertown, PA)	15-1420
Insulation Board	Cotronics (Brooklyn, NY)	360-2
Temperature Controller	Omega (Stamford, CT)	CN76020
Solid State Relay	Omega (Stamford, CT)	SSR240DC10
Heat Sink	Omega (Stamford, CT)	FHS-2
2 × Metering Valve	SGE (Austin, TX)	1236032
4 × Brass Bulkhead Union	Swagelok (Solon, OH)	
Strip Heater	Thermal Corporation (Madison, AL)	05-5-3-250W-120V
2 × OFHC Copper Gaskets	MDC Vacuum Prod. (Hayward, CA)	191013

ceramic tube to achieve about 11 ohm resistance. The heating coils provided a maximum GC oven heating rate of 300°C/min. In order to allow for repetitive injections when GC temperature ramps were used, the GC oven had to be rapidly cooled after separations. A solenoid valve (not shown in Fig. 3-12) was mounted on the GC oven front wall and connected to a 25L liquid nitrogen dewar flask by 1/4 in. o.d. insulated copper tubing. The dewar flask was pressurized with dry air from a Balston (Lexington, MA) air dryer. When the pressure in the dewar flask was about 7 psi, the GC oven could be cooled from 280°C to -20°C in about 30 seconds (600°C/min). Introducing liquid nitrogen into the GC oven also facilitated the use of sub-ambient

separation temperatures. However, it was easier to maintain isothermal cryogenic temperatures by flowing cool nitrogen gas from the dewar to the GC oven rather than spraying liquid nitrogen. Whether conducting isothermal or temperature ramp GC separations, the chromatograph oven temperature was controlled by using an Omega CN3202 heat/cool temperature controller, which varied the heating element current and energized the liquid nitrogen valve to maintain temperature setpoints (c.f. wiring in Appendix A).

The GC/MS interface was contained within a 6 in. × 6 in. × 9 in. aluminum oven. One-half in. thick ceramic board wrapped by insulating cloth covered the inside walls of the interface oven. The front and top walls of the interface oven could be removed. One side wall was cut to fit the mass spectrometer vacuum chamber inlet. A 3 in. × 5 in., 250W strip heater was used to heat the interface oven as high as 300°C. The interface oven temperature was maintained by an Omega CN76020 temperature controller (c.f. wiring in Appendix A). Two splitter valves were used to control the flow of gases into the mass spectrometer ionization chamber. One was connected to port #4 of the manual valve in the reactor oven (labeled "outlet" in Figs. 3-6 and 3-7) and facilitated Reactor-MS experiments. The 1/16 in. stainless steel tube connecting port #4 of the manual valve and this splitter valve passed through the GC oven. The end of the capillary GC column was connected to the other splitter valve to facilitate Reactor-GC/MS experiments.

II.5 Addition of a Flame Ionization Detector

The flame ionization detector (FID) is a mass-sensitive detector that is rugged and easy to use. It has a 10^{-10}g limit of detection, high sensitivity $\sim 10^{-13}$g/s, and large dynamic range (from 10^{-10} to 10^{-4}g). Its drawbacks are the facts that it is a bulk property detector and it destroys the sample. FID is the GC detector of choice for quantitative analysis of hydrocarbons. When pyrolyzed in the detector flame, hydrocarbons produce ions and electrons that conduct

electricity through the flame. "The number of ions produced is roughly proportional to the number of reduced carbons".[5] Although mass spectrometric detection is as sensitive as FID, it has a lower limit of detection (10^{-12}g), and provides structure specific information, its use for quantitative analysis is limited by its smaller dynamic range (10^4, from 10^{-12} to 10^{-8}g). Furthermore, mass spectrometer signal reproducibility strongly depends on the stability of the ion source. For these reasons, it was decided to add an FID to the reactor system to facilitate better quantitative measurements of hydrocarbons. A ca. 3 foot long piece of uncoated fused silica was used to connect the outlet of the GC/MS splitter valve (Fig. 3-12) to the inlet of an FID mounted to an HP 5980 Series II gas chromatograph. It is important to note that this line was at room temperature, which means that only hydrocarbons that are volatile at room temperature could be detected by the FID. Also, the dead volume between the splitter valve and the FID inlet resulted in a loss of chromatographic resolution. Initially, FID chromatograms were recorded by a chart recorder. However, this was unacceptable because data could neither be saved nor integrated. A 12 bit A/D converter was built to digitize the 0-1 V analog FID signal. Only one-fifth of the converter range was initially used, as it accepted input signals in a 0-5V range. The FID signal was subsequently amplified by a factor of five to match the A/D dynamic range. Figure 3-13 shows the amplifier and analog/digital converter circuit diagram. The A/D is based on a MAX187 chip bought from Digi-Key Corporation (Thief River Falls, MN). The amplification was achieved by using a TLC2262 dual operational amplifier from Texas Instruments (Dallas, TX). The amplifier gain was determined by the ratio of R2/R1. We used R1=200Ω and R2=1kΩ to obtain a 5 fold amplification. Digitized signal values were sent to the parallel port of an IBM compatible computer. The software used for data acquisition (Appendix B) also permitted signal averaging and integration. Figure 3-14a shows chromatographic peaks digitized with and without amplification. Figure 3-14b shows expansion

Figure 3-13 : Amplifier and Analog/Digital Converter

63
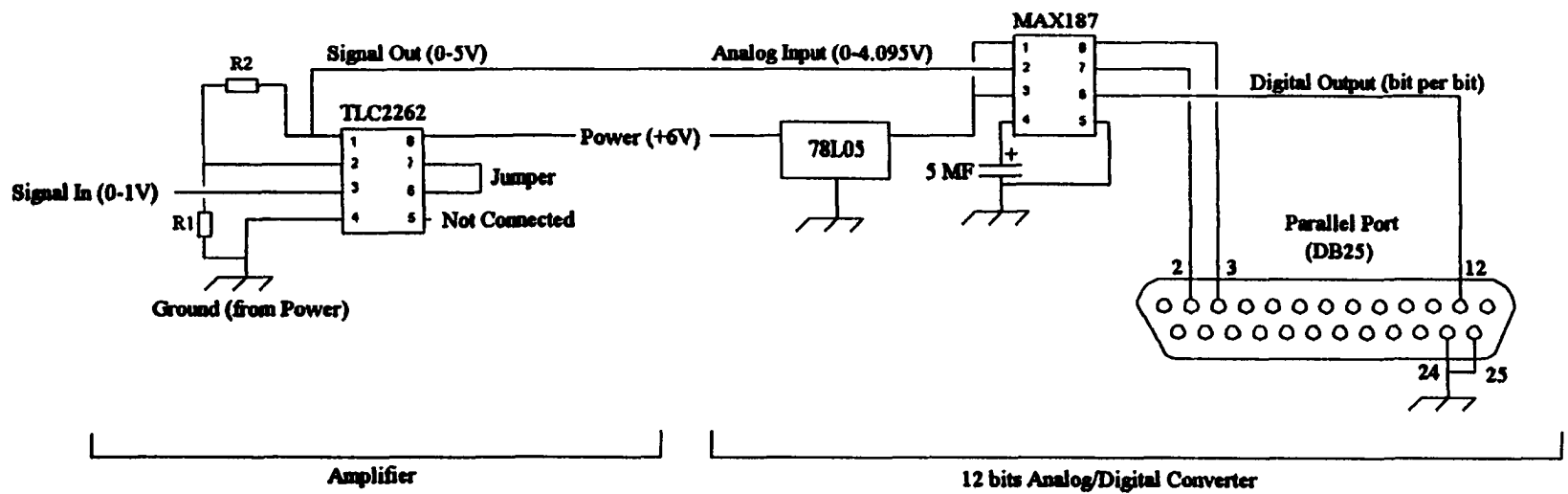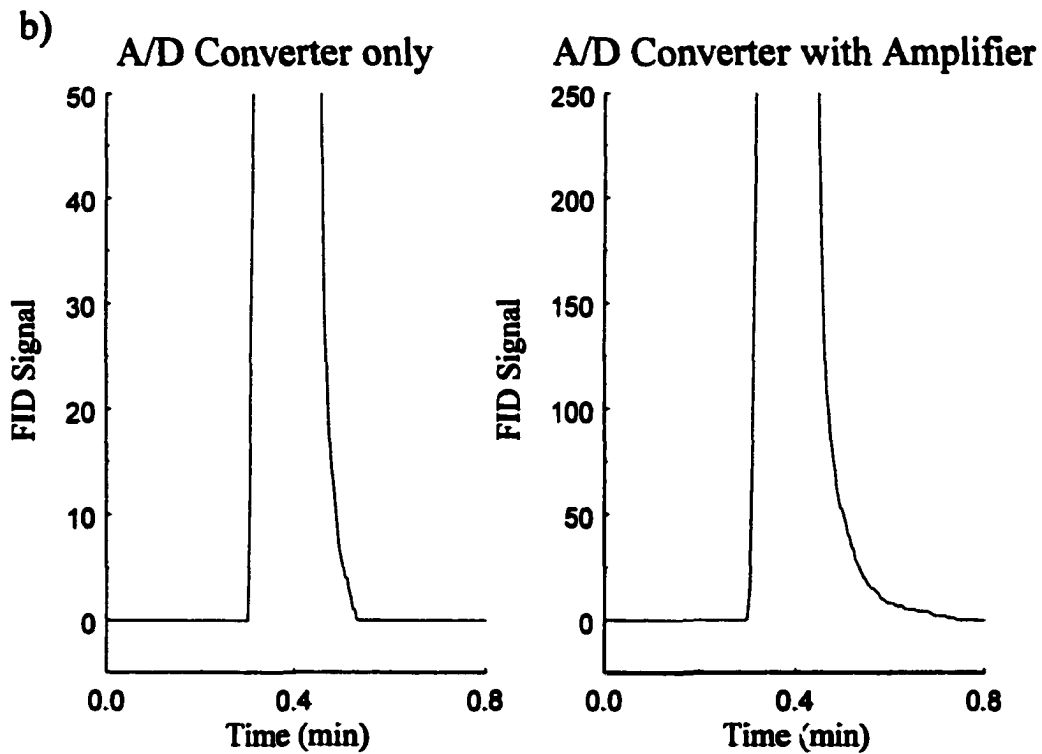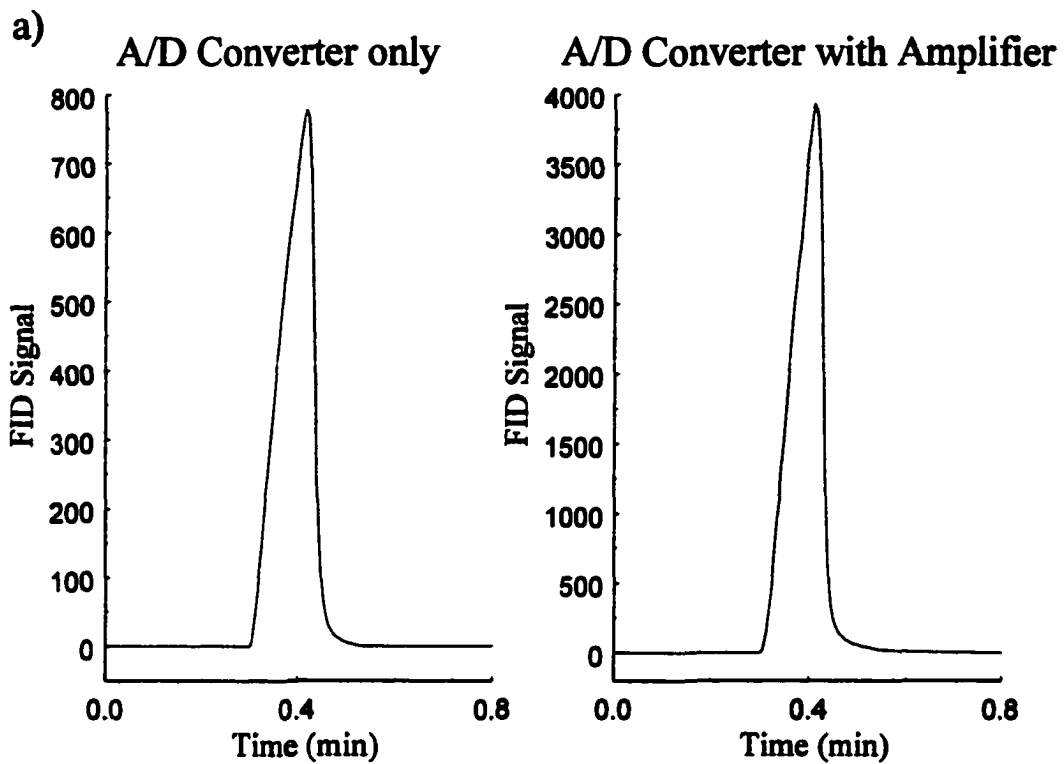
Figure 3-14 : Effect of Amplifier on FID Signal Digitization

of Figure 3-14a at the base of the peaks. Without signal amplification, the tailing portion of the peak was truncated. Peak definition was clearly improved by amplifying the FID signal prior to digitization. The peak heights of 800 and 4000 in Figure 3-14a correspond to 20 and 98% of the 12 bit A/D converter maximum range of $2^{12} = 4096$.

II.6 Current Microreactor-GC/MS-FID Design

Figure 3-15 is a drawing of the current microreactor-GC/MS-FID system that was used for studies described here. This figure is similar to Figures 3-5 and 3-12 that show the microreactor system and the GC and GC/MS interface. The GC column and the line used for reactor-MS studies are shown in Figure 3-15. All other connections have been excluded for clarity, but numbers indicate which parts were connected. The FID connection is also denoted on this figure. Figure 3-16 is the current microreactor-GC/MS-FID system flow diagram. The microreactor system flow diagram is identical to that shown in Figure 3-6. In addition, the GC and GC/MS interface flows are depicted in this figure. One of the splitter valves located in the GC/MS interface oven was connected to port #4 of the manual valve (M) and facilitated Reactor-MS experiments. The other valve split the GC effluent between the mass spectrometer and the FID.

Future modifications will include the incorporation of an FID in the interface oven, the addition of a Jade™ injector on the GC purge line in the reactor oven to allow for the injection of standards, and addition of a similar injector on the reactant line to permit pulse addition of reactants.
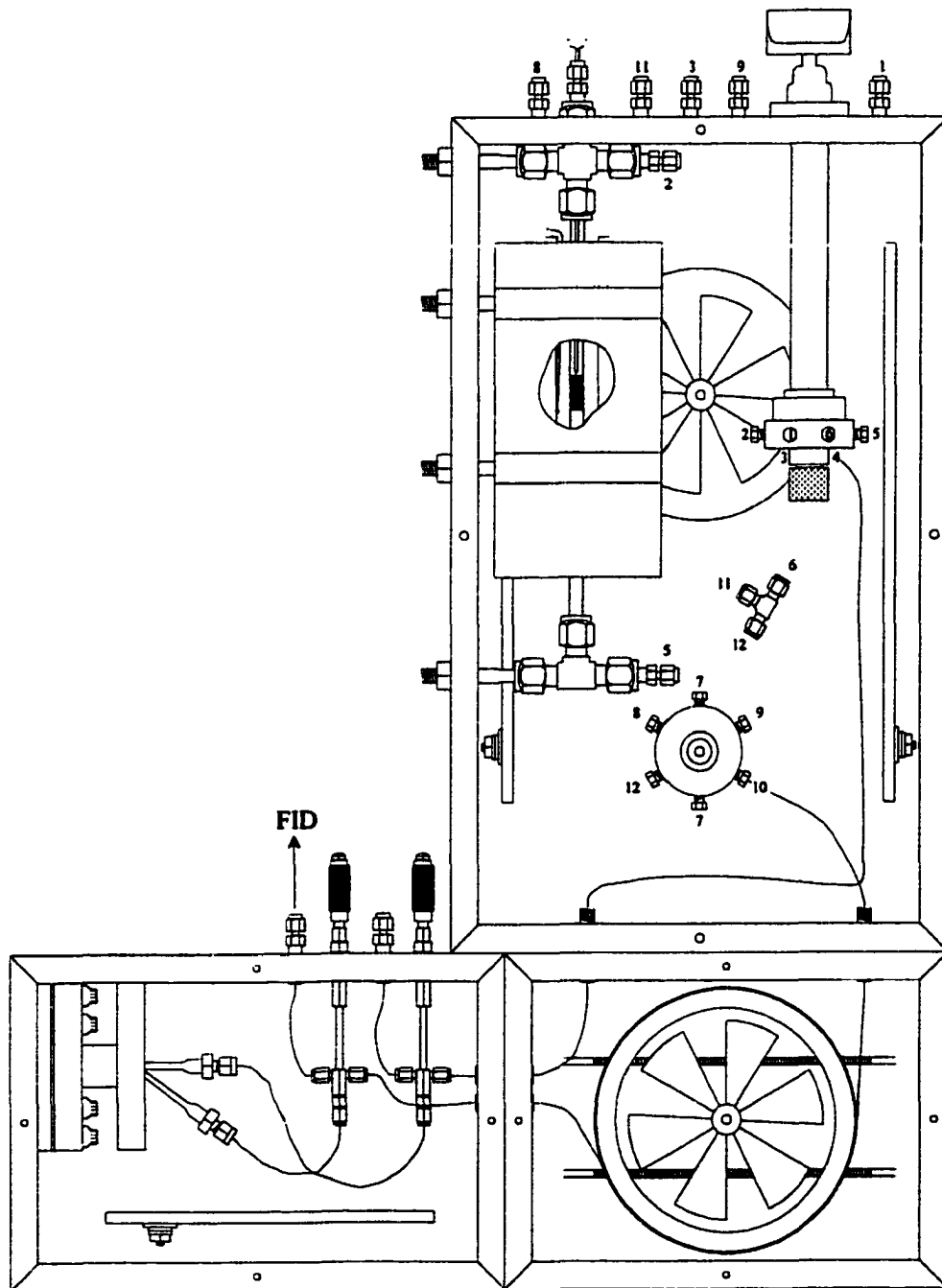
Figure 3-15 : Current Microreactor-GC/MS-FID System Design
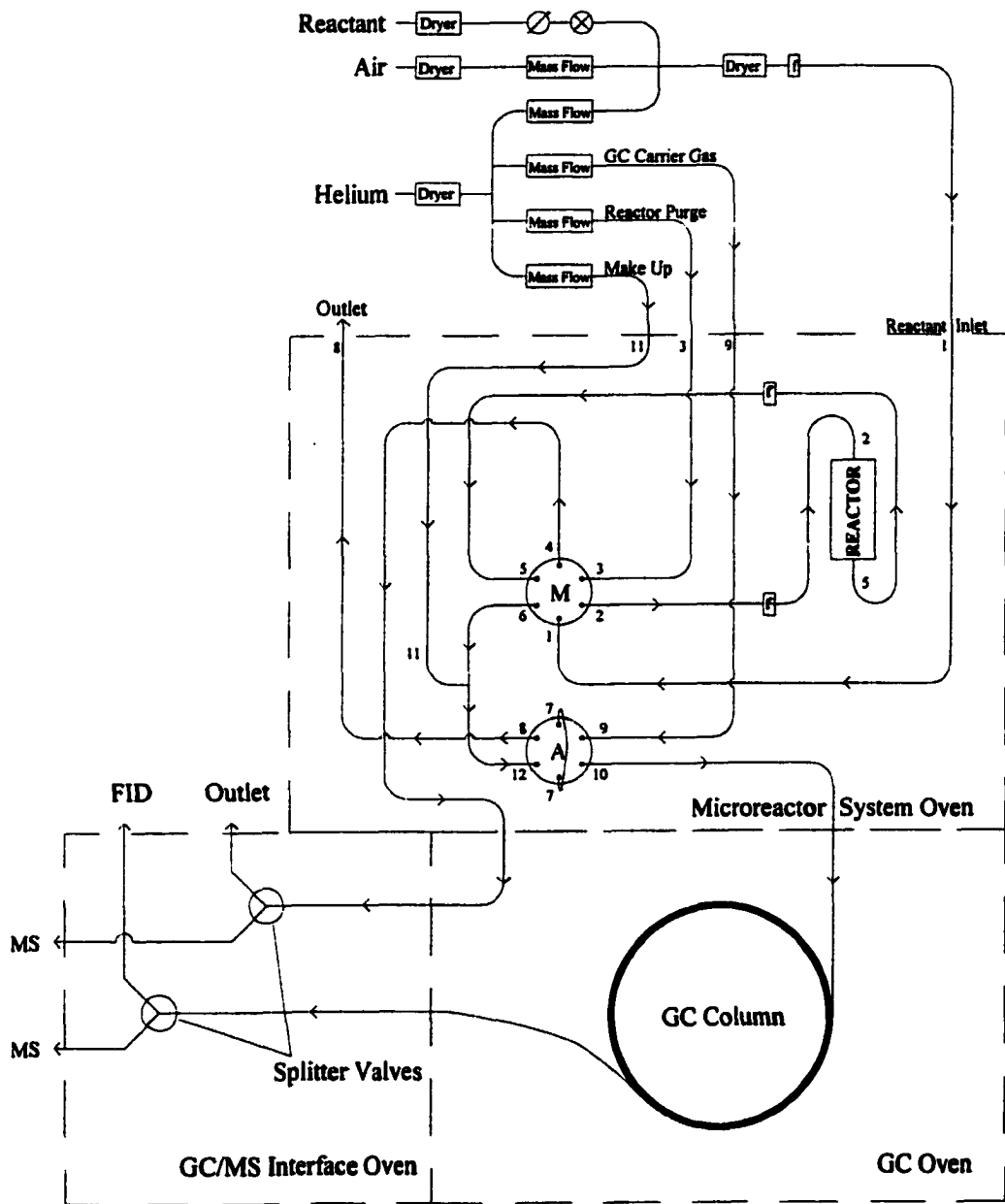
Figure 3-16 : Current Microreactor-GC/MS-FID System Flow Diagram

67

III. BENCHMARK STUDIES

Before applying the microreactor system to study new catalytic systems, the various operating modes of the system were evaluated with well characterized catalytic reactions. The following benchmark studies were used for this purpose :

- cracking of n-hexane by HZSM-5 zeolite catalyst, to test reactor-GC/MS-FID reproducibility and quantitative analysis capabilities.

- ammonia temperature programmed desorption (TPD), to test reactor-MS reproducibility and quantitative analysis capabilities.

- 1-butene oligomer desorption/decomposition, to characterize the repetitive chromatographic separation performance of the gas chromatograph.

III.1 n-Hexane cracking

The cracking of n-hexane by HZSM-5 zeolite has been extensively studied and was chosen to characterize our reactor GC/MS feature.[6-14] The ability of a solid acid to crack n-hexane is commonly employed to assess hydrocarbon cracking activity [6-11] and is designated as the α test.[10] Two mechanisms have been proposed for paraffin (e.g. n-hexane) cracking by aluminosilicate (e.g. HZSM-5) zeolites :[11,13]

Mechanism A : Initiation:[15,16] $\underbrace{C_nH_{2n+2}}_{RH} + SH \longrightarrow C_mH_{2m+2} + \underbrace{C_{n-m}H^+_{2(n-m)+1}}_{R_l^+} \ S^-$

$$RH + R_l^+ \longrightarrow R^+ + R_lH$$

$$\text{then } R^+ \longrightarrow \text{Reaction products}$$

Mechanism B : $RH + SH \longrightarrow S^- + RH_2^+$

$$\text{then } RH_2^+ \longrightarrow \text{Reaction products}$$
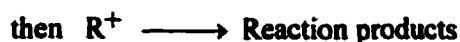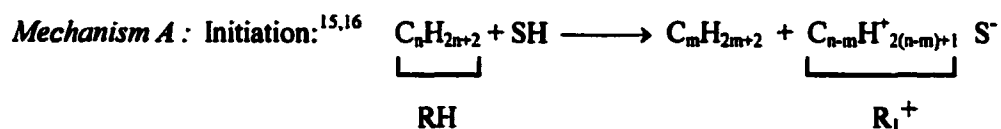
where SH is a catalyst Brønsted acid site, RH is the paraffin, R^+ is a carbenium ion derived from the paraffin, and RH_2^+ is a carbonium ion. In mechanism A, the first step after initiation is a hydride transfer that results in a carbenium ion (R^+). Subsequent beta-scission generates reaction products. In mechanism B, the paraffin reacts first with a catalyst Brønsted acid site to form a carbonium ion (RH_2^+). Decomposition of this relatively unstable ion forms the reaction products. The cracking of n-hexane by the medium pore HZSM-5 zeolite is believed to occur almost exclusively by mechanism B:[11]

$$n\text{-}C_6H_{12} + SH \longrightarrow S^- + C_6H_{13}^+ \longrightarrow SH + 2 C_3H_6$$

Hydrogen transfer between n-hexane and the intermediate ion $(C_6H_{13}^+)$, oligomerization, and further cracking of the light olefins can also occur, but are insignificant under typical reaction conditions. The cracking of n-hexane by HZSM-5 is first order with respect to hexane concentration. The protolytic first step is rate limiting. A recent publication gives a value for the n-hexane cracking by HZSM-5 apparent activation energy of 108 kJ/mol,[17] and others report apparent activation energy values ranging from 105 to 149 kJ/mol.[12] An advantage of the use of this catalytic system as a benchmark for our microreactor system is that n-hexane cracking can be achieved without significant catalyst deactivation or residue formation when low conversion conditions (i.e. short contact times) are employed.[12] This permits the use of a single catalyst sample for long periods of time, which is particularly helpful for assessing the long term stability of our detection methods.

One goal of the n-hexane cracking study was to measure the activation energy for this reaction and compare it to literature values. To do so, n-hexane cracking activity must be measured at different temperatures. For a single catalytic process, activity is often given in terms of conversion. Both fractional and percent conversion can be used. Here, n-hexane conversions were calculated as follows :

$$\text{Fractional Conversion} = \frac{[\text{n} - \text{hexane}]_0 - [\text{n} - \text{hexane}]}{[\text{n} - \text{hexane}]_0} \qquad (1)$$

$$\text{Percent Conversion} = \text{Fractional Conversion} \times 100\% \qquad (2)$$

where $[\text{n-hexane}]_0$ is the initial n-hexane concentration and $[\text{n-hexane}]$ is the instantaneous concentration of unreacted n-hexane. Apparent activation energies were obtained by application of the Arrhenius method.

III.1.a Experimental Conditions

Because n-hexane cracking by HZSM-5 exhibits no significant catalyst deactivation when performed at low conversion (i.e. less than 30% conversion[12]), the initial goal of this study was to find the temperature range over which this condition was satisfied. n-Hexane was introduced into the reactor gas flow by passing 60mL/min helium through a bubbler filled with 99.9% n-hexane obtained from Sigma (Saint-Louis, MO) and maintained at room temperature. The resulting gas mixture entered the reactor through the reactant inlet and passed through 10mg of HZSM-5 previously calcined in-situ in 25mL/min air for 2 hours at 550°C. Calcination removed species (mainly water) adsorbed on the HZSM-5 surface. After calcination, the catalyst temperature was ramped from 300°C to 700°C at 2°C/min, while in contact with the n-hexane reactant. Reactor effluent ($\sim 80\mu L$) was automatically injected every 4°C (2 min) into a 10 meter DB-5 capillary gas chromatographic column maintained at 50°C. The GC carrier gas was 3mL/min helium. After separation, the GC flow was split in the 200°C interface by opening the reactor-GC/MS splitter valve so that the mass spectrometer ion source pressure reached 1×10^{-6} Torr. The remaining GC flow was directed through the interface outlet to the external FID. The MS detector sampling rate was dictated by the mass spectrometer scan rate. To maximize the MS scan rate in order to provide the best possible GC/MS peak definition, only selected ions were scanned (m/z = 26-30, 37-45, 55-58, 69-71, 78, 86, and 91). These ions were determined to

be representative hexane and hexane derived hydrocarbons based on previous studies in which all ions in the m/z 20-180 mass range were detected. By restricting the number of ions scanned, the mass spectrometer sampling rate was increased by a factor of 6 (from 1.02 to 6.13 scans/second) compared to scanning the entire m/z 20-180 mass range. Figure 3-17 shows 62 successive chromatograms obtained during n-hexane cracking plotted versus catalyst temperature over the 450-700°C range derived from the MS (a) and the FID (b). The y-axes denote the respective detector signals: MS total ion current (TIC) and relative FID current. Below 450°C, chromatograms contained a single peak of constant area corresponding to uncracked n-hexane. As the catalyst temperature increased from 450°C to 700°C, the n-hexane peak diminished and a peak corresponding to propene grew. This was expected, because conversion increased with temperature. However, the relative peak heights for the n-hexane and propene peaks were different for the two detectors. Relative to n-hexane, the propene TIC peaks were much smaller than the FID derived peaks. Figure 3-18 shows TIC (a) and FID (b) chromatograms obtained at catalyst temperatures of 452°C, 596°C and 692°C. X-axes represent retention time from 0 to 1.75 minutes. Comparison of each chromatogram pair shows that FID chromatographic peaks were narrower than TIC chromatographic peaks. This was unexpected, because the FID connection included additional dead volume that should cause a reduction in peak resolution. Instead, peak resolution calculated for chromatograms obtained at catalyst temperatures of 596°C indicated that the resolution was almost a factor of two better for the FID (R=9.7) than for the MS (R=5.4) chromatographic peaks. This can be explained by the difference in the detection methods. In the FID, hydrocarbons pass rapidly through a flame, whereas hydrocarbons entering the ion source must diffuse out. The time required for diffusion results in peak broadening.

a)

b)
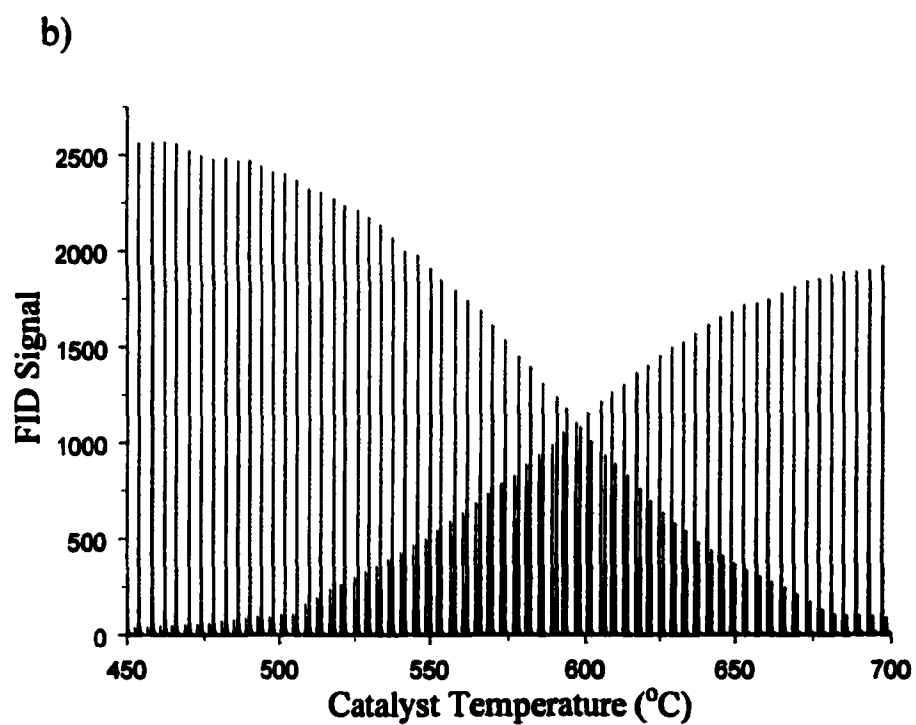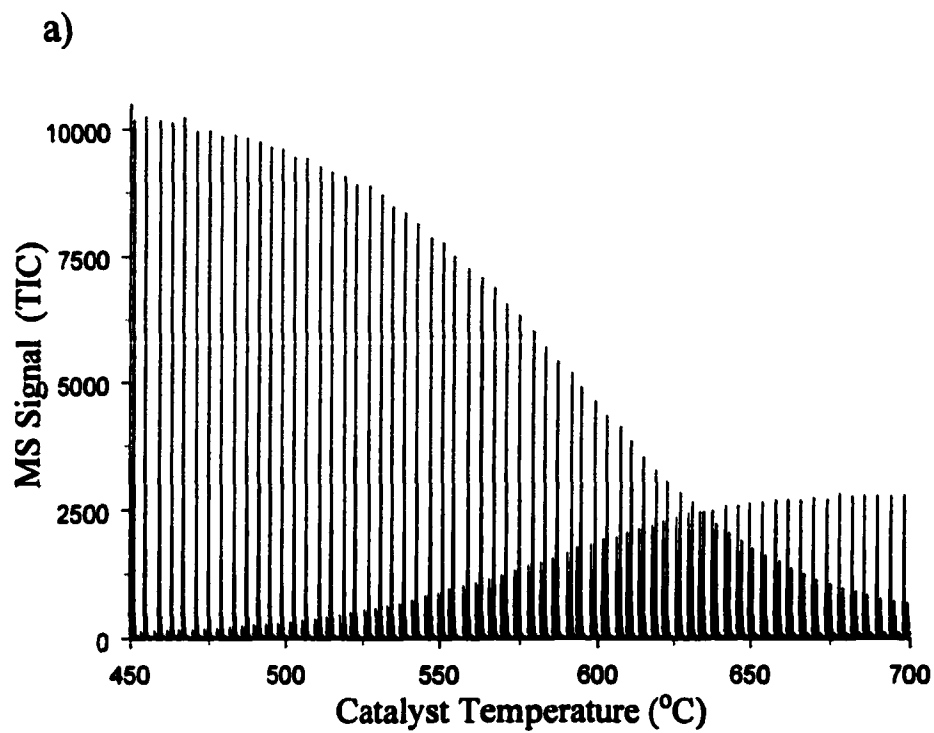
Figure 3-17 : Effect of Catalyst Temperature on Peak Heights : (a) TIC and (b) FID

72

a)

propene

n-hexane

452°C

Reactor Furnace Injection Temperature (°C)

propene

n-hexane

596°C

propene

n-hexane

alkyl aromatics

692°C

b)

propene

n-hexane

452°C

Reactor Furnace Injection Temperature (°C)

propene

n-hexane

596°C

propene

n-hexane

alkyl aromatic

692°C
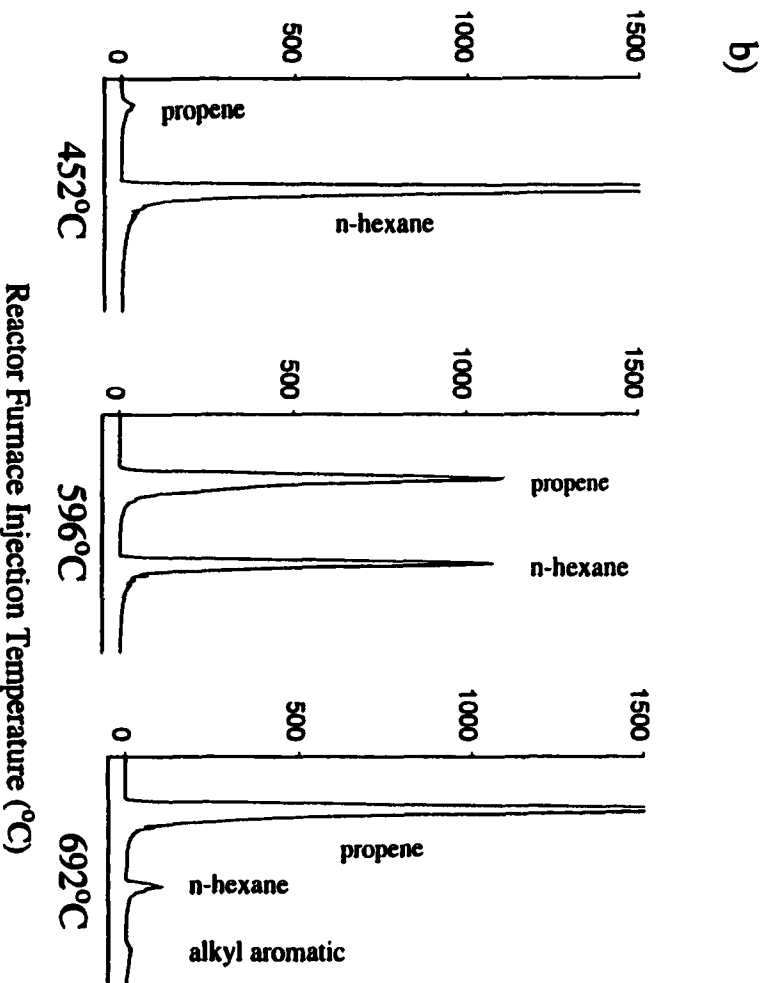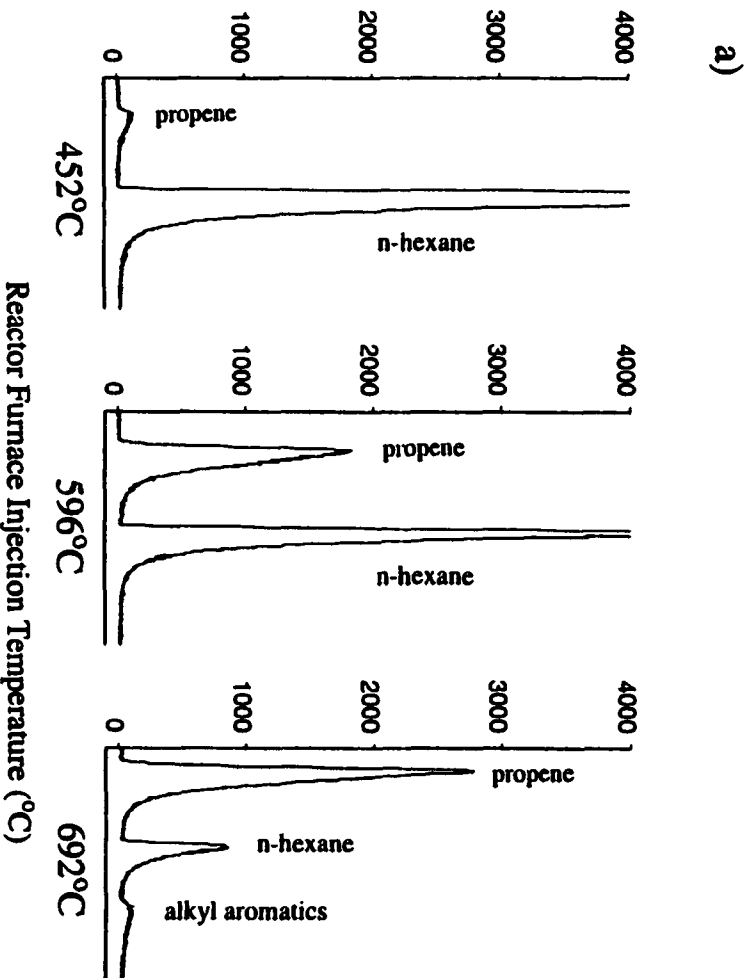
Figure 3-18 : Chromatograms at different HZSM-5 Temperatures for (a) TIC and (b) FID

73

At 452°C, the largest peak in both chromatograms corresponded to n-hexane and a small peak corresponding to propene can be observed. At 596°C, the FID chromatogram consisted of two peaks of similar intensity corresponding to propene and n-hexane. The TIC chromatogram obtained at the same catalyst temperature consisted of two peaks with significantly different intensities. The propene peak was much shorter than the n-hexane peak. At 692°C, the largest peak in both chromatograms corresponded to propene. The small n-hexane peak indicated that conversion was not complete. In addition to peaks for propene and n-hexane, the 692°C chromatogram contained an additional peak. The mass spectrum obtained during elution of this substance contained ions at m/z 78 and 91, which are characteristic of alkyl aromatics. Thus, at high temperatures, n-hexane cracking by HZSM-5 occurred with high conversion and formation of volatile alkyl aromatics in addition to significant amounts of residue. This residue is the source of catalyst deactivation.[18-20] The n-hexane peak height decreased with catalyst temperature similarly in both chromatograms (Fig. 3-17). However, the propene relative peak height was larger for the FID than for the MS. This was caused by the intrinsic properties of each detector. The FID response depended on the number of reduced carbons. When an n-hexane molecule is transformed into two propene molecules, the total number of carbons is unchanged. Thus, the sum of the FID signals for n-hexane and propene remained relatively constant throughout the cracking temperature range. The n-hexane and propene FID peaks were of nearly equal height when the catalyst temperature reached about 596°C, denoting a conversion of about 50%. The MS detector response depends on the ionization properties of the substances when they are bombarded by electrons. n-Hexane and propene molecules have significantly different sizes and chemical functionalities, resulting in different ionization properties.

Figure 3-19 shows (a) TIC and (b) FID peak areas for n-hexane (solid line) and cracking products (dotted line) plotted versus catalyst temperature over the 450-700°C range. The peak area of every eighth injection is marked with ● or ▲ to denote MS and FID results respectively.

Interestingly, although the MS and FID propene relative peak heights were significantly different (Fig. 3-17), relative peak areas were similar. The relative propene peak height differences for the FID and MS results evident in Figure 3-17 were attributed to peak shape variations. In fact, the chromatograms obtained at the 596°C catalyst temperature (Fig. 3-18) show that the propene TIC peak (a) was wider than the corresponding FID peak (b). Figure 3-19 shows that the temperature corresponding to 30% conversion is approximately 550°C. As a result, catalyst temperatures below 550°C must be used for the kinetic studies to avoid catalyst deactivation effects. The temperature range for which conversion is below 30% can be determined more precisely by calculating the percent conversion, X, for each injection :

$$X = \% \text{ Conversion} = \left(\frac{\text{Area}_{\text{Hexane/No Conversion}} - \text{Area}_{\text{Hexane}}}{\text{Area}_{\text{Hexane/No Conversion}}} \right) \times 100 \qquad (3)$$

where $\text{Area}_{\text{Hexane}}$ is the n-hexane peak area for each injection and $\text{Area}_{\text{Hexane/No Conversion}}$ is the n-hexane peak area obtained when no conversion was observed. Peaks obtained at low catalyst temperatures or when the reactor was bypassed were used to determine the zero conversion peak area. Figure 3-20 shows percent conversion obtained for each injection plotted versus catalyst temperature over the 450-700°C range. The ● and ▲ symbols represent every eighth injection and denote MS and FID data respectively. Figure 3-20 shows a very good correlation between the MS and FID data. The horizontal line at 30% conversion represents the maximum conversion that can be used to crack n-hexane without significant catalyst deactivation. This graph shows that the catalyst temperature must be maintained below 540°C to avoid deactivation and above 480°C to have significant conversion.

75

a)

b)
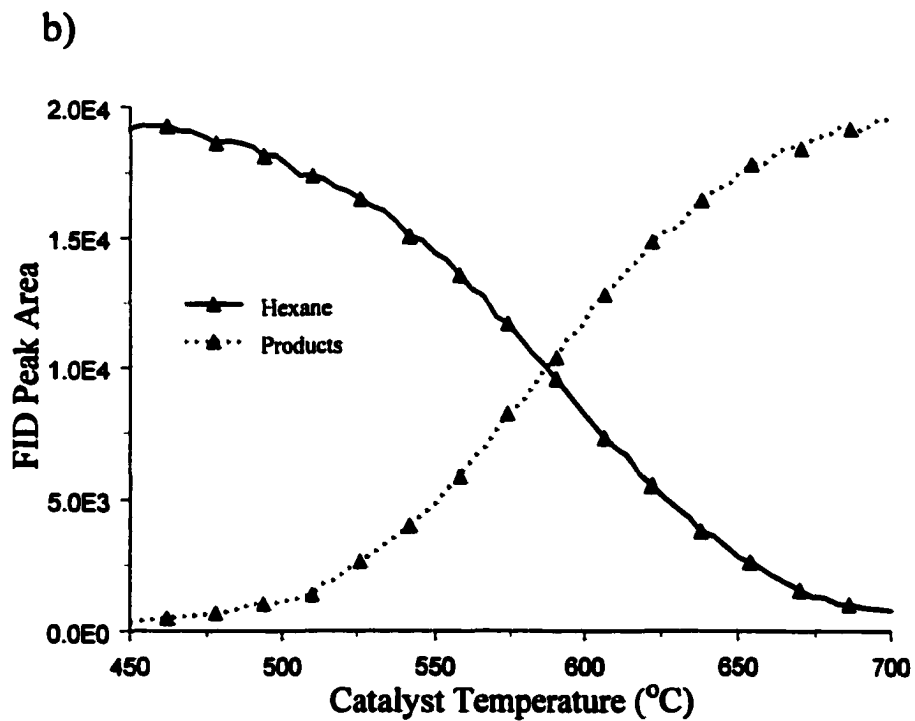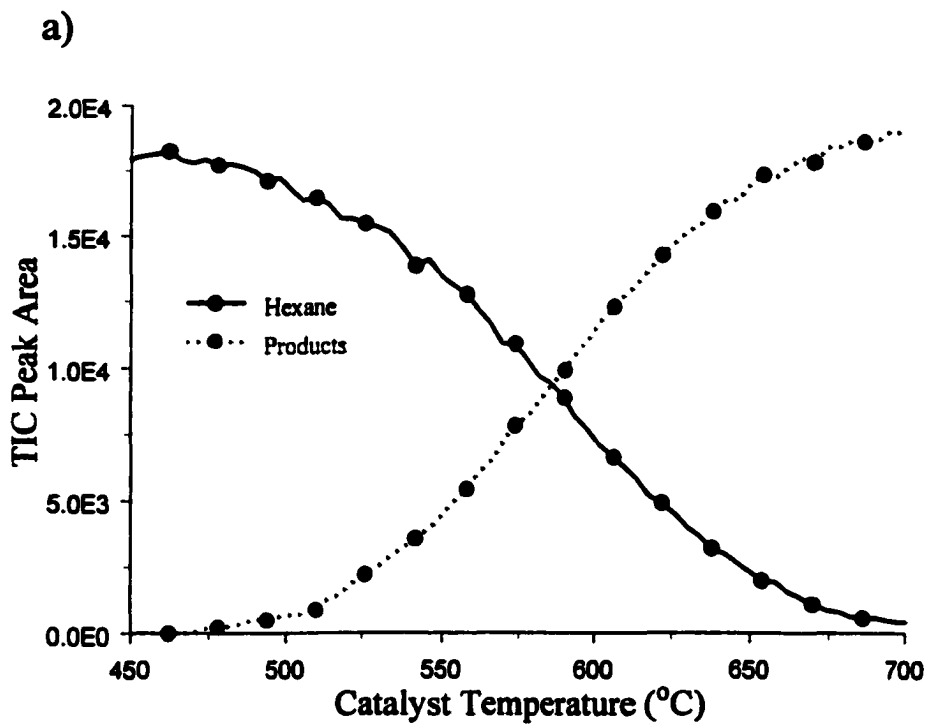
Figure 3-19 : Effect of Catalyst Temperature on Peak Areas : (a) MS and (b) FID
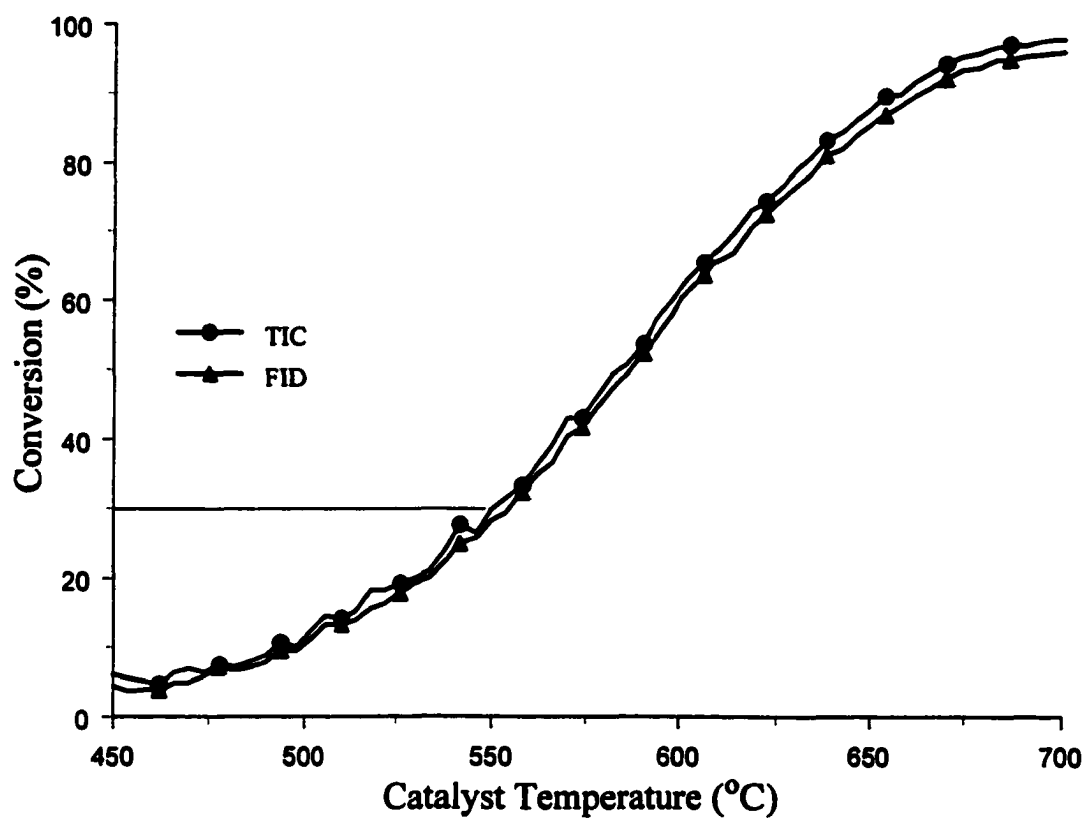
Figure 3-20 : Effect of Catalyst Temperature on n-Hexane Conversion

III.1.b Kinetic Study

For a given chemical reaction, the reaction rate constant is related to the activation energy and temperature, and can be calculated from the Arrhenius equation (defined in Chapter 1):

$$k = A \exp\left(-\frac{E_a}{RT}\right) \quad (4)$$

where k is the rate constant, A is the pre-exponential factor (also called frequency factor), E_a is the activation energy in Joules per mole, R is the gas constant with the value 8.314 J mol^{-1} K^{-1}, and T is the temperature in Kelvin. n-Hexane cracking by HZSM-5 is a first order process. The activation energy can be determined from the slope, $-E_a/R$, of the straight line obtained by plotting the natural logarithm of the rate constant against the reciprocal absolute temperature :

$$\ln k = -\frac{E_a}{R} \times \frac{1}{T} + \ln A \quad (5)$$

Conversion is directly proportional to and can therefore be substituted for the rate constant k (c.f. Appendix C). Consequently, the activation energy can be obtained from the slope, $-E_a/R$, of the straight line obtained by plotting the natural logarithm of the fractional conversion (X) versus the reciprocal absolute temperature :

$$\ln X = -\frac{E_a}{R} \times \frac{1}{T} + \ln A' \quad (6)$$

Isothermal n-hexane conversions were measured at catalyst temperatures of 480°C, 500°C, 520°C, and 540°C. However, plots of lnX versus 1/T were not linear for the MS or the FID data. By collecting n-hexane chromatograms overnight while bypassing the reactor, it was determined that the amount of n-hexane present in the gas flow varied with time. n-Hexane was introduced to the reactor gas flow by allowing helium to bubble through liquid n-hexane maintained at room temperature. Thus, the amount of n-hexane in the gas flow depended on the n-hexane vapor pressure, which varied with the ambient temperature. Room temperature variations were

sufficient to change the amount of n-hexane present in the gas flow during isothermal catalytic reaction measurements. As a result, the bubbler temperature was regulated by using a refrigerated water recirculator (model CFT-75 from Neslab, Portsmouth, NH). The bubbler was maintained at a temperature below room temperature to avoid n-hexane condensation in unheated transfer lines. The effect of bubbler temperature on the relative amount of n-hexane present in the reactant gas flow is illustrated by Figure 3-21, which shows n-hexane MS and FID peak areas plotted as a function of the bubbler temperature. Peak areas derived from each detector were directly proportional to the bubbler temperature. Peak areas (relative n-hexane concentrations) nearly doubled when the bubbler temperature was increased from 10.6°C to 21.6°C.

In a second attempt to measure the n-hexane cracking activation energy, n-hexane chromatogram peaks (injections at 2 minute intervals) were collected for ten minutes in the bypass mode, then for ten minutes under isothermal reactor conditions at 480°C, 500°C, 520°C and 540°C. Fractional conversions at each catalyst temperature, T, were calculated by equation 7. Five chromatogram peak areas obtained in bypass mode, $Area_{Hexane\ Bypass}$, and at each isothermal temperature, $Area_{Hexane\ T}$, were averaged.

$$\text{Fractional Conversion }_T = \left(\frac{\sum_{n=1}^{n=5}Area_{Hexane\ Bypass} - \sum_{n=1}^{n=5}Area_{Hexane\ T}}{\sum_{n=1}^{n=5}Area_{Hexane\ Bypass}} \right) \qquad (7)$$

The natural logarithm of the fractional conversion was plotted versus the reciprocal temperature. Figure 3-22 shows the plots generated from FID and MS data. Both detectors yielded straight lines. However, the slopes of these lines were significantly different. The activation energies calculated from these slopes were consequently different also. This should not be possible because the detection method should not affect the n-hexane cracking kinetics. During subsequent experiments, n-hexane peak areas obtained in the bypass mode were recorded both at
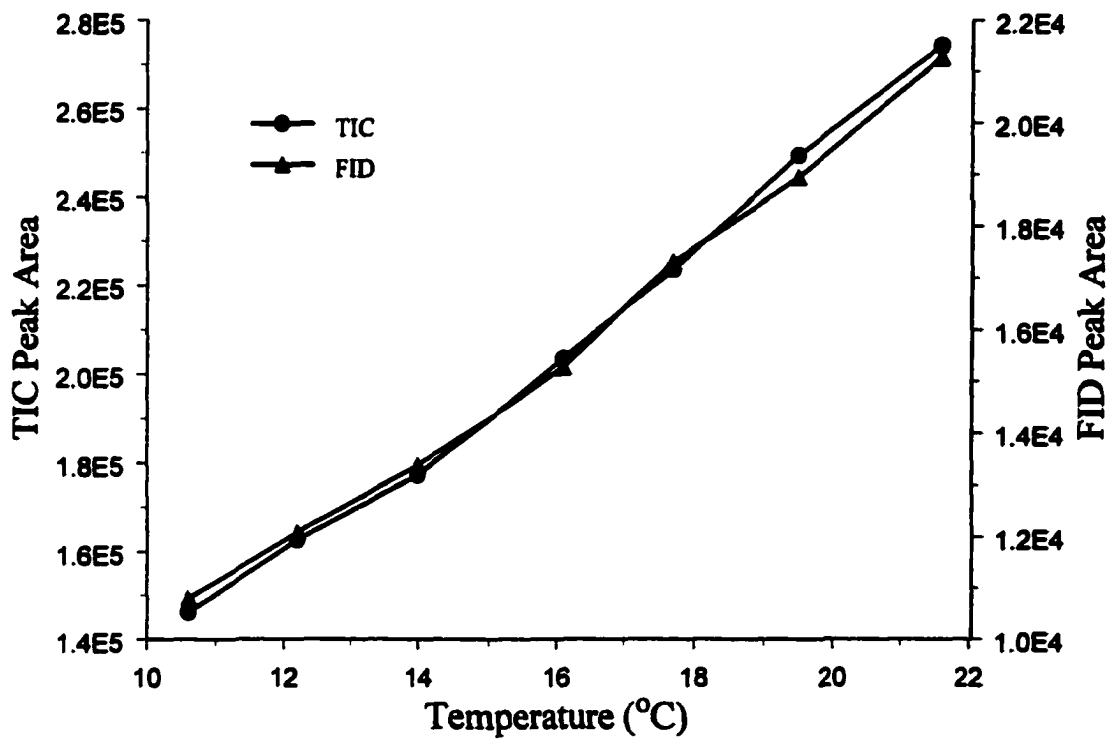
Figure 3-21 : Effect of n-Hexane Bubbler Temperature
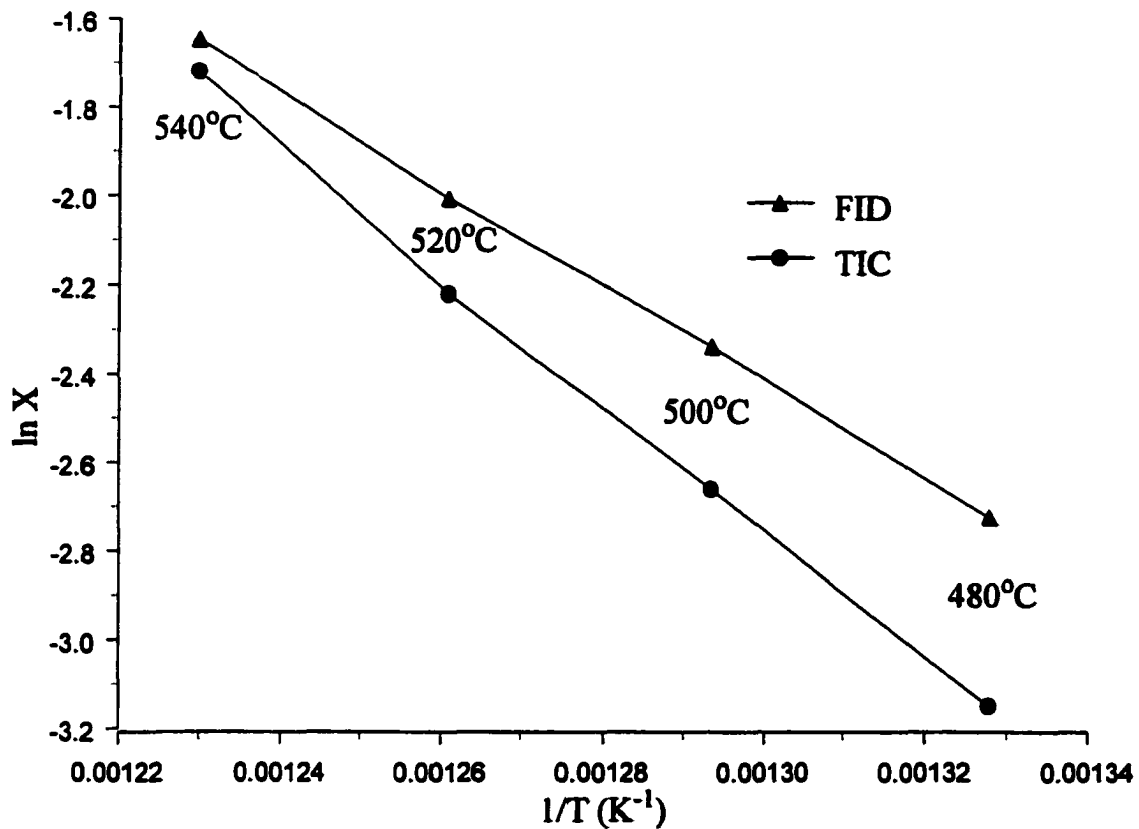
Figure 3-22 : Arrhenius Plots for n-Hexane Cracking derived from FID and MS Data

the start and the end (i.e. after all isothermal temperature data were collected) of the experiment. FID n-hexane peak areas were essentially identical, whereas the TIC peak areas obtained after isothermal measurements were significantly smaller than those obtained before reaction. The n-hexane signal obtained through the bypass at each detector was recorded for over 4 hours. Figure 3-23 shows the chromatographic detector signal and n-hexane peaks areas obtained by using the FID (a) and the MS (b) detectors. FID peak heights and areas were constant with time whereas MS peak heights and areas clearly decreased with time. The large amount of n-hexane that entered the mass spectrometer on each injection may have contaminated the ion source, which would reduce the MS signal. This effect seems to be reversible because no significant signal loss was observed when the experiment was repeated after allowing the MS to pump down overnight. This MS signal decrease during chromatographic measurements was a significant problem. Although we were unable to avoid this problem, acceptable data were obtained by changing the experimental procedure. Figure 3-24 shows a flowchart representing the new data collection procedure. After the catalyst was calcined in situ, n-hexane was first introduced via the bypass mode. When the n-hexane partial pressure was constant and the catalyst temperature was stable at 480°C, data collection began. GC injections were made at 2 minute intervals. During the first 10 minutes, chromatograms were obtained while n-hexane flowed through the reactor bypass. The manual valve was then switched and n-hexane was cracked in the reactor at 480°C. After 10 minutes, the manual valve was switched back to bypass and the catalyst was heated to the next temperature, in this case, 490°C. At the same time, chromatograms were collected in the bypass mode for 10 minutes (from 20 to 30 minutes in Fig. 3-24). During that time, the reactor furnace reached 490°C. The manual valve was switched again and n-hexane was cracked for 10 minutes at 490°C. This process was repeated so that each isothermal n-hexane cracking measurement was performed between two zero conversion bypass
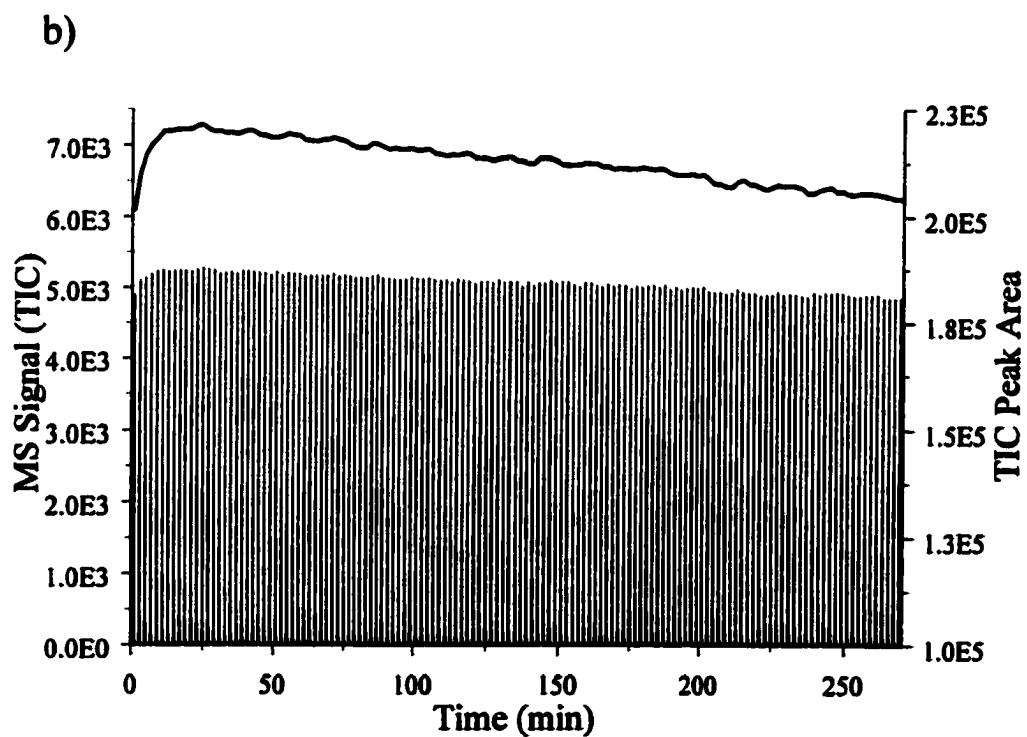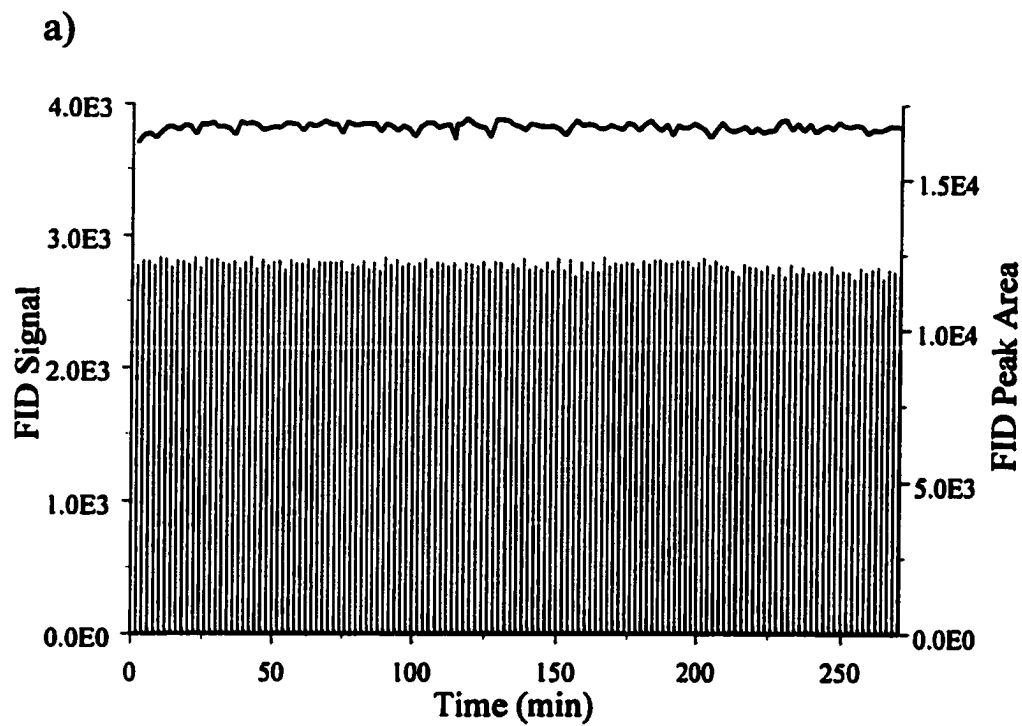
Figure 3-23 : Effect of Time on (a) FID Signal and (b) TIC Signal
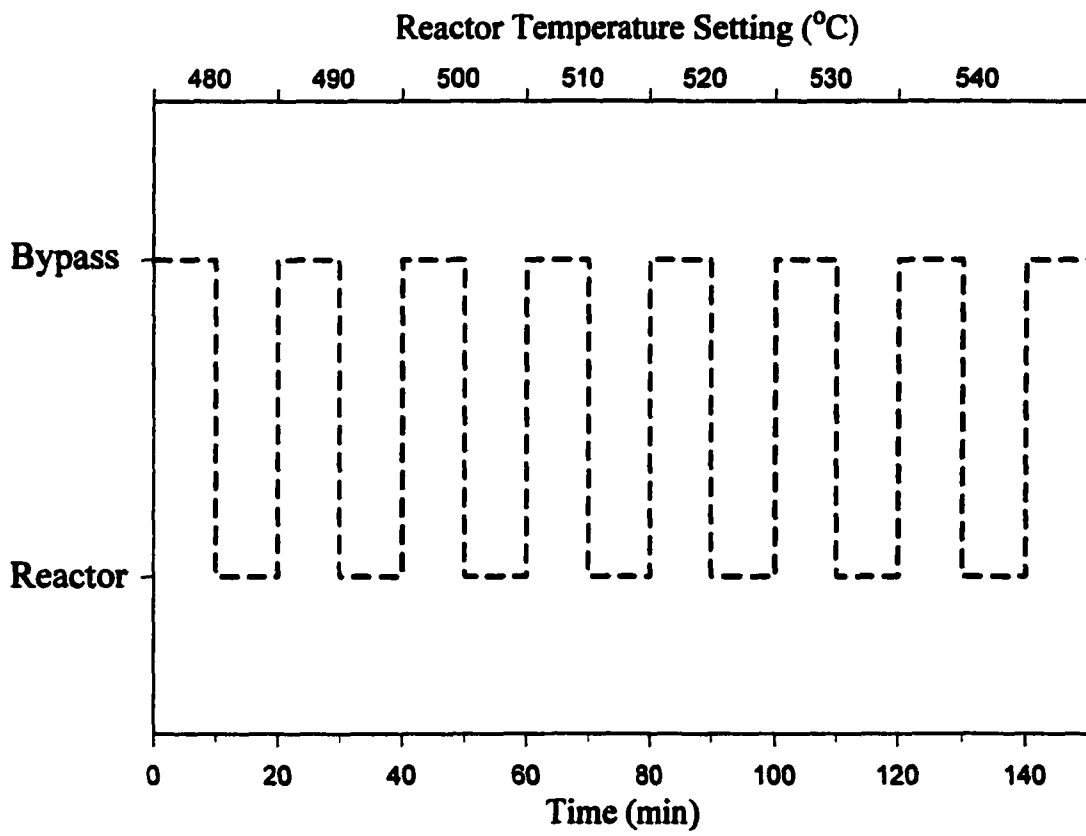
Figure 3-24 : Experiment Flowchart

mode measurements. Fractional conversion was calculated in such a way that the effect of the MS signal decrease was minimized :

$$\text{Fractional Conversion}_T = \left(1 - 2 \times \frac{\sum_{n=1}^{n=5}\text{Area}_{\text{Hexane},T}}{\sum_{n=1}^{n=5}\text{Area}_{\text{Hexane},Before} + \sum_{n=1}^{n=5}\text{Area}_{\text{Hexane},After}}\right) \qquad (8)$$

where $\text{Area}_{\text{Hexane},T}$ was the n-hexane average peak area obtained while cracking n-hexane at temperature T, and $\text{Area}_{\text{Hexane},before}$ and $\text{Area}_{\text{Hexane},after}$ were the average n-hexane peaks areas obtained at zero conversion (bypass mode) just before and after collection of chromatograms representing cracking at temperature T. Arrhenius plots obtained by using this procedure are shown in Figure 3-25a. FID and TIC plots overlap. Activation energies for n-hexane cracking by HZSM-5 derived from the slopes of these lines were calculated to be 110kJ/mol. The fact that the activation energies calculated from FID and TIC data gave the same exact numerical value (110kJ/mol) was only a coincidence. The uncertainty associated with this value, calculated from peak area reproducibility, was found to be ±2kJ/mol.

When cracking n-hexane, both n-hexane and propene peaks were detected. The amount of propene formed was directly related to the amount of n-hexane lost. Thus, the activation energy for the first order process can also be determined from changes in the propene peak area. Figure 3-25b shows Arrhenius plots obtained by using propene peak areas. The FID and TIC data produced relatively straight lines with similar slopes, but they did not overlap. However, these lines were not expected to overlap. The natural logarithms of the absolute detector signals used to make these plots are different for the FID and MS signals. The propene peak areas were much smaller than the hexane peak areas because of the required low conversion conditions. The relative propene peak area uncertainty was consequently higher, as was the uncertainty in the activation energy. The FID and TIC derived values (111kJ/mol and 106kJ/mol respectively) were nevertheless very close to those derived from fractional n-hexane conversion.
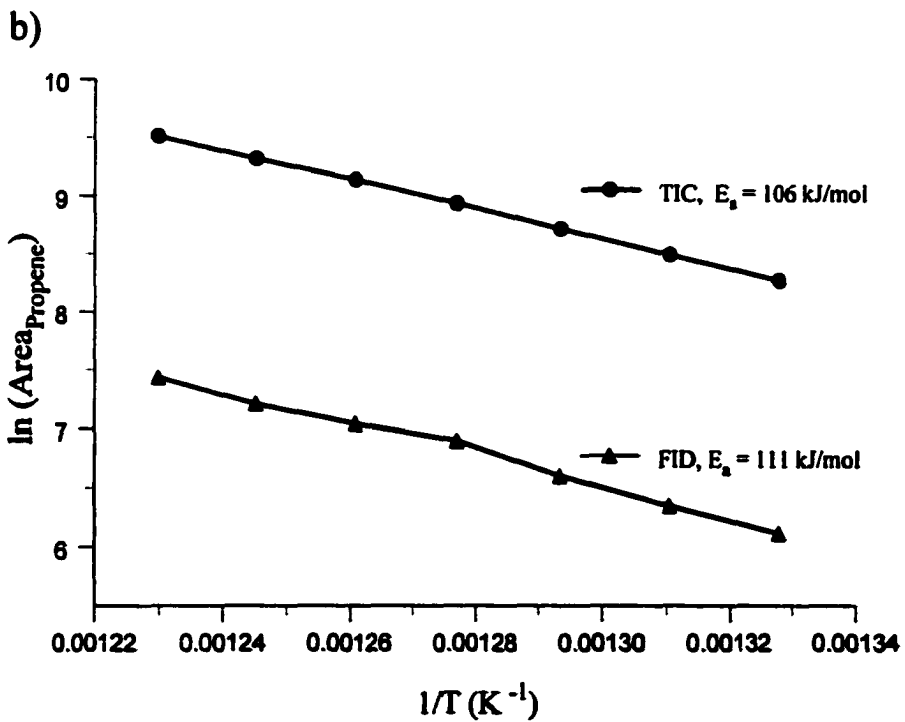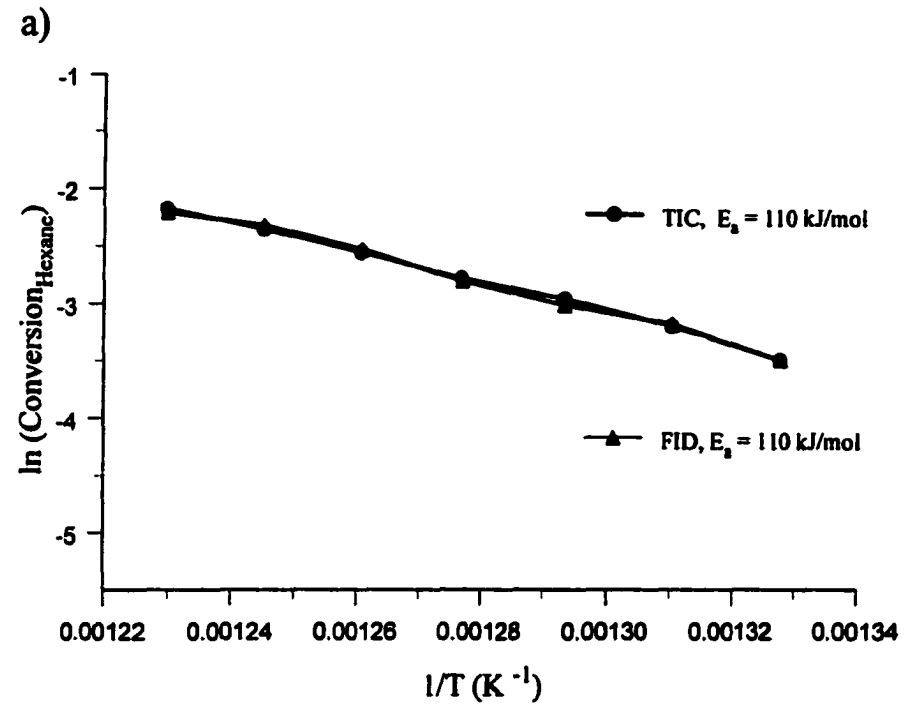
Figure 3-25 : Arrhenius Plots for n-Hexane Cracking by HZSM-5 derived from
a) n-Hexane Conversion and b) Propene Formation

III.2 Ammonia Temperature Programmed Desorption

Ammonia temperature programmed desorption (TPD) is commonly used to characterize catalyst acidities and was chosen to characterize our reactor-MS feature.[21,22] Unlike n-hexane cracking, the FID could not be used to confirm MS results because ammonia provides no FID signal. Instead, reactor-MS ammonia TPD results were compared to those obtained by thermogravimetry and VT-DRIFTS.

Active site acidities of catalysts are often characterized by studying the interactions between these sites and basic probe molecules such as ammonia and pyridine. However, water readily adsorbs onto these sites at room temperature. As illustrated by Figure 3-26, adsorbed water can be removed by heating the catalyst. Figure 3-26a shows VT-DRIFTS spectra measured while heating HY zeolite from 50 to 500°C at 2°C/min. IR apparent absorbance (y-axis) is plotted against wavenumber (x-axis) for the 4000-800 cm^{-1} range. Although spectra were acquired at 5°C intervals, only 4 spectra corresponding to catalyst temperatures of 50°C, 125°C, 200°C, and 400°C are shown in this figure. Figure 3-26b shows expansions of Figure 3-26a in the 3600-3200 and 1800-1400 cm^{-1} ranges. At 50°C, water adsorbed on the HY surfaces resulted in a broad absorbance feature (3700-2500cm^{-1}) and a sharp absorbance band (1650cm^{-1}). As the catalyst temperature increased, water desorbed revealing the IR bands of the Brønsted acid sites (3650 and 3550cm^{-1}). Water was completely desorbed by 400°C. After water desorption, the catalyst must be cooled in a dry environment to avoid re-adsorbtion of water on catalyst surfaces prior to ammonia exposure.

Qualitative acid strength profiles can be obtained by monitoring the temperature dependence of ammonia desorption. Temperatures at which ammonia desorbs from catalyst surfaces depend on the strengths of interactions between the adsorbed base and the acid sites. Under conditions for which ammonia does not re-adsorb (i.e. efficient purge) and readily

a)

Apparent Absorbance

b)

Apparent Absorbance
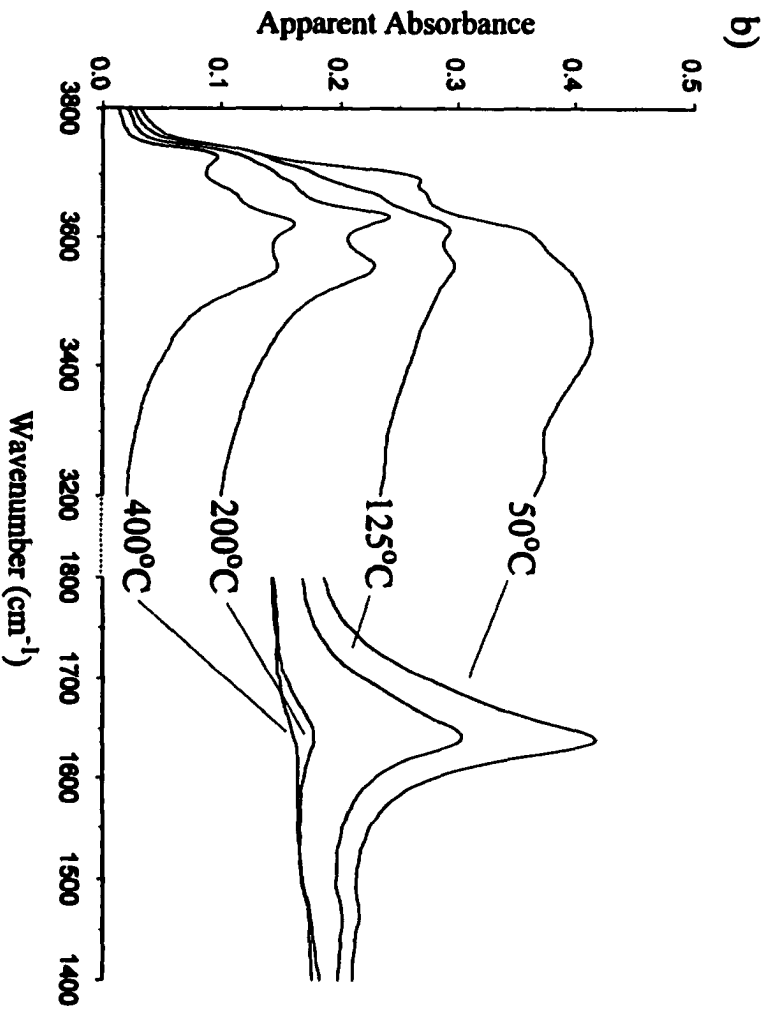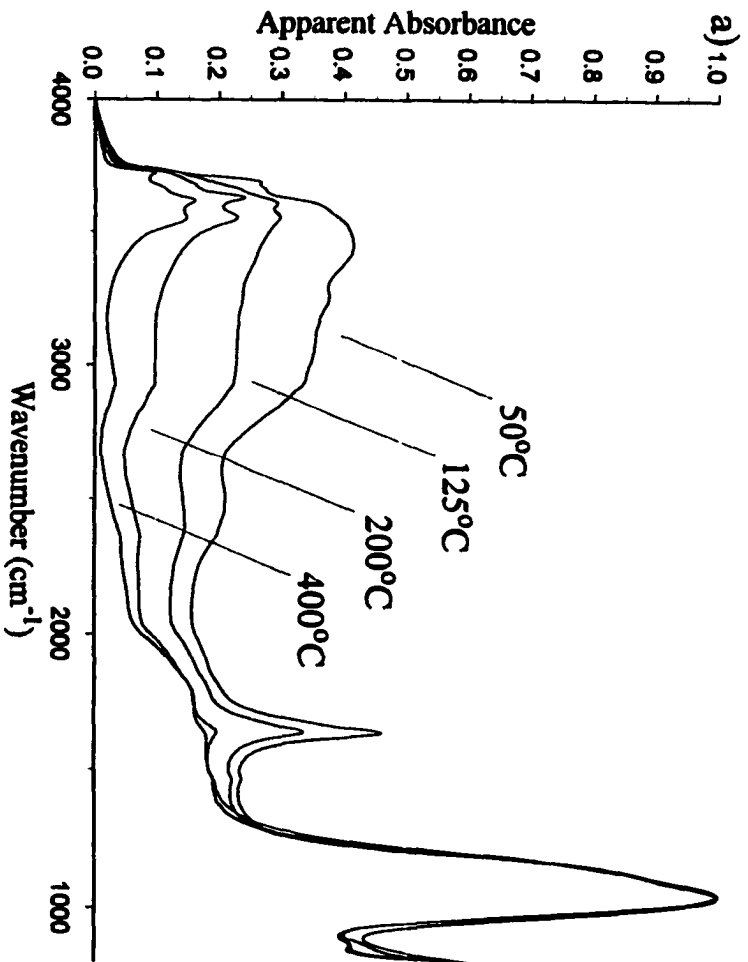
Figure 3-26 : HY Dehydroxylation

88

diffuses through the catalyst pores, desorption temperature profiles represent measures of catalyst site acidity distributions. Figure 3-27 shows ammonia desorption from 30 mg of HY zeolite monitored by thermogravimetry. The left y-axis in Figure 3-27 represents percent weight loss and the right y-axis represents the first derivative of the weight loss. The percent weight loss (solid line) and its first derivative (dotted line) are plotted against the catalyst temperature (x-axis) over the 100-550°C range. The HY sample was heated to 650°C in air (25mL/min) to remove adsorbed water, then cooled to 100°C and flushed with helium before it was exposed to ammonia. After ammonia exposure, the sample was purged for 30 minutes and finally heated in 25mL/min helium from 100 to 650°C at 10°C/min to desorb ammonia. Most of the sample weight loss occurred below 550°C. The weight loss first derivative profile represents the HY acid strength distribution. Unfortunately, because thermogravimetric analysis provides only sample weight change information, this technique provides only the overall (combined Lewis and Brønsted) acid strength distribution. Furthermore, effects from water re-adsorption prior to or after ammonia exposure cannot be discerned by thermogravimetry. Bagnasco reported that water can replace ammonia bound to Lewis acid sites.[23] In fact, this can be used to distinguish Lewis and Brønsted acid sites by comparing thermogravimetry TPD results obtained with and without water vapor addition.

Ammonia interacts with Lewis and Brønsted acid sites differently, resulting in distinct and well separated infrared bands.[24-26] Figure 3-28a shows DRIFTS spectra measured in the 4000-800 cm⁻¹ range when HY and NaY zeolite samples were exposed to ammonia. Both zeolite samples were heated to 500°C in flowing helium to remove adsorbed water and then cooled to 100°C before they were exposed to ammonia. Figure 3-28b shows expansions of Figure 3-28a in the 3800-3100 and 1800-1300 cm⁻¹ ranges. In both figures, apparent IR absorbance (y-axis) is plotted against wavenumber (x-axis). Y-axes are not shown in these figures because the HY
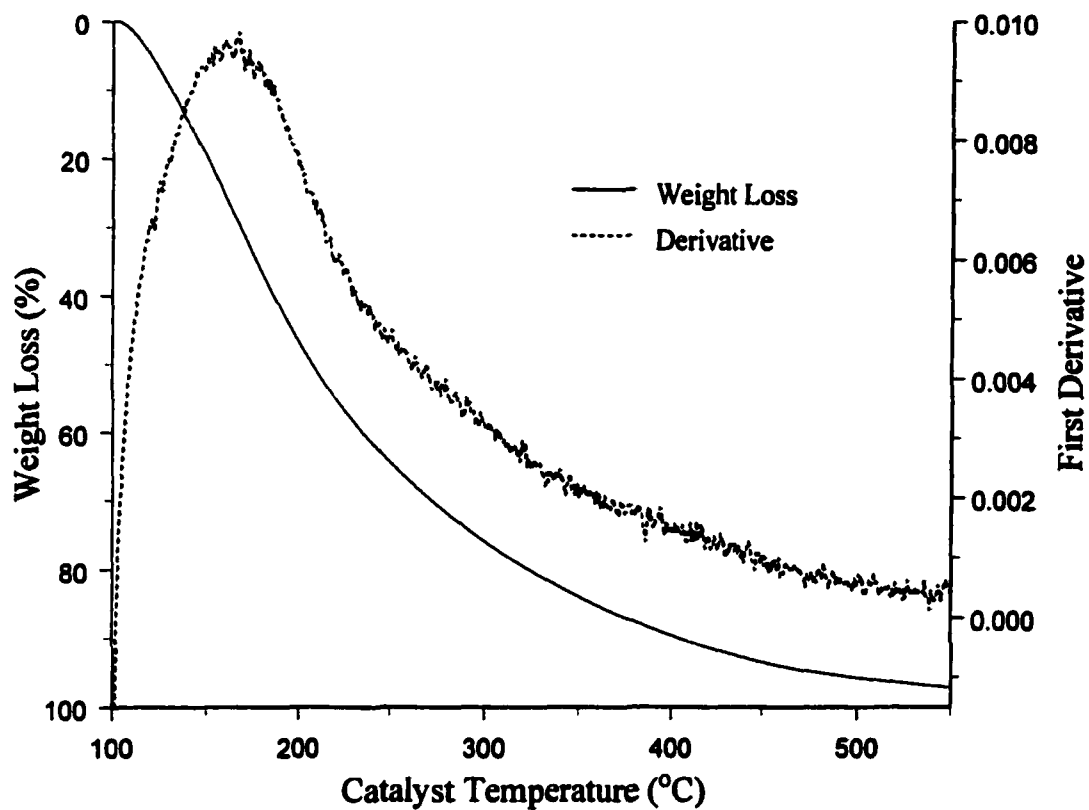
Figure 3-27 : HY Ammonia TPD Monitored by Thermogravimetry

a)

Apparent Absorbance

HY

NaY

4000   3000   2000   1000
Wavenumber (cm⁻¹)

b)

Apparent Absorbance

HY

NaY

3700 3500 3300 3100   1800 1700 1600 1500 1400 1300
Wavenumber (cm⁻¹)
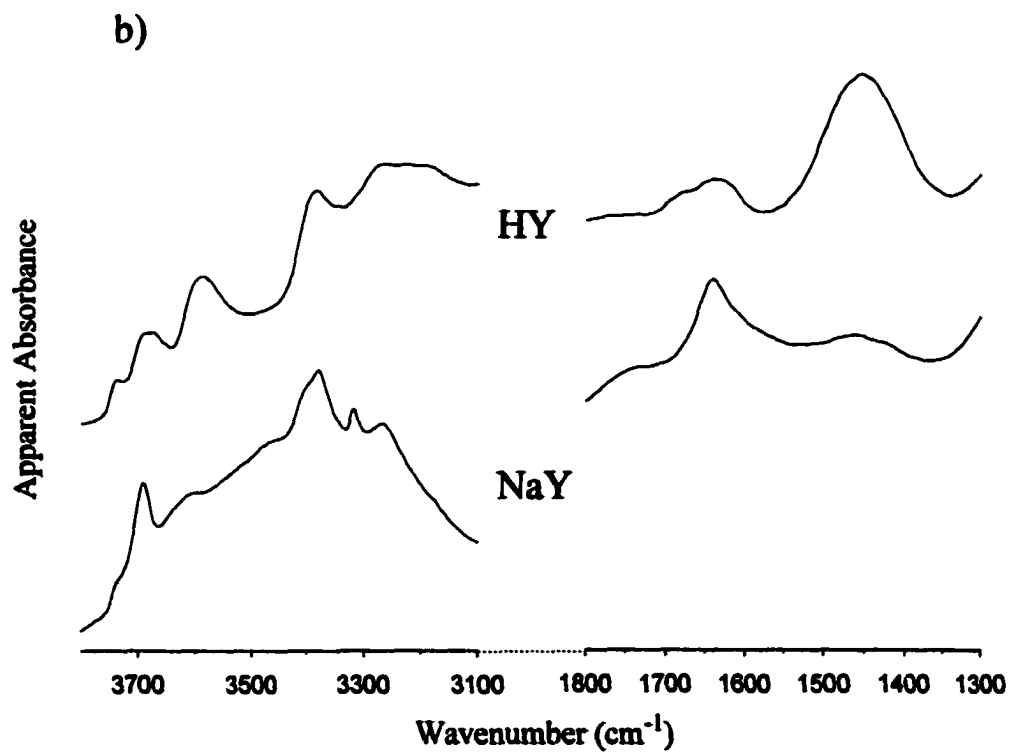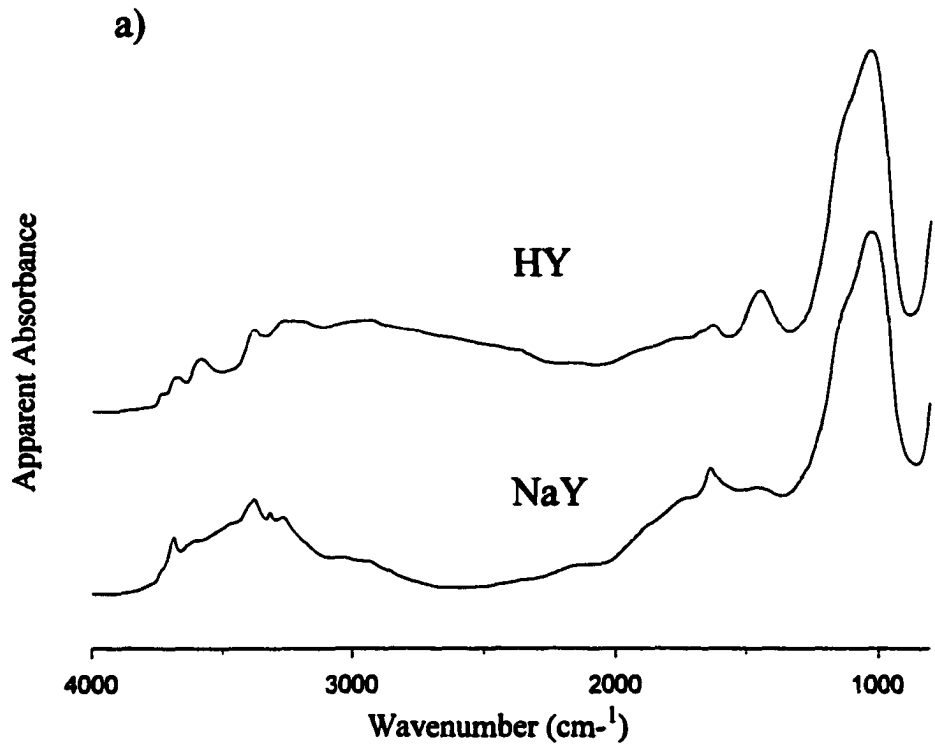
Figure 3-28 : Ammonia Adsorbed on HY and NaY

91

spectra were artificially offset to permit comparisons to the NaY spectra. Ammonia adsorbed on NaY Lewis acid sites yielded absorbance bands between 3400 and 3300 cm^{-1} due to N-H stretching vibrations and a band at 1640 cm^{-1} characteristic of ammonia bending vibrations. In contrast, ammonia adsorbed on HY Brønsted acid sites yielded broad N-H stretching vibration absorptions and a band at 1450 cm^{-1} assigned to the NH_4^+ bending vibration. The HY zeolite also showed weak absorbance at $1640cm^{-1}$ suggesting that the ion exchange was not complete and that some Lewis sites remained.

Figure 3-29 shows ammonia TPD from HY (a) Brønsted and (b) Lewis acid sites monitored by VT-DRIFTS. Ammonia was completely removed from the HY Lewis acid sites ($1640cm^{-1}$) by heating to 275°C, whereas ammonia adsorbed on HY Brønsted acid sites ($1450cm^{-1}$) did not desorb until the temperature reached 200°C and continued to desorb until 400°C. Clearly, interactions between ammonia and Brønsted acid sites were much stronger than interactions between ammonia and Lewis acid sites.

The microcatalytic reactor was used to generate ammonia TPD curves for different solid acid catalysts, namely HY, HZSM-5, MCM-41, silica alumina, and unpromoted and 1% Fe promoted sulfated zirconia. When available, TPD curves were compared with published results. The reproducibility of the ammonia TPD curves was also tested.

About 100mg of catalysts were calcined in-situ at 600°C (550°C for HZSM-5) in 25mL/min air for 2 hours. During calcination, the microreactor system oven was heated to 100°C to facilitate water removal from all transfer lines. After calcination, the catalyst sample was allowed to cool to 100°C and was then flushed with 25mL/min helium. Anhydrous ammonia from Airgas (Radnor, PA) was added either as a very low flow (2mL/min for a couple of minutes) or as a 10 psi pulse. In both cases, excess ammonia was added and catalyst samples were flushed with 25mL/min helium through the reactor purge line until ammonia could no
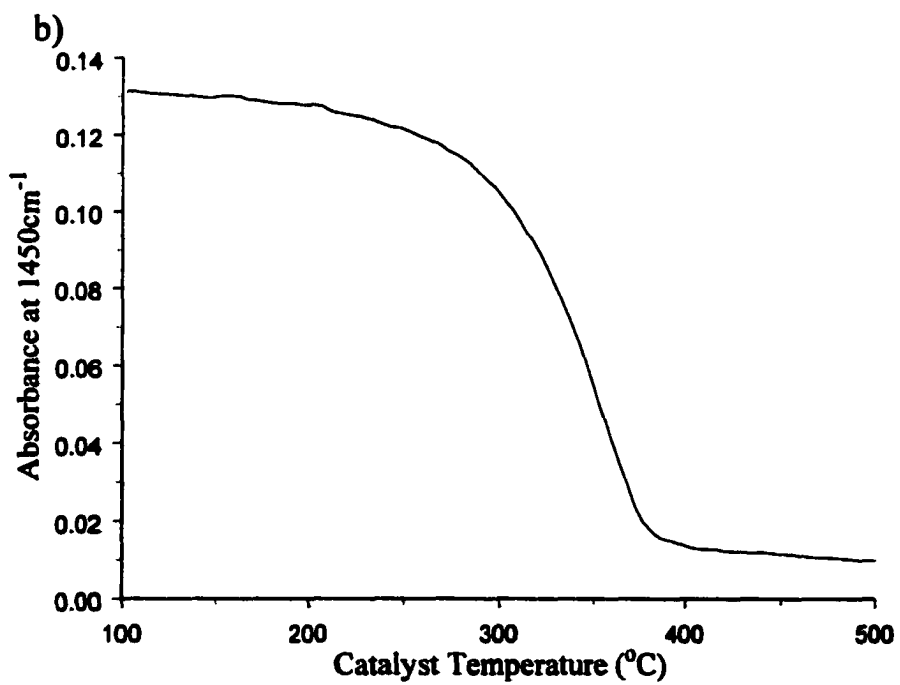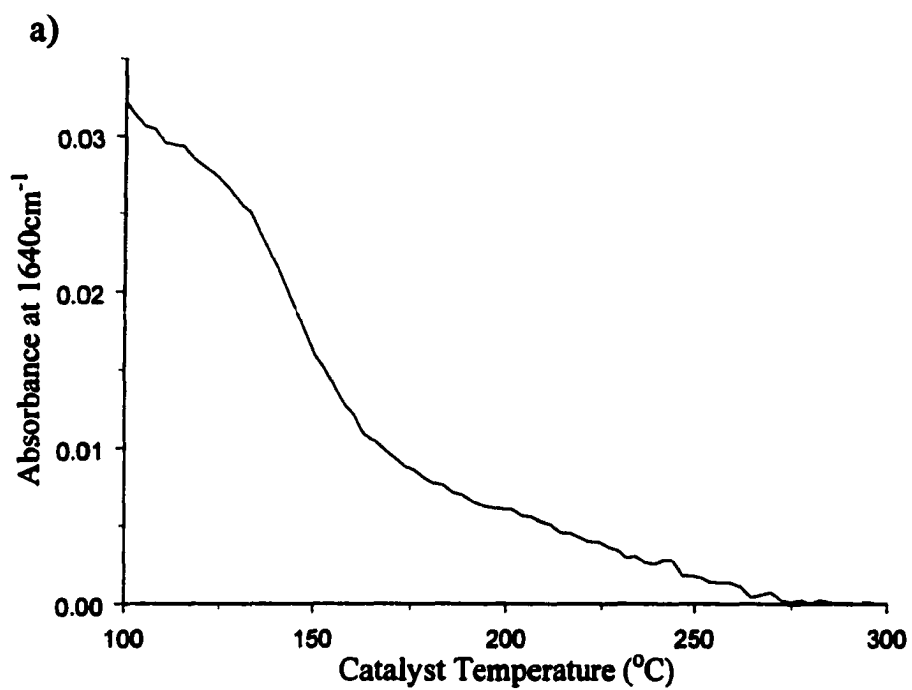
Figure 3-29 : HY Ammonia TPD from (a) Lewis and (b) Brønsted acid sites

longer be detected in the reactor effluent by the mass spectrometer. The mass spectrometer ion source pressure was adjusted depending on how much ammonia adsorbed onto each catalyst. Ion source pressures ranging from 1×10^{-6} to 2×10^{-5} Torr (for HY and silica alumina, respectively) were used for TPD experiments. Ammonia was desorbed by heating the reactor furnace from $100^\circ C$ to $700^\circ C$ at $10^\circ C/min$. The mass spectrometer was set to detect ions in the 12-150 m/z range. This wide range permitted detection of ammonia desorption as well as possible contaminants or catalyst decomposition. MS scans were signal averaged to record 2 to 3 spectra per minute. Figure 3-30a shows results from HY zeolite ammonia TPD. The x-axes denote catalyst temperatures and the y-axes represent the mass spectrometer signal, which was either total ion current (left axis) or selected ion current (right axis). The total ion current (solid line) and the ammonia molecular ion m/z 17 selected ion profile (dashed line) exhibited similar shapes, indicating that ammonia was the primary evolved product. However, the water molecular ion at m/z 18 (dotted line) also had significant intensity. This means that water also desorbed from the catalyst surface. Although dessicant traps were used on gas cylinders and the microreactor system oven was heated to $100^\circ C$ during TPD experiments, it was not possible to completely remove water. The water mass spectrum contains a signal at m/z 17 that is about one third of the intensity of the m/z 18 molecular ion. Consequently, the TPD ion signal at m/z 17 did not solely result from ammonia. The ammonia ion at m/z 14 (N^+) could be used to represent ammonia evolution without water interference. However, the m/z 14 ion signal is about 6 times smaller than m/z 17 in the ammonia mass spectrum. Instead, a signal representative of ammonia was obtained by subtracting the water contribution from the m/z 17 ion signal. This was done by subtracting one third of the m/z 18 ion signal from the measured m/z 17 ion signal:

$$\text{Ammonia Signal} = \text{Signal}_{m/z\ 17} - (1/3 \times \text{Signal}_{m/z\ 18}) \tag{9}$$
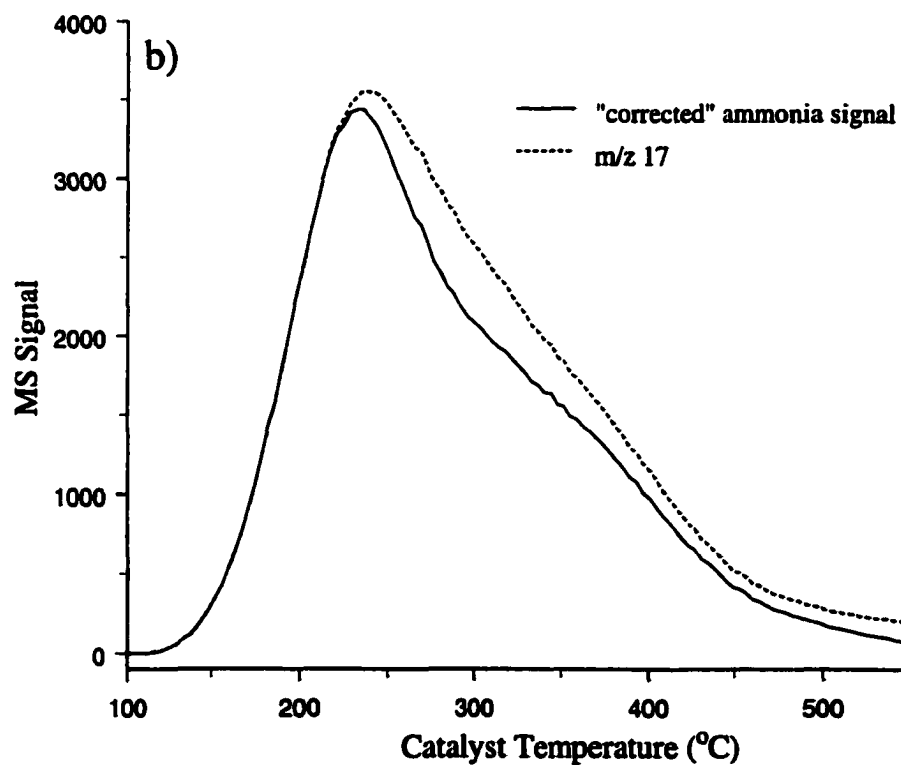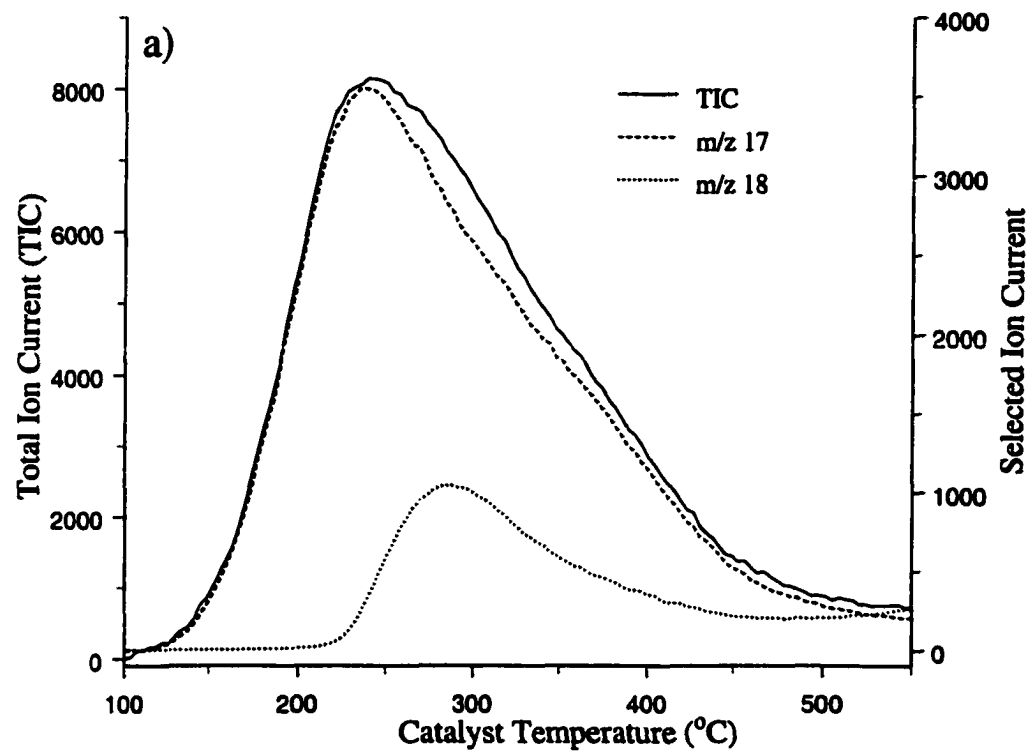
Figure 3-30 : HY Ammonia TPD Monitored by Microreactor

Figure 3-30b shows the HY acid strength distribution corrected for water desorption. The solid line in Figure 3-30b corresponds to the "ammonia signal" calculated by using equation 9. The dashed line in this figure represents the m/z 17 signal before correction. Ammonia temperature programmed desorption from HY resulted in a characteristic assymetric peak previously reported by Hidalgo and coworkers.[21] Ammonia started to desorb around 120°C and continued to desorb until 550°C. This temperature range is different from that determined by using VT-DRIFTS. In that study, the start of ammonia evolution occurred just above 100°C, the temperature at which ammonia adsorbed on Lewis acid sites began to desorb. VT-DRIFTS measurements showed that ammonia was completely removed from Brønsted acid sites at 400°C. The discrepancy between VT-DRIFTS and Reactor-MS results may be due to the higher sensitivity of the mass spectrometer compared to the FTIR. The FTIR may not be able to detect the last 9% of ammonia evolution (area of TPD profile above 400°C in Fig. 3-30b).

The reproducibility of ammonia TPD experiments was verified by repeating the measurement for each catalyst type. In order to compare ammonia TPD curves, MS signals were normalized so that TPD curves could be superimposed. The "Normalized MS Signal" was calculated by dividing the "Ammonia Signal" calculated by equation 10 by the maximum signal for each data set :

$$\text{Normalized MS Signal} = \frac{\left(\text{Ion}_{m/z17} - [\text{Ion}_{m/z18}/3]\right)}{\left(\text{Ion}_{m/z17} - [\text{Ion}_{m/z18}/3]\right)_{max}} \tag{10}$$

This calculation normalized the MS data to a 0-1 range. Figures 3-31 to 3-33 represent replicate ammonia TPD curves for HY, HZSM-5, MCM-41, silica-alumina, unpromoted and 1% Fe promoted sulfated zirconia catalysts. In these figures, the normalized MS signal corrected for water evolution is plotted against the catalyst temperature. For all six catalysts, ammonia TPD curves obtained for replicate samples were very similar. The two ammonia TPD curves obtained for HY shown in Figure 3-31a are almost completely superimposed. One of the curves is the same as that presented in Figure 3-30b. Of all six catalysts, HY adsorbed ammonia the most.

a)

b)
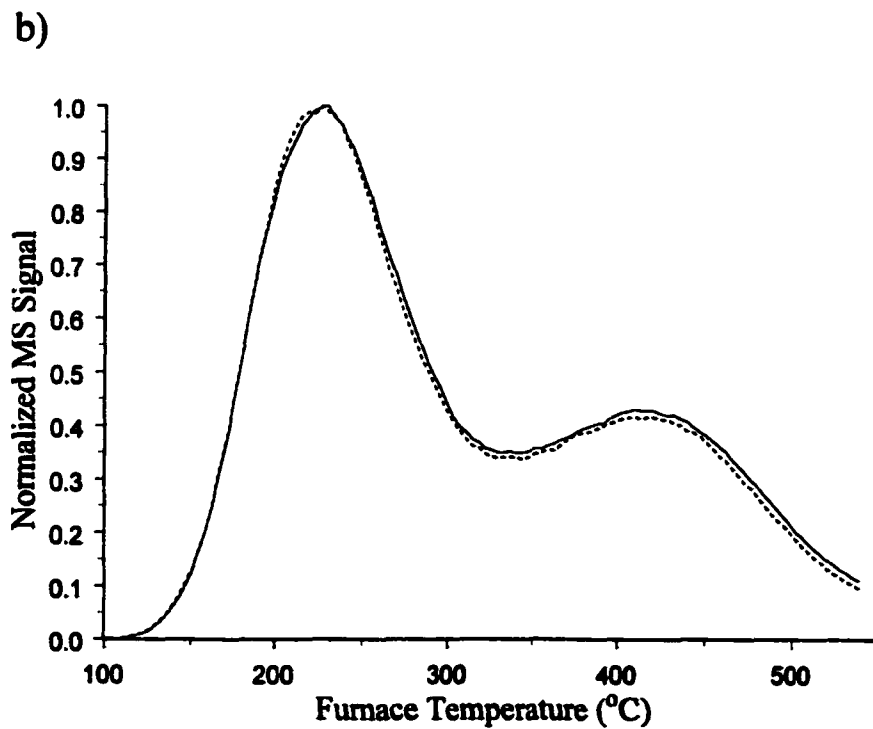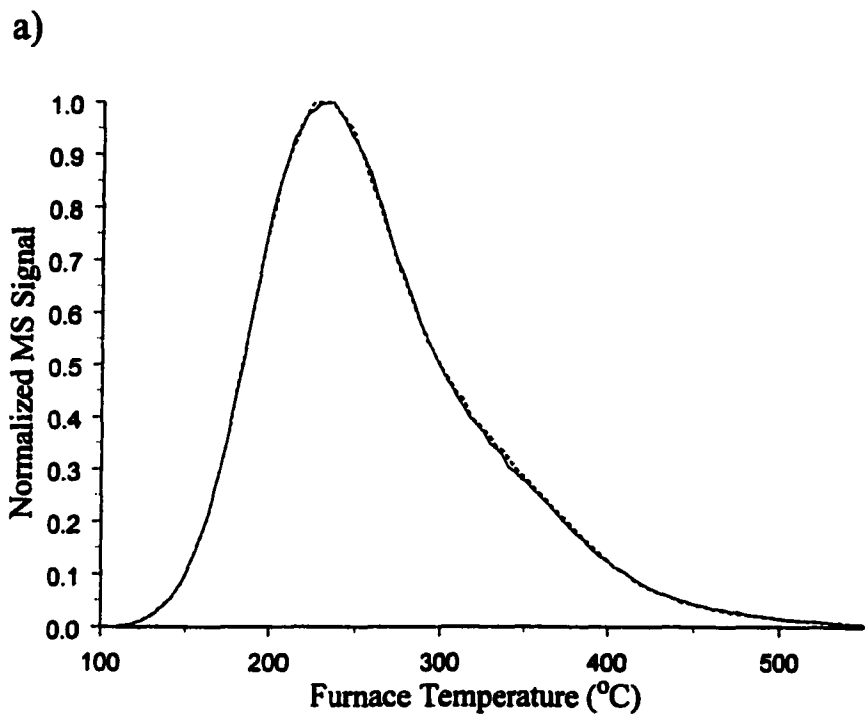
Figure 3-31 : NH$_3$ TPD from a) HY and b) HZSM5
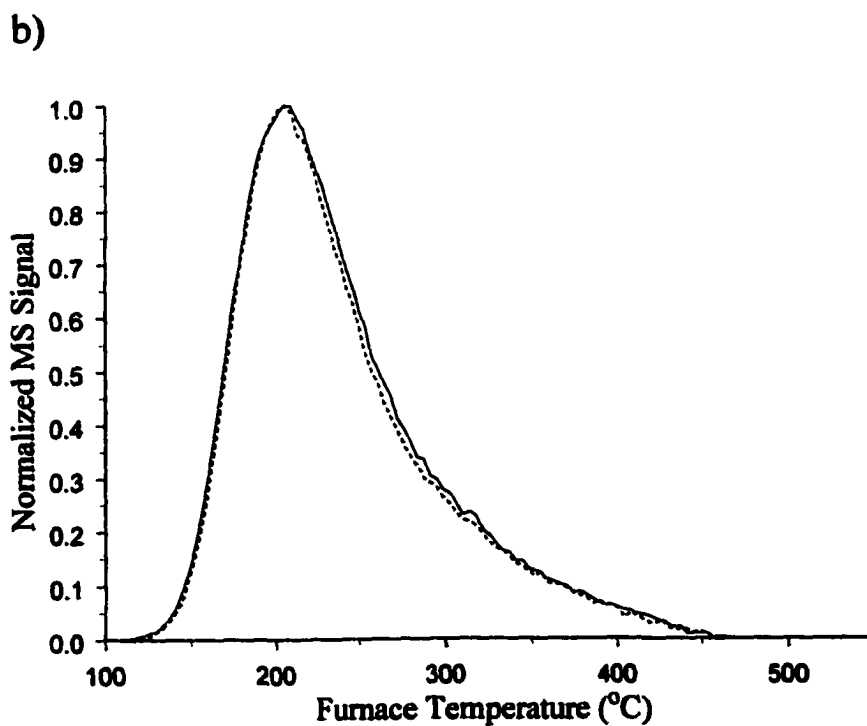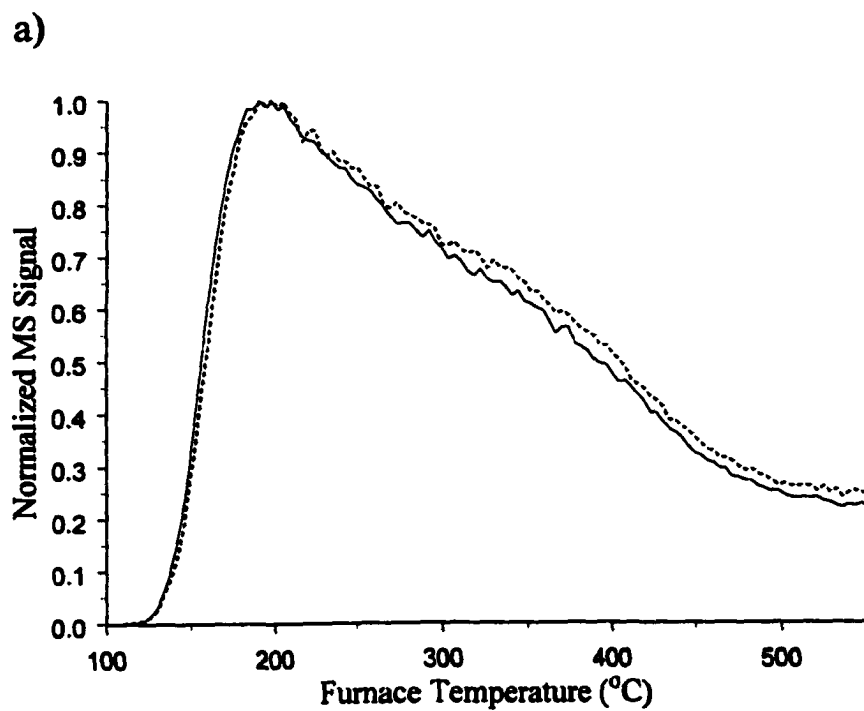
Figure 3-32 : NH$_3$ TPD from a) MCM41 and b) SiAl

a)

b)
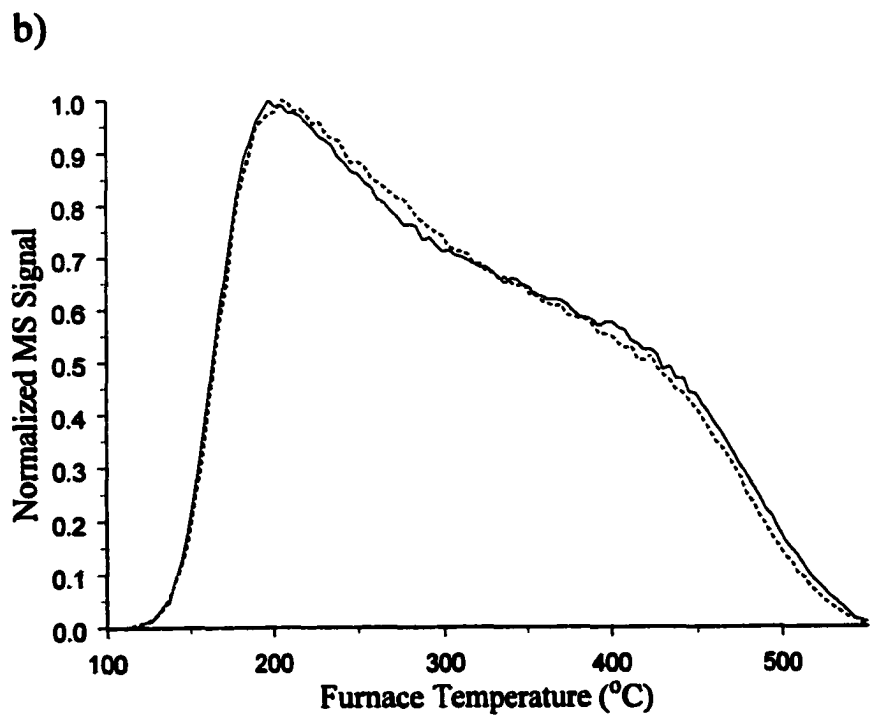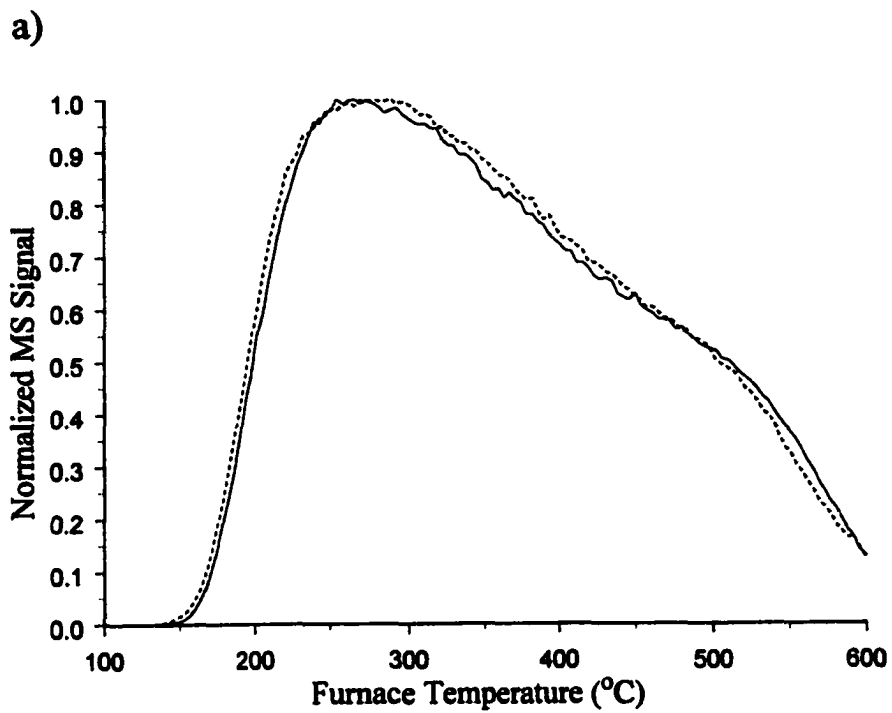
Figure 3-33 : NH$_3$ TPD from a) unpromoted and b) 1% Fe promoted Sulfated Zirconia

The ammonia TPD curves obtained for HZSM-5 (Fig. 3-31b) consisted of two characteristic peaks, as described in the literature.[14,23,27] The low temperature peak was attributed to desorption from Lewis acid sites based on the fact that ammonia liberated at these temperatures could be displaced by water, whereas ammonia responsible for the high temperature peak could not be displaced by water.[23] The low temperature peak maximized at 225°C, whereas the high temperature peak maximum occurred near 415°C. Ammonia desorption was nearly complete by 550°C.

Figure 3-32a shows ammonia TPD curves for MCM-41. They consist of a broad tailing peak that maximizes at about 200°C. Unlike the zeolites, ammonia desorption was not complete by 550°C. These results are consistent with previous studies of the acid properties of mesoporous MCM-41 using ammonia as a probe molecule that showed that MCM-41 has a broad acid strength distribution.[28-30]

Silica-alumina TPD curves (Fig. 3-32b) consisted of a sharp peak that maximized at about 205°C. Ammonia desorption was complete by 450°C, which is consistent with the low acidity reported for silica-alumina.[31-33]

Unpromoted and 1% Fe promoted sulfated zirconia ammonia TPD curves (Figs. 3-33a and 3-33b) are similar and consist of broad peaks. When iron was present, the curve shifted to lower temperature. In addition to ammonia desorption, mass spectrometric analysis indicated that sulfated zirconia catalysts decomposed. Ions at m/z 64 and m/z 32, characteristic of SO_2, were observed when the reactor furnace temperature reached 450°C for the 1% Fe promoted sulfated zirconia and 500°C for the unpromoted sulfated zirconia catalyst. SO_2 evolution maximized at 525°C and 600°C for the 1% Fe promoted and the unpromoted sulfated zirconia catalysts respectively. These results are consistent with previously published results.[34]

III.3 1-Butene Temperature Programmed Desorption

In the past, we used 1-butene TPD to characterize metal promoted sulfated zirconias.[35] Olefins react with Brønsted acid sites on inorganic oxide catalyst surfaces to form carbenium ions. Volatile species detected during TPD studies typically include oligomers and oligomer cracking products. As a result, a large range of products are evolved during 1-butene TPD experiments. We previously used 1-butene TPD to test the chromatographic separations capabilities of our repetitive injection gas chromatography-mass spectrometry apparatus.[36,37] Similar studies were conducted to assess the performance of the GC built for use with our microreactor system.

Sulfated zirconia has attracted considerable attention as a catalyst for skeletal isomerization of alkanes at low temperatures.[38] Oligomerization reactions such as those that have been proposed to form C_8 intermediates in the isomerization of n-butane involve reactions of carbenium ions.[39] We investigated the reactivities of carbenium ions on unpromoted sulfated zirconia catalyst by using reactor-GC/MS to analyze volatiles produced during TPD of surface species resulting from 1-butene adsorption. About 100mg of sulfated zirconia was calcined in situ at 600°C in 10mL/min air for 2 hours. During calcination, the microreactor system oven was heated to 100°C. The catalyst sample was then allowed to cool to 50°C. When the catalyst temperature reached 50°C, the air flow was replaced by 10mL/min helium. A pulse of 1-butene from Specialty Products & Equipment (Houston, TX) was introduced to the catalyst. This was accomplished by opening the 1-butene lecture bottle until the pressure gauge read 10psi and then immediately closing it. A 10mL/min helium flow was used to remove the excess 1-butene. When hydrocarbons could no longer be detected in the reactor effluent by the mass spectrometer, the microreactor oven was set to 60°C. At that point, the reactor-GC/MS splitter valve was opened so that the pressure in the mass spectrometer ion source reached 4.8×10^{-6} Torr. The sulfated zirconia catalyst was heated from 50 to 300°C at 2°C/min, while the

microreactor oven was heated from 60 to 200°C at 2°C/min and held at 200°C until the catalyst temperature ramp was completed. Volatile products evolved during the heating ramp where analyzed by GC/MS every 15°C from 70 to 280°C. The capillary column employed was a 10m x 25mm x 25μm AT™-1 from Alltech (Deefield, IL). A 2mL/min helium GC carrier gas flow was employed. The GC/MS interface was maintained at 200°C during the experiment. The catalyst temperature range was selected based on a separate thermogravimetry experiment, in which 1-butene oligomerization products were desorbed from 30mg of sulfated zirconia over the 50 to 400°C temperature range. Figure 3-34a shows the results from the thermogravimetry and microreactor-GC/MS experiments. The x-axis in Figure 3-34a represents the catalyst temperature. The tick marks on this axis denote the GC/MS injections. The right y-axis denotes the percent weight loss for adsorbed hydrocarbons. The left y-axis represents the mass spectrometer total ion current for the 15-200 mass range. The dotted line in Figure 3-34a is the thermogravimetry percent weight loss. It clearly indicates that most of the weight loss (>90%) occurred below 300°C. The solid line represents GC/MS total ion current chromatograms measured when reactor effluent was injected into the mass spectrometer. The GC/MS total ion current represents 15 successive capillary gas chromatograms obtained over the 70-280°C catalyst temperature range. The numerous peaks in the reactor-GC/MS chromatograms suggest that 50°C was sufficient for 1-butene oligomerization on sulfated zirconia catalyst. Figure 3-34b shows the gas chromatogram obtained by injecting reactor effluent into the gas chromatographic column when the catalyst temperature reached 175°C. The mass spectrometer total ion current (left y-axis) and the GC oven temperature (right y-axis) are plotted against the retention time (x-axis). The dotted line in Figure 3-34b represents the gas chromatographic oven temperature program employed to separate volatile products. Subambient temperatures were required at the beginning of the temperature program to separate low boiling point hydrocarbons such as

a)

b)
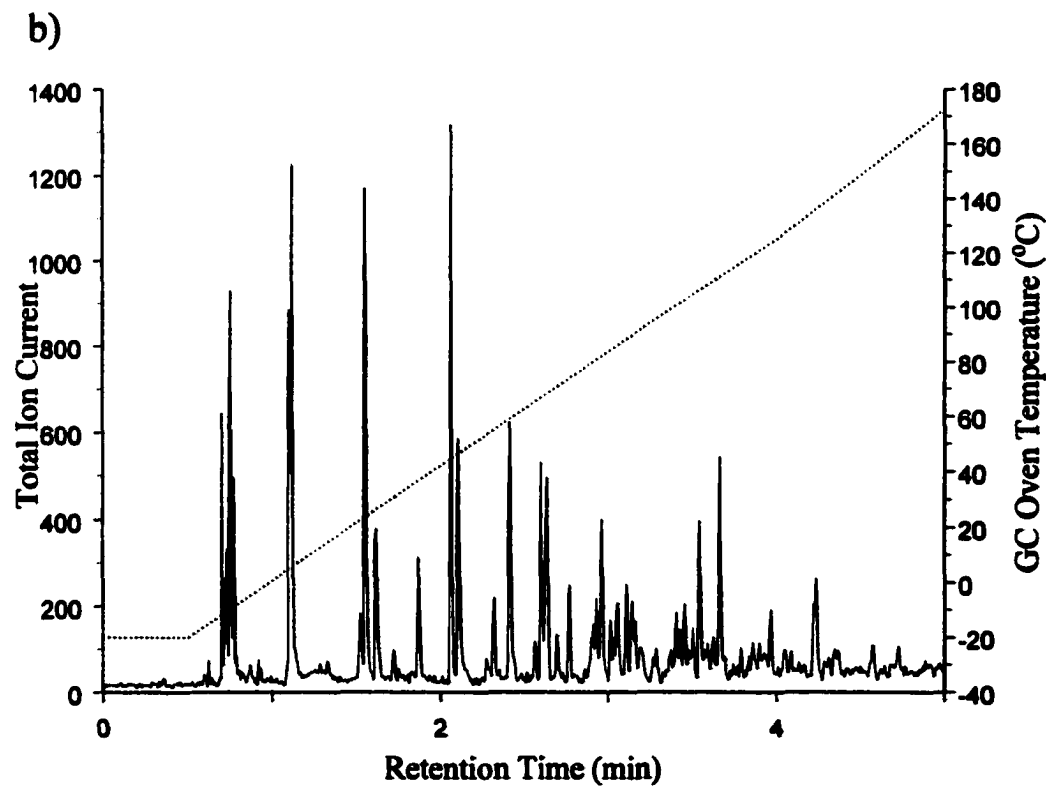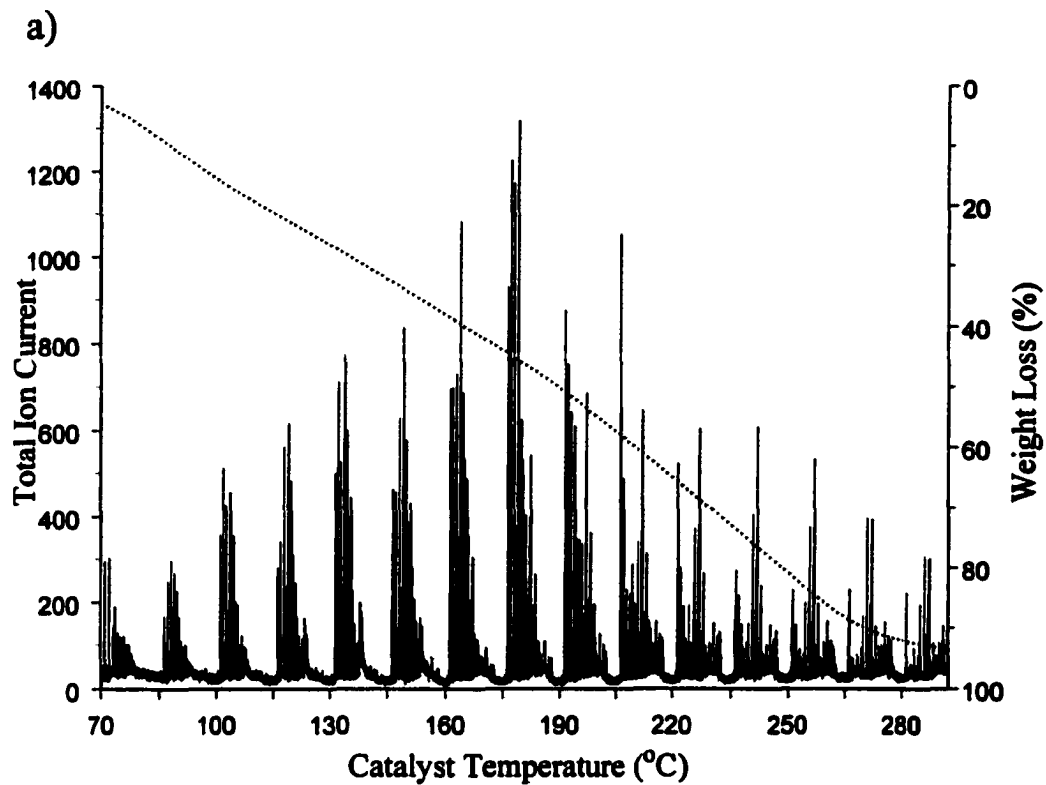
Figure 3-34 : Butene Oligomerization Products Desorption from Sulfated Zirconia

propene and butenes. After a 30 second isothermal period at -20°C, the GC temperature was increased to 125°C at a rate of 40°C/min and then to 220°C at a rate of 50°C/min. The gas chromatograph temperature program required about 6 minutes. Cooling the GC oven back to -20°C required approximately 30 seconds. By allowing one minute equilibration at -20°C before the next injection, chromatograms were obtained at 7.5 minute intervals, which corresponded to 15°C catalyst temperature intervals. The chromatogram (solid line) in Figure 3-34b contains more than 50 eluent peaks, many of which are baseline resolved. Mass spectra obtained during reactor-GC/MS analyses confirmed that most evolved products were hydrocarbons in the C_3-C_{10} range. Although the majority of the volatile products were saturated hydrocarbon isomers, unsaturated species and aromatics were also detected. The volatile products detected during reactor-GC/MS analysis of the sulfated zirconia catalyst containing adsorbed 1-butene are consistent with the following reaction scheme:[35]

$$C_4H_8 + HS \longleftrightarrow C_4H_9^+ + S^-$$

$$\uparrow\downarrow C_4H_8$$

$$C_8H_{16} + HS \longleftarrow C_8H_{17}^+ + S^- \xrightarrow{C_4H_8} \text{higher oligomers}$$

β-scission   rearr   H⁻

$$R_2(\text{unsat'd}) + R_1^+ + S^- \xleftarrow{\text{β-scission}} C_8H_{17}^+ + S^- \xrightarrow{H^-} C_8H_{18} + S^-$$

H⁻

$$R_1(\text{unsat'd}) + HS \qquad R_1(\text{sat'd}) + S^- \qquad C_8H_{16} + HS$$
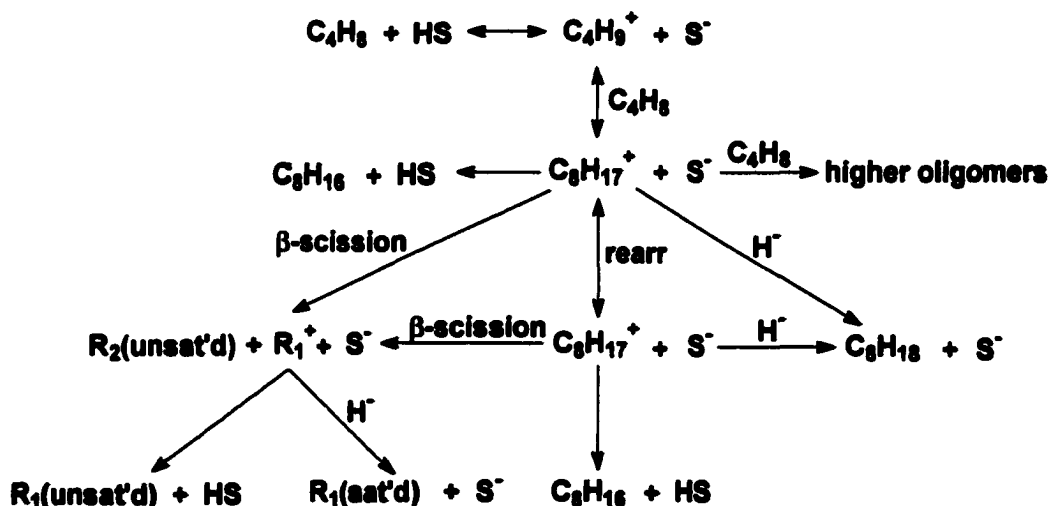
In this reaction scheme, C_4H_8 represents butene and HS denotes a Brønsted acid site on the catalyst surface. Butenes detected by reactor-GC/MS analysis may have resulted from deprotonation of $C_4H_9^+$ species when the thermal energy due to sample heating exceeded the interaction energy between the carbenium ion and the catalyst surface. Reactions of 1-butene with $C_4H_9^+$ carbenium ions to form $C_8H_{17}^+$ must have occurred to form the volatile products that

were larger than C_4. Initially formed $C_8H_{17}^+$ carbenium ions may rearrange, react with 1-butene to form larger carbenium ions, or may be converted to volatile products by : deprotonation to regenerate HS Brønsted acid sites and form C_8H_{16} species, hydride abstraction from neighboring adsorbates to form C_8H_{18} species, or β-scission to produce unsaturated products and smaller carbenium ions. Small carbenium ions may desorb as olefins or abstract hydrides and desorb as saturated hydrocarbons. Many of the hydrocarbons detected by reactor-GC/MS likely resulted from β-scission of large oligomeric carbenium ions. Apparently, most unsaturated β-scission products were too large to be volatile at the temperature at which scission occurred. The small carbenium ions formed by these scissions subsequently reacted by hydride abstraction to form saturated hydrocarbon products.

The large number of eluent peaks in Figure 3-34a illustrates the magnitude of the repetitive injection GC/MS data reduction problem. The data for this typical repetitive injection experiment consisted of 17,558 mass spectra and 15 chromatograms. The first step in creating species-specific evolution profiles from repetitive injection GC/MS data is to identify the substances responsible for selected chromatographic peaks. This is usually accomplished by comparing retention times and mass spectra of known materials with those associated with unknown chromatographic eluents. After the substance responsible for a chromatographic peak is identified, information regarding the concentration of this species in the reactor effluent can be obtained by computing the total ion current (TIC) chromatographic peak area. To generate species-specific evolution temperature profiles, chromatographic peaks representing the same substance in successive reactor-GC/MS gas chromatograms must be integrated. A profile is generated by plotting TIC peak areas for a particular substance against the sample temperatures at which the chromatographic injections were made. Commercially available GC/MS software is designed for manipulating single chromatograms. Therefore, each species-specific reactor-

GC/MS peak must be located and integrated manually when these data reduction tools are employed. Consequently, the task of generating species-specific evolution profiles using commercially available GC/MS data reduction software can be very time consuming. To simplify reactor-GC/MS data reduction procedures, a filtering algorithm that compares structure-specific mass spectral patterns to determine which chromatographic peaks represent selected eluents was employed.

The chromatogram peak extraction algorithm compares all reactor-GC/MS mass spectra with a target mass spectrum and extracts chromatogram segments from the data set when the mass spectra match the target spectrum. After isolating the chromatogram peaks representing a selected eluent, their areas are computed and plotted as a function of the sample temperature at the time of the chromatographic injection. The mass spectrum filter employs a spectral comparison method that has been used for library searching [40] and is supplied with many MS data systems. In this method, mass spectra are represented as multidimensional vectors. Vector dimensionality is determined by the number of ions scanned to obtain the spectrum (i.e. the mass range). The orientation of a mass spectral vector in multidimensional space is determined by relative ion signal abundances and is therefore dependent on the structure of the substance that produced the mass spectrum. Angles between vectors derived from reactor-GC/MS mass spectra and a target mass spectrum are obtained by computing vector dot products. Small angles are obtained when mass spectra are very similar, whereas large angles result when poor matches are obtained. An operator-specified threshold angle is employed to determine which chromatogram segments are extracted from the original set. With the appropriate choice of threshold angle value, the chromatogram peaks derived from mass spectra that closely resemble the target mass spectrum are selected from the reactor-GC/MS data set.

106

Figure 3-35 shows how a species-specific temperature profile was generated from the entire data set in Figure 3-34a by using the mass spectrum filtering algorithm. Figure 3-35a shows the gas chromatogram obtained by injecting reactor effluent when the catalyst temperature reached 175°C. The mass spectrum corresponding to the maximum of a chromatographic peak marked with an asterisk in Figure 3-35a was selected as the target mass spectrum and is shown in Figure 3-35b. Library search indicated that this mass spectrum corresponded to that of 2-methylbutane. Figure 3-35c shows the chromatographic peaks that were extracted from the entire data set, Figure 3-34a, by using the mass spectrum filtering algorithm and the 2-methylbutane target mass spectrum. Chromatogram peaks are plotted against the injection temperature. With appropriate choice of a vector angle threshold value, these peaks could be attributed solely to 2-methylbutane elutions. The 2-methylbutane species-specific evolution temperature profile, shown in Figure 3-35d, was obtained by plotting the integrated peak areas of the chromatographic peaks extracted by the filtering algorithm (Figure 3-35c) against the injection temperature.

Species-specific temperature profiles can be generated for each chromatographic eluent by repeating the process described for the 2-methylbutane. Figure 3-36 shows another example of species-specific profile generation. A different chromatographic peak (marked with an asterisk in Figure 3-36a) was selected from the gas chromatogram obtained by injecting reactor effluent when the catalyst temperature reached 175°C. The corresponding mass spectrum is shown in Figure 3-36b. Library search provided no match for this mass spectrum. However, the ion at m/z 134 and the presence of an ion at m/z 91 (tropylium ion) suggested that the target mass spectrum corresponded to a C_4-benzene. Although a single mass spectrum was selected as the target, more than one chromatogram peak was extracted from some chromatograms (Figure 3-36c). Because mass spectra representing the C_4-beneze isomers are virtually indistinguishable,
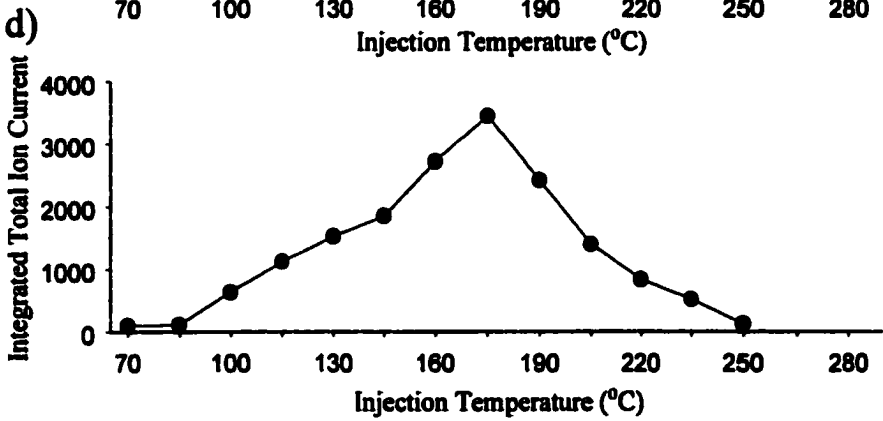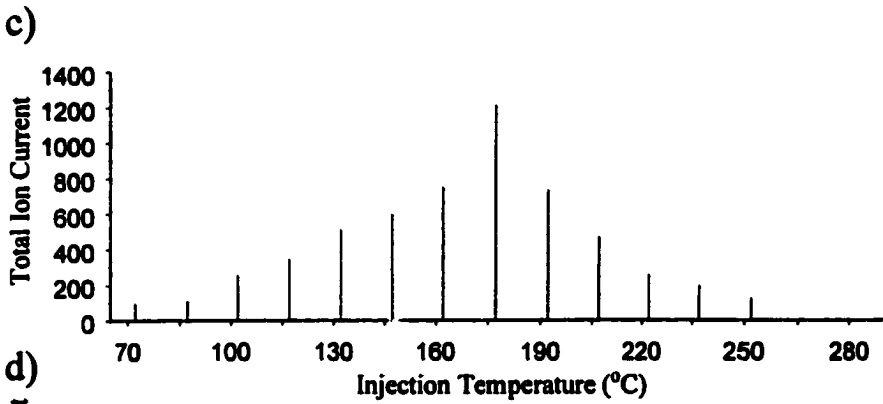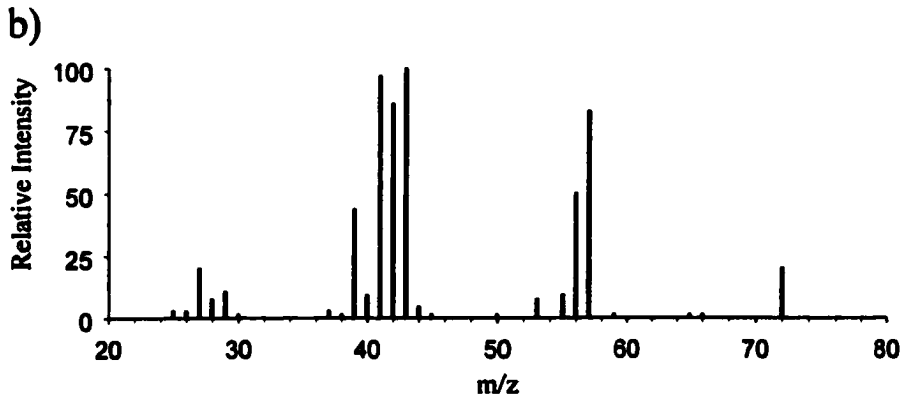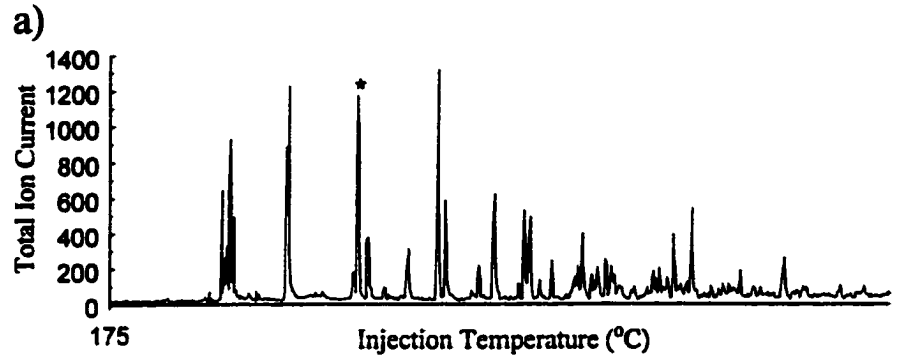
Figure 3-35 : 2-Methylbutane Evolution Profile Extraction

108
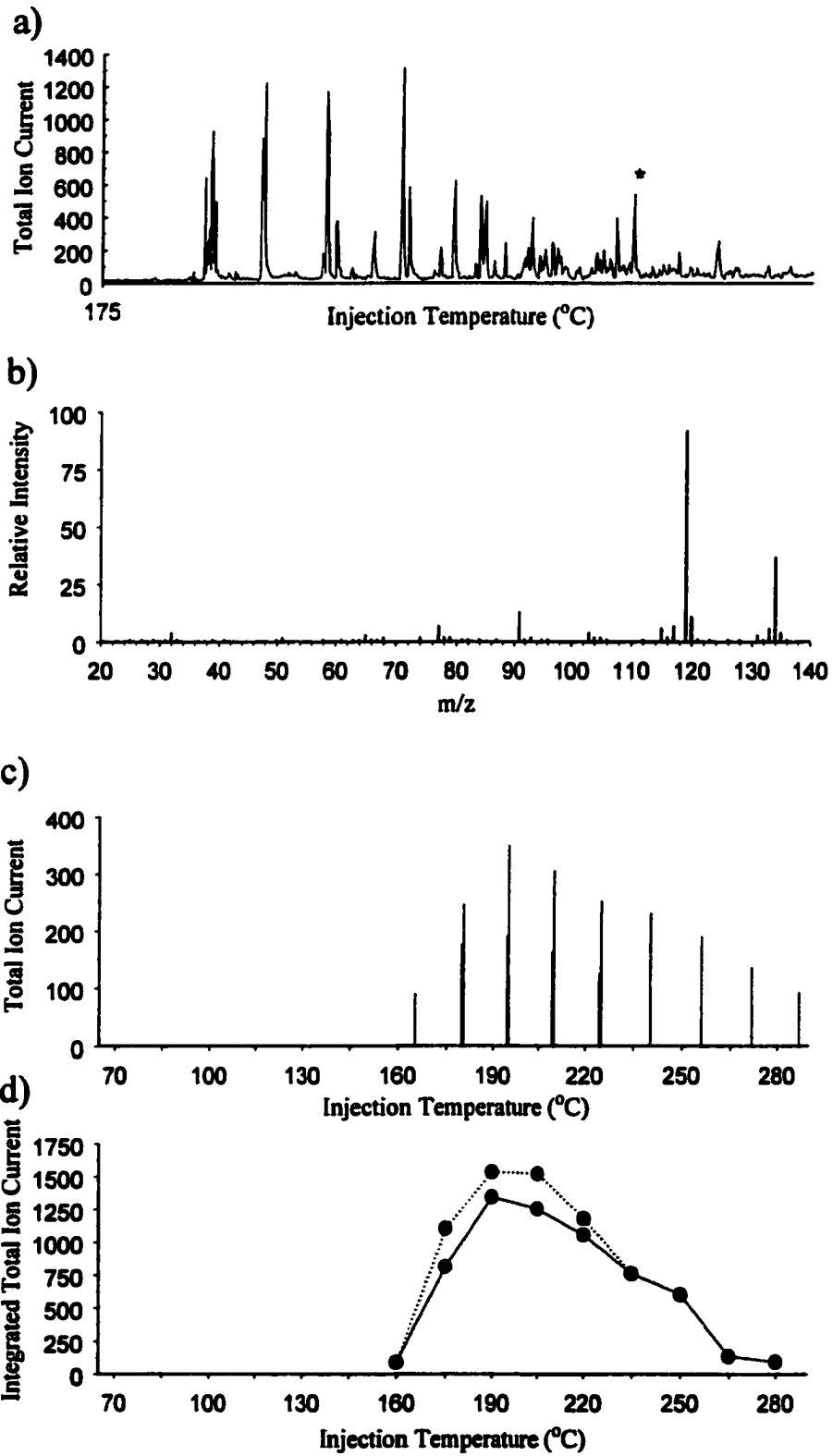
Figure 3-36 : C4-Benzene Evolution Profile Extraction

109

it was not possible to restrict mass spectrum filtering to a single component. The peaks corresponding to each C_4-benzene isomer were manually separated based on their retention times in each chromatogram. Then, the evolution temperature profile representing a selected C_4-benzene isomer was be obtained (solid line in Figure 3-36d). Alternatively, the peak area of both C_4-benzene isomers can be added to generate a C_4-benzene specific temperature profile (dotted line on Figure 3-36d).

Comparing figures 3-35d and 3-36d shows that evolution profiles may vary for different substances. 2-Methylbutane evolution occurred over catalyst temperatures in the 70-250°C range and maximized when the catalyst reached 175°C. In contrast, C_4-benzene evolution was not detected before the catalyst temperature reached 160°C. The C_4-benzene evolution maximized between 190 and 205°C and continued until the reactor effluent was no longer monitored (last injection at 280°C). Products that exhibit similar evolution temperature profiles may be formed by the same pathway, whereas different evolution temperature profiles often denote products that are formed by different mechanisms. The difference in the 2-methylbutane and C_4-benzene temperature profiles clearly indicates that these products originated from different pathways. This was expected, because aromatic compounds likely originated from the decomposition of polyene segments that were formed at lower temperatures.

IV. n-BUTANE ISOMERIZATION

n-Butane isomerization by 1% Fe promoted sulfated zirconia was studied because this was the original application for which the reactor was built. Unlike the benchmark studies, these experiments were not expected to provide information regarding specific aspects of the apparatus. Instead, results were compared to previous catalytic reactor studies of the isomerization of n-butane to iso-butane conducted in Dr. Resasco's laboratory.[2]

A few years ago, Hsu and coworkers [41] were the first to report that sulfated zirconia promoted with Fe and Mn exhibited significantly higher activity for n-butane isomerization. Since then, sulfated zirconia has attracted considerable attention as a catalyst for alkane isomerization. A comprehensive review was subsequently published by Song and Sayari.[38] Although several theories have been proposed, the cause of the enhanced catalytic activity of metal promoted sulfated zirconia is still unknown. One explanation is that metal promoters increase the catalyst acidity. Most proposed mechanisms involve reactions of carbenium ions formed at sulfated zirconia acid sites. However, initial carbenium ion formation is a poorly understood process. Carbenium ions can be formed by abstraction of hydrides from n-butane by a strong Lewis acid site, A:

$$n\text{-}C_4H_{10} + A \longrightarrow C_4H_9^+ + HA^-$$

However, this requires an extremely strong Lewis acid site. Another hypothesis is that strong Brønsted acid sites, HS, can abstract hydrides from n-butane:

$$n\text{-}C_4H_{10} + SH \longrightarrow C_4H_9^+ S^- + H_2$$

However, hydrogen gas has not been detected. Alternatively, carbenium ions were thought to be generated by reaction of an olefin, which was present as an impurity in the feed or formed by thermal cracking, and a Brønsted acid site, HS:

$$n\text{-}C_4H_8 + HS \longrightarrow C_4H_9^+ + S^-$$

This proposal was not really convincing and more recently it was suggested that carbonium ions can be formed by reaction with a Brønsted acid site, HS:

$$n\text{-}C_4H_{10} + SH \longrightarrow \underset{\text{carbonium ion}}{C_4H_{11}^+ S^-} \longrightarrow \underset{\text{parrafin \ carbenium ion}}{C_iH_{2i+2} + C_{4\text{-}i}H_{2(4\text{-}i)} S^-}$$
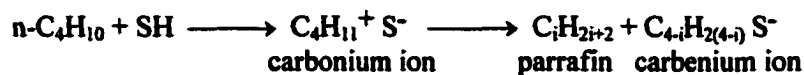
It is now widely believed that protolysis (dissociation of an intermediate carbonium ion into a paraffin and a carbenium ion) of the n-butane feed molecule by a strong Brønsted acid site is responsible for the initial formation of carbenium ions, such as $C_4H_9^+$. Then, intramolecular or intermolecular isomerization can take place:[38,42]

Intramolecular

$$C_4H_9^+ \longrightarrow \longrightarrow \underset{\text{Primary Carbenium Ion}}{} \longrightarrow \text{i-}C_4H_{10}$$

Intermolecular

$$C_4H_9^+ \longrightarrow \text{Butene} \longrightarrow C_8H_{17}^+ \rightleftharpoons$$

Secondary Carbenium Ion   Tertiary Carbenium Ion

$$\text{i-}C_4H_{10} \qquad \text{reacts with carbenium ion}$$
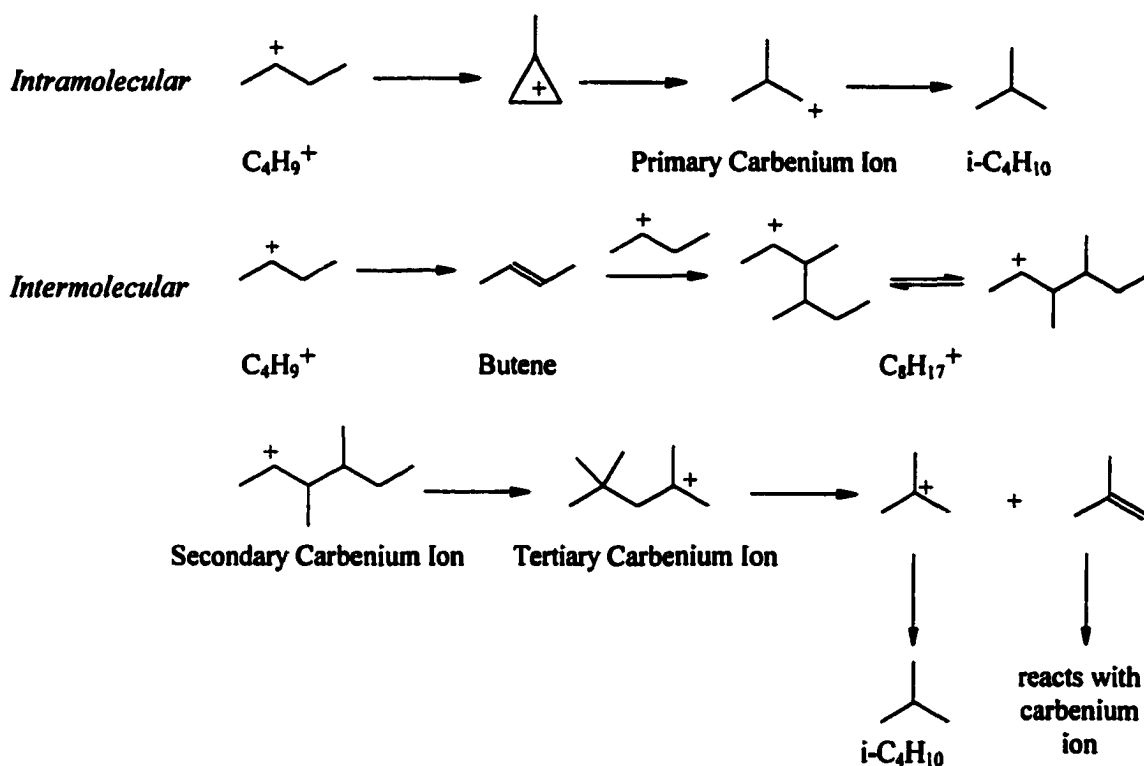
The intermolecular pathway, involving a C_8 intermediate, is energetically favored because it is expected to include secondary and tertiary carbenium ions which are more stable than the primary carbenium ions in the intramolecular model. However, the intermolecular pathway is based on the hypothesis that the butene formed reacts with the C_4 carbenium ion.[42]

112

In previous studies, metals (such as Cr, Fe, and Mn) were incorporated into sulfated zirconias and their promoting effects were evaluated for n-butane isomerization by using Dr. Resasco's catalytic reactor.[43,44] Catalytic activity measurements were made and deactivation rates were determined from plots of n-butane conversion against time on stream. n-Butane percent conversion was calculated by using equation (11) :

$$\text{n-Butane Percent Conversion} = \frac{\text{Area}_{i-butane}}{\text{Area}_{i-butane} + \text{Area}_{n-butane}} \times 100 \qquad (11)$$

Catalysts were calcined in-situ by heating them in dry air at 600°C for 2 hours. They were then cooled in air to 100°C, flushed with helium, and finally exposed to a mixture of 10mL/min n-butane and 20mL/min helium. Figure 3-37 shows results of n-butane isomerization by 1% metal (Fe, Cr, and Mn) promoted sulfated zirconia at 100°C. n-Butane conversion for each of the metal promoted sulfated zirconia samples increased to a maximum and then decreased with time on stream. The induction period was attributed to the formation and accumulation of intermediate species at the catalyst surface.[2] Fe promoted sulfated zirconia, represented by the solid line in Figure 3-37, exhibited the highest overall activity, and all catalysts had similar deactivation rates.

n-Butane isomerization studies were similar to n-hexane cracking in the sense that the hydrocarbon reactant flowed through a catalyst sample. However, the amount of n-butane (33% vol.) was much greater that of n-hexane (0.0026% vol. or 17 mg/L). Even after make up helium dilution, the high n-butane concentration resulted in a large pressure pulse (~100 fold) when the peak eluted into the mass spectrometer. As a result, the large sample loop (~80µL) could no longer be used. Instead, a 15µL sample loop was employed for n-butane isomerization studies.
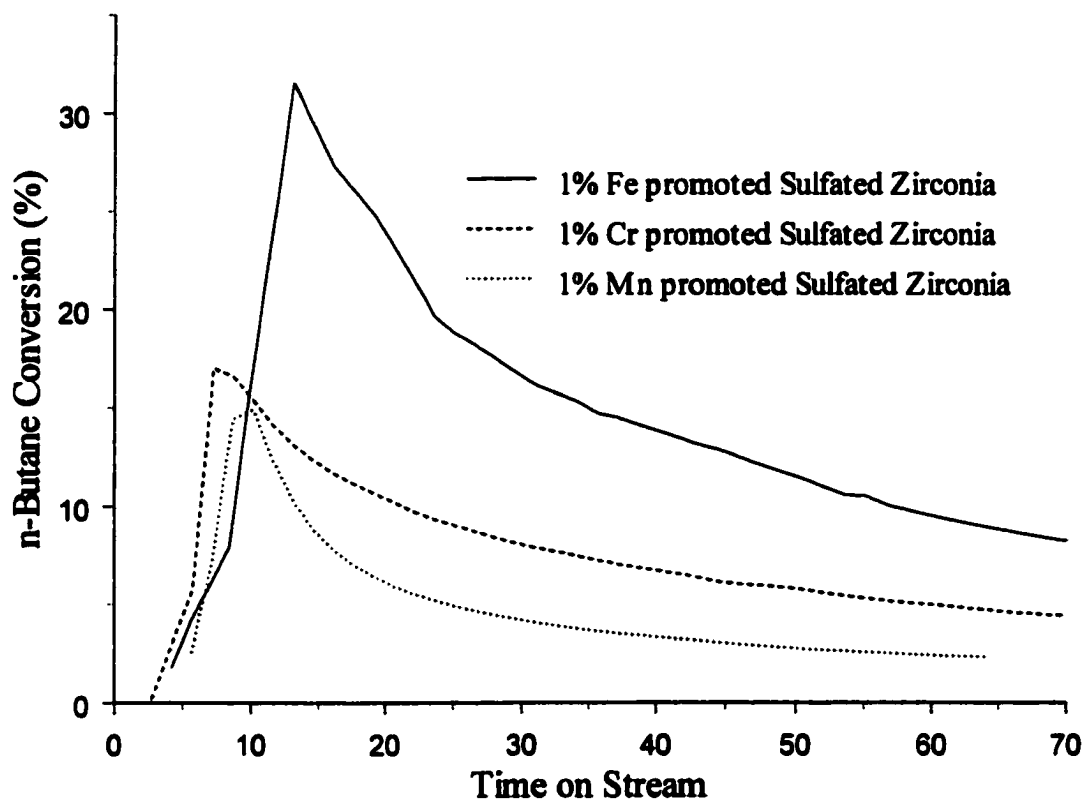
Figure 3-37 : Effects of Metal Promoters on n-Butane Isomerization by Sulfated Zirconia

Initial results from n-butane isomerization by 1% Fe promoted sulfated zirconia showed that automatic injections into the GC were not reproducible. Figure 3-38 shows successive chromatograms obtained while measuring n-butane concentrations in the "Bypass Mode" prior to reactor experiments. The y-axis denotes mass spectrometer total ion current (TIC). The variable peak heights are similar to those that were obtained in n-hexane cracking studies prior to adding the make up gas at the reactor exit (Fig. 3-8). Although the addition of make up gas allowed for reproducible n-hexane injections, the irreproducible n-butane injections likely resulted from pressure variations. The 15μL sample loop restricted gas flow and may have caused pressure variations when the automatic valve was rotated. One way to solve this problem would be to ensure that flow paths were identical regardless of the automatic valve position (Fig. 3-7). However, this could not be achieved with a 6-port valve, because the sample loop can only be part of one flow path. As a result, the 6-port gas switching valve was replaced with an 8-port gas switching valve that could accommodate two 15μL sample loops. Figure 3-39 shows the 8-port valve connections. The numbers on this figure correspond to those used for the current microreactor-GC/MS-FID design (Fig. 3-15) and current reactor flow diagram (Fig. 3-16). In position 1, port #12 was connected to the outlet (port #8) through sample loop 1. The GC carrier gas (port #9) was connected to the GC/MS column (port #10) through sample loop 2. In position 2, ports #12 and #8 were connected through sample loop 2 and the GC carrier gas (port #9) swept the reactor effluent trapped in sample loop 1 into the GC column (port #10). The only difference between the two valve positions was which sample loop was being loaded and which was being injected. It is however important to note that each 8-port valve rotation resulted in an injection while every other 6-port valve rotation produced an injection. Thus, the programmed time intervals at which the 8-port valve rotated had to be doubled to maintain the same injection time intervals.
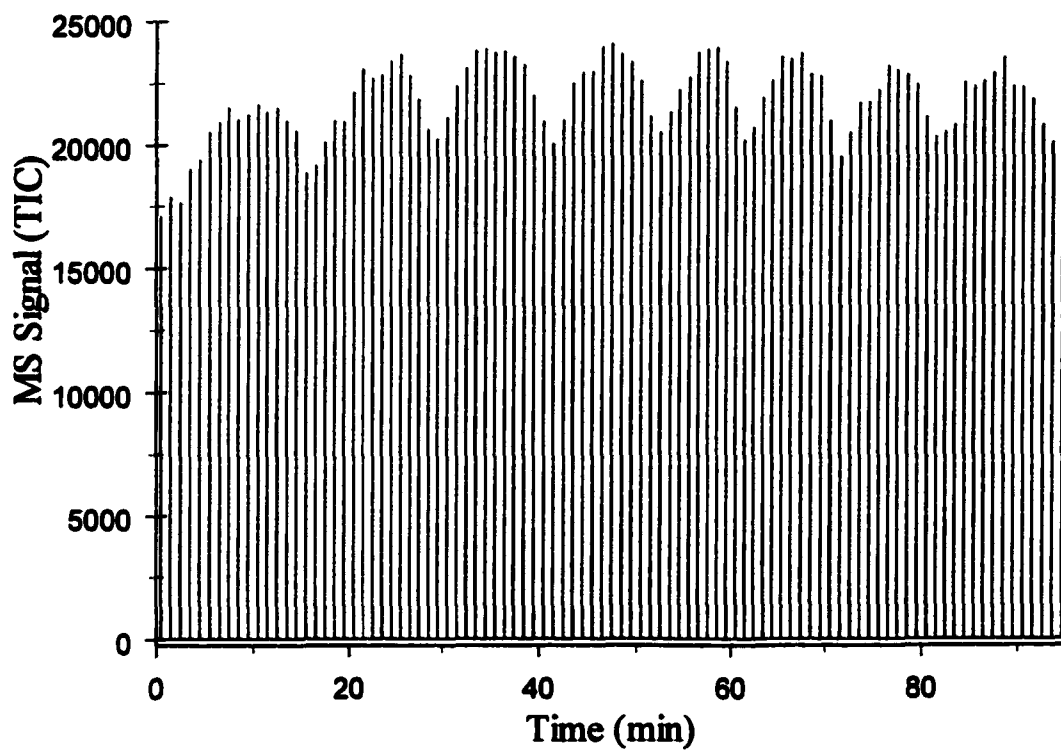
Figure 3-38 : Irreproducible GC Injections of n-Butane

POSITION 1

to Outlet
8

Sample Loop 1

Sample Loop 2

GC Carrier Gas 9 ————— 10 to GC/MS

Sample Loop 2

Sample Loop 1

12
from Manual Valve

POSITION 2

to Outlet
8

Sample Loop 1

Sample Loop 2

GC Carrier Gas 9 ————— 10 to GC/MS

Sample Loop 2

Sample Loop 1

12
from Manual Valve
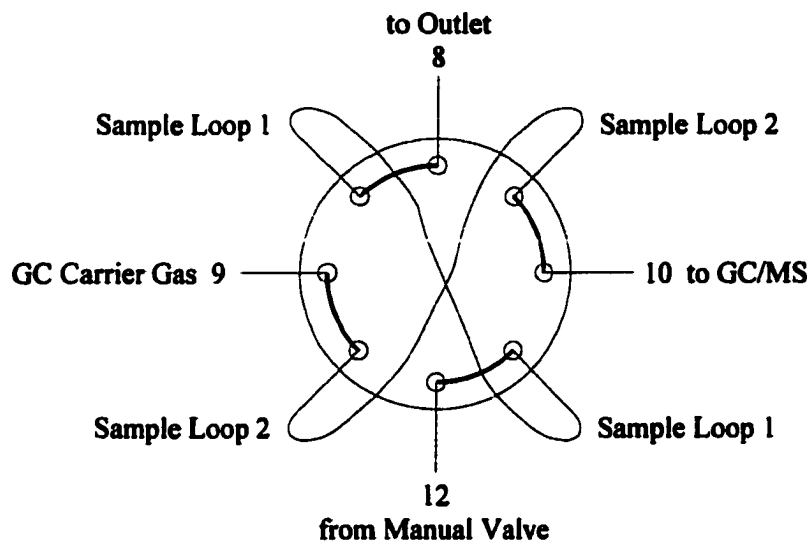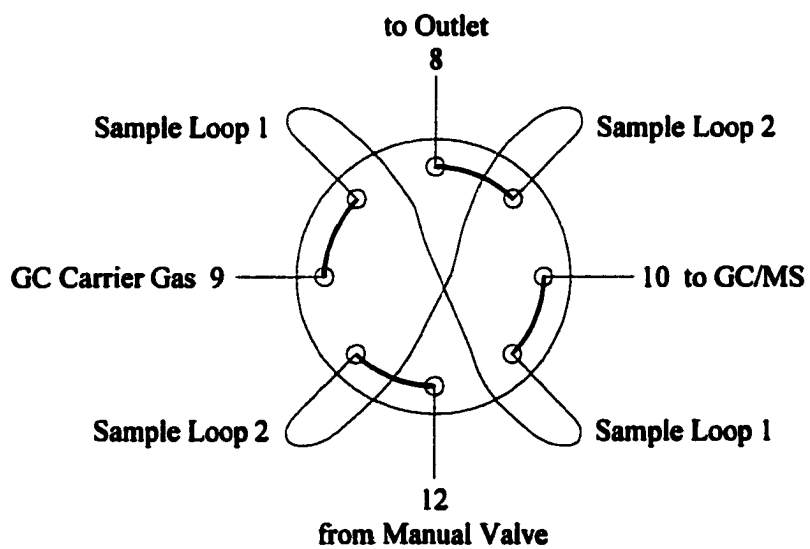
Figure 3-39 : 8-port Valve Positions

117

n-Butane isomerization by 1% Fe promoted sulfated zirconia was characterized by using our microreactor-GC/MS system. About 100mg of a freshly synthesized 1% Fe promoted sulfated zirconia was calcined in situ at 600°C in 20mL/min air for 2 hours. During calcination, the microreactor system oven was heated to 100°C. The catalyst sample was then allowed to cool to 100°C. When the catalyst temperature reached 100°C, the air flow was replaced by 20mL/min helium and 25mL/min make up helium was added at the microreactor exit. The manual valve was placed in the Bypass Mode and 10mL/min n-butane was added. The reactor-GC/MS splitter valve was then opened so that the pressure in the mass spectrometer ion source reached 2.8×10^{-7} Torr. GC/MS injections were used to determine when the n-butane partial pressure (chromatographic peak height) reached equilibrium. The catalyst was maintained at 100°C during isomerization measurements. The manual valve was switched to the Reactor Mode to admit n-butane to the catalyst (time on stream=0) and the automatic valve began to inject effluent into the GC/MS at one minute intervals. The GC oven temperature was maintained at -10°C for separations. A 10m × 25mm × 25µm AT™-1 capillary column from Alltech (Deefield, IL) was employed. A 2mL/min helium GC carrier gas flow was employed. The GC/MS interface was maintained at room temperature during studies. Figure 3-40 compares the results from this study and those from previous studies with Dr. Resasco's reactor. In this figure, the x-axes denote the time on stream in minutes but have different scales. The curve in Figure 3-40a is identical to the solid line in Figure 3-37 and represents the time dependence of n-butane isomerization by 1% Fe promoted sulfated zirconias motinored by using Dr. Resasco's reactor. As previously described, conversion increased to a maximum (about 32% after 13 minutes on stream) and then slowly decreased due to catalyst deactivation. After more than one hour on stream, n-butane conversion was still higher than 10%. Figure 3-40b shows the results obtained by using the microreactor-GC/MS system to monitor n-butane isomerization by a freshly prepared 1% Fe promoted sulfated zirconia catalyst. Maximum conversion was obtained for the
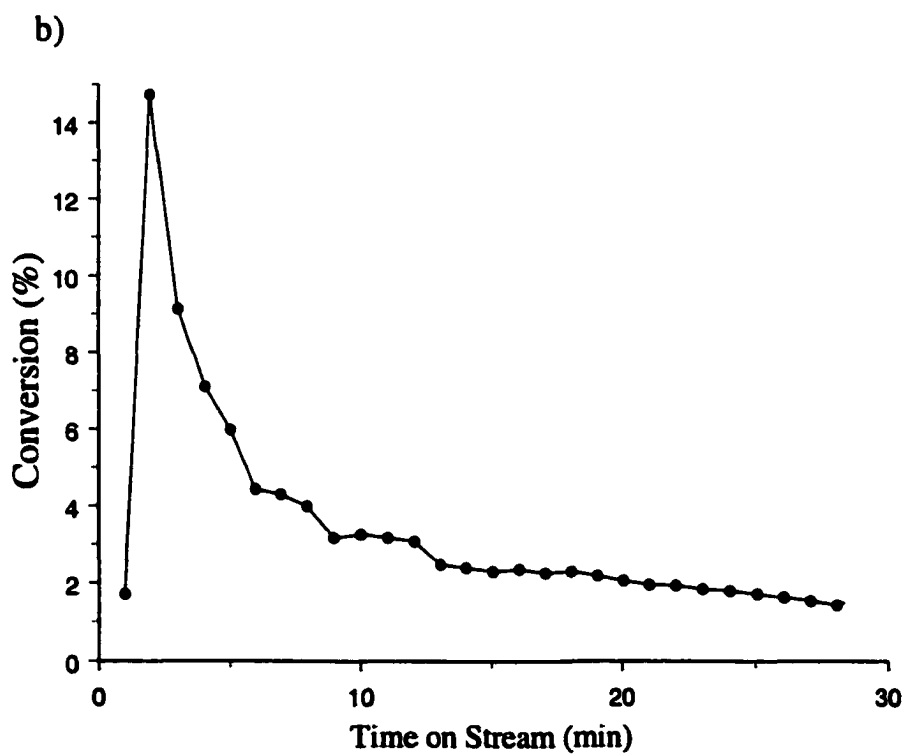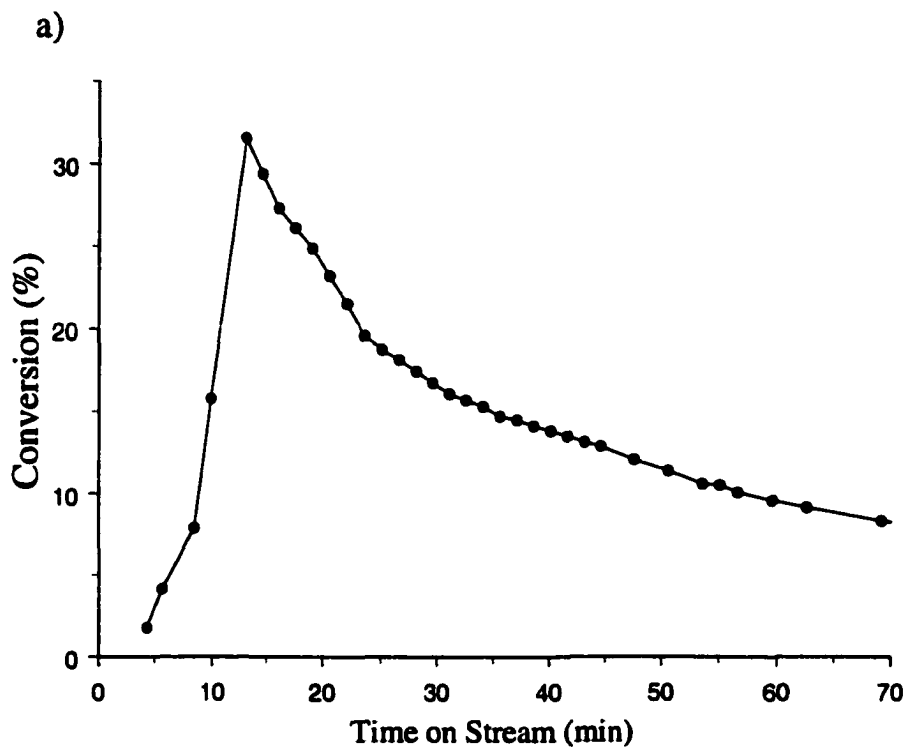
Figure 3-40 : n-Butane Isomerization Results from (a) Dr. Resasco's reactor
and (b) the new microreactor-GC/MS system

119

second injection (time on stream = 2 minutes) and no induction period was observed. n-Butane conversion did not exceed 15% and fast deactivation occurred (conversion dropped below 5% after 6 min on stream).

Catalytic activity and catalyst deactivation are known to be related and to depend on the n-butane partial pressure and catalyst temperature.[2] An increase in n-butane partial pressure or in temperature results in an increase in activity and a faster catalyst deactivation. This may explain why some authors report an induction period,[2,45] but others do not.[41] n-Butane isomerization experiments with the microreactor-GC/MS system were repeated with lower n-butane partial pressures and lower catalyst temperatures. However, results from these experiments were similar to those depicted in Figure 3-40b. Again, no induction period was observed and catalyst deactivation was very fast.

Differences in the Figure 3-40 curves may have resulted from different catalysts, different reactants (i.e. impurities in the reactant stream) or differences in the properties of the reactor system (e.g. increased pressure due to the smaller lines used in our microreactor system). To find out, it would have been useful to compare results with the same catalyst and reactant streams on both microreactor systems. However, this was not possible because the reactor in Dr. Resasco's laboratory was no longer available.

Although sulfated zirconia showed great promise for catalyzing the skeletal isomerization of alkanes, academic and industrial researchers were unable to avoid rapid catalyst deactivation. Consequently, this catalyst is no longer pursued and our research project was discontinued. As a result, minimal effort was made to find the cause of the discrepancy in the n-butane isomerization results.

V   CONCLUSION

A microreactor-GC/MS-FID system was developed in our laboratory. This system is very versatile and was used for isothermal catalytic activity determinations and temperature programmed catalyst characterization measurements. Its design made it easy to bypass the microreactor furnace or the gas chromatograph.

The microreactor-GC/MS-FID system was able to provide accurate activation energies for n-hexane cracking by HZSM-5. A very good correlation between the MS and FID data was also obtained, which indicates that MS information alone may be able to give both structural and quantitative information for most applications. Catalyst acid site distributions were characterized by ammonia temperature programmed desorption. Results from 1-butene oligomerization product desorption / decomposition showed the high performance of the GC built for this system.

The microreactor-GC/MS-FID system is now well characterized and will be used to study unknown catalytic systems.

VI REFERENCES

1. E.C. Sikabwe, Ph.D. dissertation, University of Oklahoma, 1997, "Investigations of the Effects of Iron, Manganese, and Nickel on the Properties of Sulfated Zirconia Catalysts"

2. M.A. Coelho, W.E. Alvarez, E.C. Sikabwe, R.L. White and D.E. Resasco, *Catal. Today*, 28 ` (1996) 415-429

    "Induction of activity and deactivation of Fe, Mn-promoted sulfated zirconia catalysts"

3. G.C. Bond, *Heterogeneous Catalysis - Principles and Applications*, Second Edition, Oxford Science Publications: London, England, 1987

4. M. Bowker, *The Basis and Applications of Heterogeneous Catalysis*, Oxford Chemistry Primers, Oxford Science Publications: London, England, 1998

5. D.A. Skoog, F.J. Holler, and T.A. Nieman, *Principles of Instrumental Analysis*, Fith Edition, Saunders College Publishing: 1998

6. P.B. Weisz and J.N. Miale, *J. Catal.*, 4 (1965) 527-529

    "Superactive Crystalline Aluminosilicate Hydrocarbon Catalyst"

7. J.N. Miale, N.Y. Chen, and P.B. Weisz, *J. Catal.*, 6 (1966) 278-287

    "Caralysis by Crystalline Aluminosilicates IV. Attainable Catalytic Cracking Rate Constants, and Superactivity"

8. M. Guisnet, F.X. Cormerais, Y.S. Chen, G. Perot, and E. Freund, *Zeolites*, 4 (1984) 108-109

    "Effect of Sodium Content on the Activity of ZSM-5 Zeolite"

9. D.S. Santilli, *Appl. Catal.*, 60 (1990) 137-141

    "Mechanism of Hexane Cracking in ZSM-5"

10. S.I. Ivanov and V.I. Timoshenko, *Kinet. Catal.*, 34 (1993) 447-450 translated from *Kinetika i Kataliz*, 34 (1993) 500-503

    "n-Hexane Cracking on a ZSM-5 Type Zeolite and Zeolite-Containing Catalyst Deactivated under Conditions of Steam Treatment"

11. D.B. Lukyanov, V.I. Shtral, and S.N. Khadzhiev, *J. Catal.*, 146 (1994) 87-92

"A Kinetic Model for the Hexane Cracking Reaction over H-ZSM-5"

12. S.M. Babitz, B.A. Williams, J.T. Miller, R.Q. Snurr, W.O. Haag, and H.H. Kung, *Appl. Catal. A*, **179** (1999) 71-86

"Monomolecular Cracking of n-Hexane on Y, MOR, and ZSM-5 Zeolites"

13. D.B. Luk'yanov, *Zeolites*, **11** (1991) 325-328

"The Role of Enhanced Activity Sites in Hexane Cracking over ZSM-5 Zeolites"

14. J.G. Post, J.H.C. van Hoof, *Zeolites*, **4** (1984) 9-14

"Acidity and Activity of H-ZSM-5 Measured with NH_3-TPD and n-Hexane cracking"

15. K.A. Cumming, and B.W. Wojciechowski, *Catal. Rev.-Sci. Eng.*, **38**, (1996) 101-157

"Hydrogen Transfer, Coke Formation, and Catalyst Decay and Their Role in the Chain Mechanism of Catalytic Cracking"

16. B.W. Wojciechowski, *Catal. Rev.-Sci. Eng.*, **40**, (1998) 209-328

"The Reaction mechanism of Catalytic Cracking: Quantifying Activity, Seletivity, and Catalyst Decay"

17. S. Kotrel, P.M. Rosynek, and J.H. Lunsford, *J. Phys. Chem. B*, **103**, (1999) 818-824

"Intrinsic Catalytic Cracking Activity of Hexane over H-ZSM-5, H-β and H-Y Zeoiltes"

18. B. Gielen and M.G. Palekar, *Zeolites*, **9** (1989) 208-216

"Some Observations on Coke Precursor on ZSM-5 during n-Hexane Cracking"

19. W.A. Groten, B.W. Wojciechowski, and B.K. Hunter, *J. Catal.*, **138**, (1992) 343-350

"On the Relationship between Coke Formation Chemistry and Catalyst Deactivation"

20. D.M. Bibby, N.B. Milestone, J.E. Patterson, and L.P. Aldridge, *J. Catal.*, **97** (1990) 493-502

"Coke Formation in Zeolite ZSM-5"

21. C.V. Hidalgo, H. Itoh, T. Hattori, M. Niwa, and Y. Murakami, *J. Catal.*, **85** (1984) 362-369

"Measurement of the Acidity of Various Zeolites by Temperature Programmed Desorption of Ammonia"

22. N. Katada, H. Igi, J.-H. Kim, M. Niwa, *J. Phys. Chem. B*, **101** (1997) 5969-5977

"Determination of the Acidic Properties of Zeolite by Theoretical Analysis of Temperature-Programed Desorption of Ammonia Based on Adsorption Equilibrium"

23. G. Bagnasco, *J. Catal.*, 159 (1996) 249-252

"Improving the Selectivity of NH₃ TPD Measurements"

24. E.A. Paukshtis and E.N. Yurchenko, *Russ. Chem. Rev. (Engl. Transl.)*, 52, (1983) 242-250

"Study of Acid-Base properties of Heterogenous Catalysts by Infrared Spectroscopy"

25. T. Barzetti, E. Selli, D. Moscotti, and L. Forni, *J. Chem. Soc., Faraday Trans.*, 92 (1996) 1401-1407

"Pyridine and Ammonia as Probes for FTIR Analysis of Solid Acid Catalysts"

26. J.A. Lercher, C. Gründling, and G. Eder-Mirth, *Catal. Today*, 27 (1996) 353-376

"Infrared Studies of the Surface Acidity of Oxides and Zeolites using Adsorbed Probe Molecule"

27. K. Chao, B.H. Chiou, C.C. Cho, and S.Y. Jeng, *Zeolites*, 4, (1984) 2-4

"Temperature Programmed Desorption on ZSM-5 Zeolites"

28. J. Weglarski, J. Datka, H. He, and J. Klinowski, *J. Chem. Soc., Faraday Trans.*, 92 (1996) 5161-5164

"IR spectroscopic studies of the acidic properties of the mesoporous molecular sieve MCM-41"

29. A. Liepold, K. Roos, W. Reschetilowski, A.P. Esculcas, J. Rocha, A. Philippou, and M.W. Anderson, *J. Chem. Soc., Faraday Trans.*, 92 (1996) 4623-4629

"Textural, structural and acid properties of a catalytically active mesoporous aluminosilicate MCM-41"

30. H. Kosslick, J. Landmesser, and R. Fricke, *J. Chem. Soc., Faraday Trans.*, 93 (1997) 1849-1854

"Acidity of substituted MCM-41-type mesoporous silicates probed by ammonia"

31. A.K. Bandopadhyay, J. Das, and S.K. Roy, *J. Catal.*, 124 (1990) 241-246

"Effect of quaternary ammonium compounds on the physicochemical properties of amorphous silica-alumina"

32. H.M. Ismail, S.A.A. Mansour, and M.I. Zaki, *Thermochim. Acta*, 202 (1992) 269-280

"Acidic Sites on Silica-Alumina Catalysts with Reduced Aluminum Content"

33. N. Cardona-Martinez, and J.A. Dumesic, *J. Catal.*, 128 (1991) 23-33

"Microcalorimetric measurements of basic molecule adsorption on silica and silica-alumina"

34. E.C. Sikabwe, M.A. Cohela, D.E. Resasco and R.L. White, *Catal. Lett.*, **34**, (1995) 23-30

"Catalyst Decomposition during Temperature Programmed Desorption of Bases from Promoted Sulfated Zirconia"

35. E.C. Sikabwe, R.L. White, *Catal. Lett.*, **44** (1997) 177-183

"Effects of Iron Promoter on Reactions of 1-Butene Adsorbed on Sulfated Zirconias"

36. D.L. Negelein, E. Bonnet, R.L. White, *J. Chromatog. Sci.*, **37** (1999) 263-269

"Effluent Monitoring by Repetitive Injection Gas Chromatography-Mass Spectrometry"

37. R.L. White, D.L. Negelein, E. Bonnet, R. Lin, *Curr. Top. Anal. Chem.*, **1** (1998) 93-105

"Repetitive Injection Gas Chromatography/Mass Spectrometry for Evolved Gas Analysis"

38. X. Song and A. Sayari, *Catal. Rev.-Sci. Eng.*, **38** (1996) 329-412

"Sulfated Zirconia-Based Strong Solid-Acid Catalysts: Recent Progress"

39. V. Adeeva, G.D. Lei, and W.M.H. Sachtler, *Appl. Catal. A*, **118** (1994) L11-L15

"Isomerization of ^{13}C Labeled Butane over Fe, Mn Promoted Sulfated ZrO_2 Catalyst"

40. J.A. de Haseth and L.V. Azarraga, *Anal. Chem.*, **53**, (1981) 2292-2296

"Interferogram-based infrared search system"

41. C.Y. Hsu, C.R. Heimbush, C.T. Armes, and B.C. Gates, *J. Chem. Soc. Chem. Commun.*, (1992) 1645-1646

"A Highly Active Solid Superacid Catalyst for n-Butane Isomerization: A Sulfated Oxide Containing Iron, Manganese, and Zirconium"

42. H. Liu, V. Adeeva, G.D. Lei, and W.M.H. Sachtler, *J. Molecul. Catal. A*, **100** (1995) 35-48

"Butane Isomerization Over Platinum Promoted Sulfated Zirconia Catalysts"

43. R. Lin, and R.L. White, Unpublished results

44. R. Lin, E. Bonnet, E.C. Sikabwe, and R.L. White, *Pittcon*, March 1-5, New Orleans (1998)

"Investigation of Effects of Metal Promoters on Sulfated Zirconia Catalysts"

45. V. Adeeva, J.W. de Haan, J. Jänchen, G.D. Lei, V. Schünemann, L.J.M. van De Ven, W.M.H. Sachtler, and R.A. van Santen, *J. Catal.*, **151** (1995) 364-372

"Acid Sites in Sulfated and Metal Promoted Zirconium Dioxide Catalysts"

CHAPTER 4 : NICKEL ALUMINATE
OXIDATION STUDIES

I.   INTRODUCTION

Dr. White's laboratory has interests in the study of biomass conversion by catalytic cracking. Currently, about 97% of all transportation energy in the U.S. is derived from petroleum, which is a non-renewable feedstock. Foreign oil accounts for about one-half of the oil used in the United States. The fact that oil is a non renewable energy feedstock and that the U.S. is currently heavily reliant on foreign sources of energy are excellent incentives for developing renewable energy sources. In addition, the burning of fossil fuels has serious environmental consequences. In contrast, the use of biomass for energy provides significant environmental advantages. For example, plant growth needed to generate biomass feedstocks will deplete atmospheric carbon dioxide and offset the increase in atmospheric carbon dioxide resulting from biomass fuel combustion. There is currently no way to offset the carbon dioxide added to the atmosphere (and the resultant greenhouse effect) that results from fossil fuel (diesel, gasoline, and natural gas) combustion. Biomass renewable energy sources can be converted to oxygenated fuels and are therefore logical choices for replacing oil.[1]

The kinetics and thermal decomposition mechanisms of biomass and biomass constituents have been extensively studied. In contrast, few studies have focused on the use of catalysts for direct biomass cracking. Examples of biomass catalytic cracking studies include Arauzo et. al.,[2] who reported that nickel aluminate, $NiAl_2O_4$, could effectively convert biomass to CO and CO_2. Preliminary studies in our laboratory [3] showed that nickel aluminate catalyzes the conversion of cellulose, the major natural polymer in biomass, to primarily CO_2. The fact

that nickel aluminate promotes the formation of CO_2 in an inert atmosphere suggests that nickel aluminate has potential as an oxidation catalyst.

An oxidation catalyst is a substance that activates the oxidant (usually oxygen present in the air), the substrate, or both.[4] Oxidation catalysts should not oxidize the reaction products.[4] This is only important in partial oxidations, because complete hydrocarbon oxidation yields carbon dioxide and water that cannot be easily oxidized. Golodets proposed two possible forms of intermediates in catalytic heterogeneous reactions involving molecular oxygen.[5] The initial reactant (Reac) or substrate can form an activated complex with oxygen at the catalyst (Cat) surface to form the products (Prod) and a "deformation" mechanism occurs:

$$Reac + O_2 + Cat \longrightarrow (Reac\ O_2\ Cat)^* \longrightarrow Prod + Cat$$

This mechanism requires the simultaneous adsorption of both oxygen and reactant, which makes it particularly difficult (high negative entropy). Alternatively, in the step-wise mechanism molecular oxygen is activated by the catalyst prior to reaction with the reactant:

$$Cat + O_2 \longrightarrow (Cat\ O_2)^*$$

$$(Cat\ O_2)^* + Reac \longrightarrow Prod + Cat$$
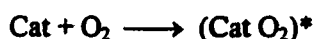
The stepwise mechanism is now accepted by most scientists. However, the nature of the activated complex still remains a point of discussion and depends on the catalyst employed.

The objectives of the study described here were first to verify the activity of nickel aluminate for production of CO_2 from cellulose and second to evaluate its potential as an oxidation catalyst. Kinetic studies similar to those for n-hexane cracking described in Chapter 3 were performed to compare the nickel aluminate activity for n-butane oxidation to that of 1% platinum on alumina, a known oxidation catalyst used in automotive three-way catalytic converters.[6-10]

II. THERMAL DECOMPOSITION OF CELLULOSE

Cellulose is the primary biopolymer in plants. It forms the basis for grasses, leaves, and stems and comprises about 50% of dry biomass. Cellulose consists of a linear chain of glucose units. Glucose molecules are joined together by 1,4-β-linkages.
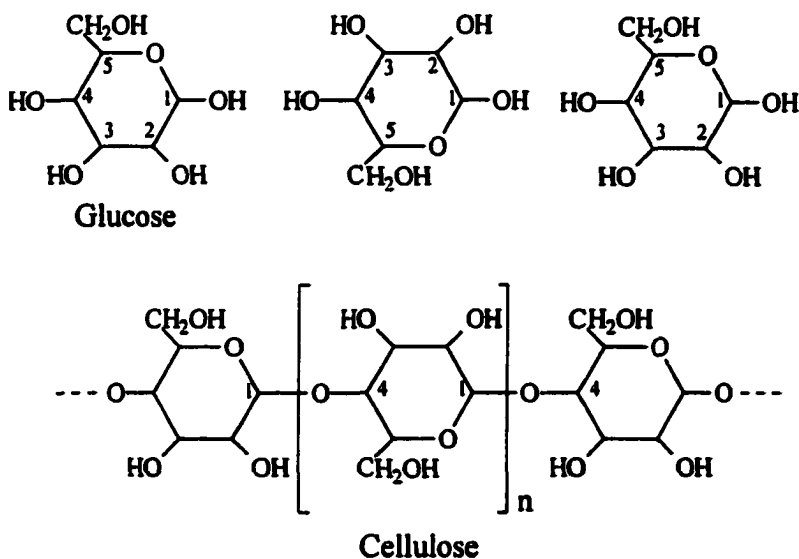
Cellulose and cellulose derivative thermal degradation processes have been extensively studied.[11-37] Interest in cellulose decompositions arise from potential fuel production and for improving the fire retardancy of cotton and wool. The role of oxygen in enhancing cellulose degradation is well known.[11] Oxidative decomposition generates carbon dioxide as the major product. In inert atmospheres, a large number of products are formed,[12] ranging from hydrocarbons (methane, ethane, etc.) to small and large oxygenated species (furan, furan derivatives, 1,6-anhydro-β-D-glucose or levoglucosan, etc.). Carbon dioxide is produced in inert environments, but the yield can be dramatically increased by mixing cellulose with a catalyst.

II.1 Thermogravimetric Analysis

Thermogravimetric analysis of neat cellulose and cellulose-catalyst samples was used to assess the effect of nickel aluminate on cellulose thermal decomposition. Cellulose powder (~20μm particles) was purchased from Aldrich (Milwaukee, WI). Cellulose-catalyst samples were prepared by mixing 10% by weight cellulose with sieved catalyst having particles sizes in the 63-150μm range.

Figure 4-1 shows the weight loss curves for neat cellulose (solid line), cellulose-$NiAl_2O_4$ (dashed line), and cellulose-1%Pt/Al_2O_3 (dotted line) obtained by heating samples from 25°C to 600°C at 10°C/min in 25mL/min helium. The x-axis in Figure 4-1 denotes sample temperature. The left y-axis denotes neat cellulose weight loss and the right y-axis denotes cellulose-catalyst sample weight loss. For easier comparisons, weight loss curves were normalized. Sample weights at 100°C corresponded to 0% weight loss and sample weights measured at 600°C was scaled to 100% weight loss for neat cellulose and 10% weight loss for the cellulose-catalyst samples.

Neat cellulose weight loss consisted of a single step that began near 300°C and was complete by 400°C. This temperature range for cellulose thermal decomposition in an inert atmosphere is consistent with results published in the literature.[13-19] Cellulose-catalyst sample weight losses exhibited a main step that occurred in the same temperature range as the neat cellulose. However, weight loss began at a lower temperature (near 100°C and 225°C for cellulose samples mixed with 1%Pt/Al_2O_3 and $NiAl_2O_4$, respectively) and continued until the temperature reached 600°C. The weight lost between 400°C and 600°C was larger for the 1%Pt/Al_2O_3 catalyst (about 2%) than for the $NiAl_2O_4$ catalyst (less than 1%).

The fact that cellulose weight loss began at lower temperature when 1%Pt/Al_2O_3 and $NiAl_2O_4$ were present suggested that both substances catalyze cellulose thermal decomposition
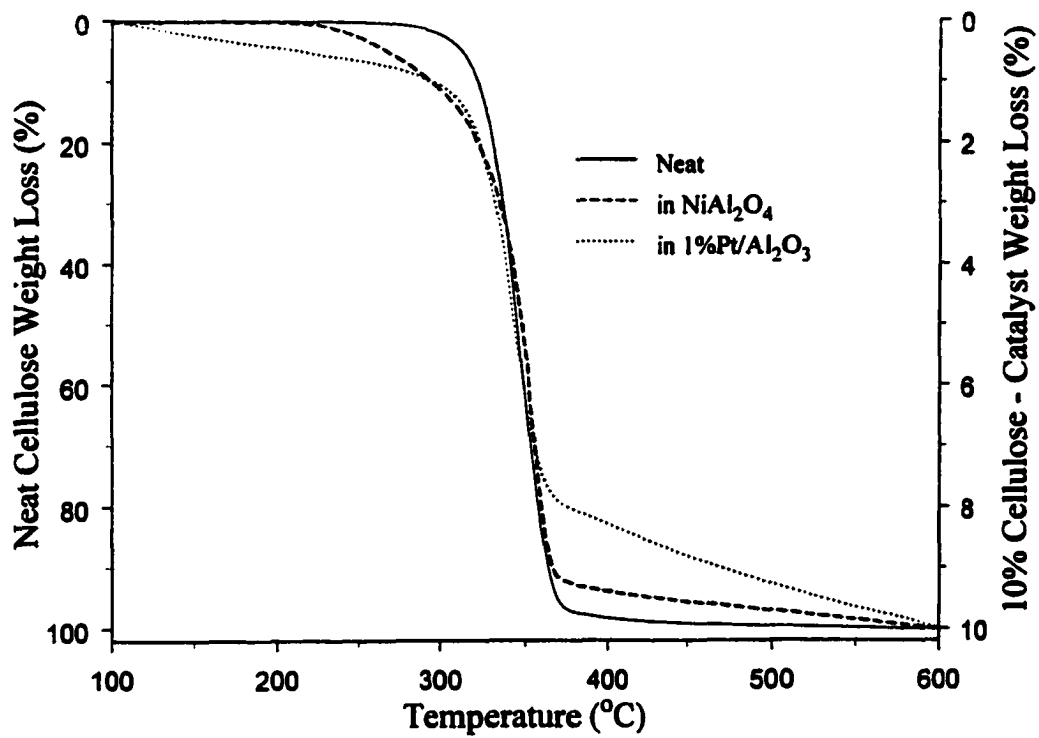
Figure 4-1 : Thermogravimetric Analysis of Cellulose Thermal Decomposition

in an inert atmosphere. However, the low temperature weight loss (<300°C) could have been due to water desorption from the catalyst rather than from cellulose decomposition. This cannot be determined by thermogravimetric analysis. Thermal Analysis-Mass Spectrometry was employed to characterize volatile thermal degradation products in order to discriminate between weight loss due to desorption of species adsorbed on catalysts and that due to cellulose decomposition.

II.2 Thermal Analysis - Mass Spectrometry

Volatiles formed during cellulose thermal decomposition were analyzed by thermal analysis-mass spectrometry (TA-MS). Results from simultaneous thermal analysis-mass spectrometric studies of cellulose decomposition have been published in the literature.[20-24] Non-oxidative cellulose thermal decomposition is known to produce large amounts of relatively non-volatile species such as levoglucosan.[12] To avoid clogging our interface with non-volatile products, TA-MS analysis was restricted to low temperature (<300°C) measurements.

About 30mg cellulose-catalyst samples were heated from 25°C to 300°C at 10°C/min in 25mL/min helium. The interface between the sample furnace and the mass spectrometer was maintained at 300°C to improve transport of volatile products to the mass spectrometer ionization chamber. In the temperature range over which weight loss was observed (i.e. starting at 100°C for the 1%Pt/Al$_2$O$_3$ sample and 200°C for the NiAl$_2$O$_4$), the TA-MS splitter valve was opened so that the mass spectrometer ion source pressure reached 1×10^{-5} Torr. Signal averaging and integration parameters were set so that one data point (mass spectrum) was recorded every 15 seconds covering the 15-150 amu mass range.

Figure 4-2 shows results from TA-MS analysis of cellulose-NiAl$_2$O$_4$ (Fig. 4-2a) and cellulose-1%Pt/Al$_2$O$_3$ (Fig. 4-2b) samples. In both figures, the x-axes represent sample

131
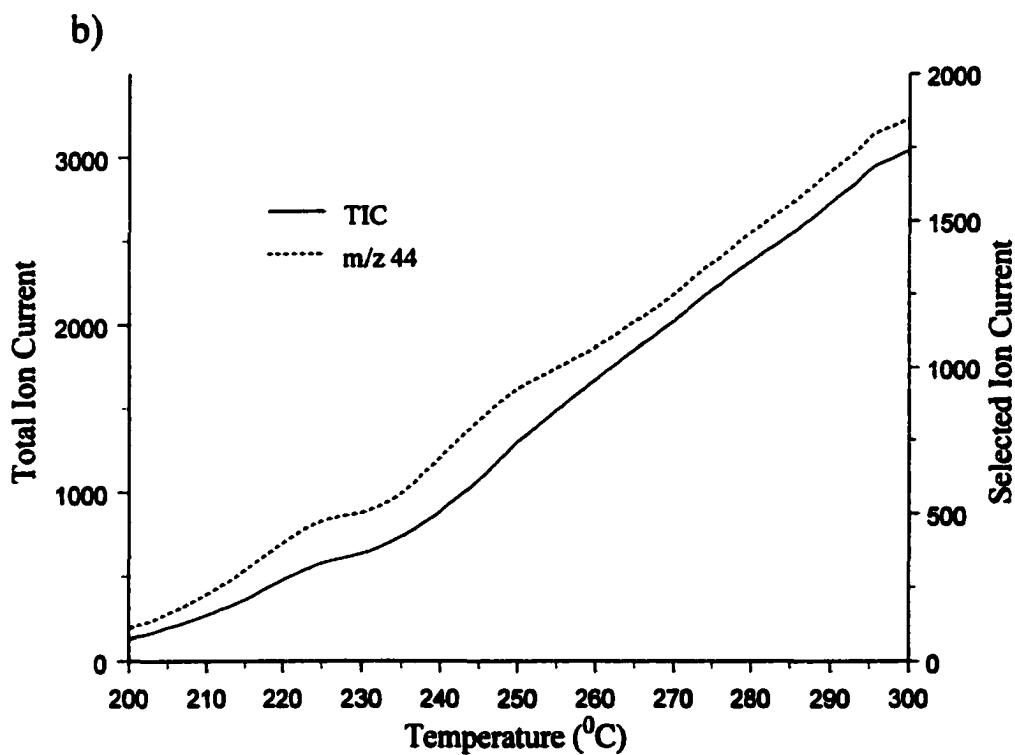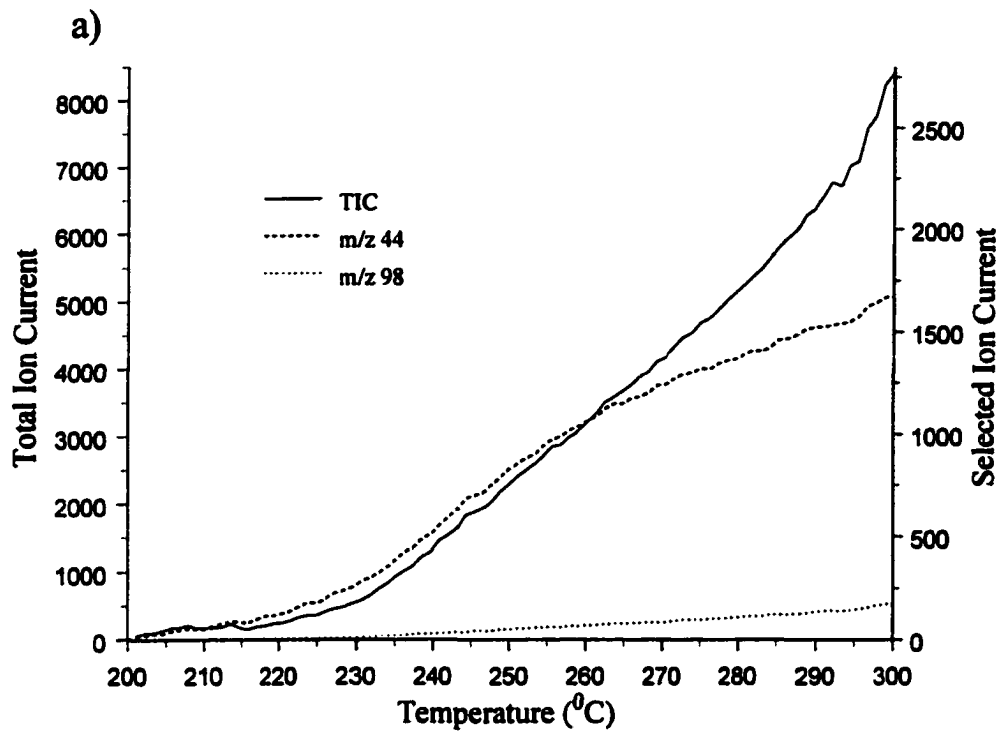
Figure 4-2 : Cellulose Decomposition Products Detected by TA-MS
a) NiAl₂O₄ and b) 1%Pt/Al₂O₃

temperature. The y-axes denote either total ion current (left y-axis) or selected ion current (right y-axis). In Figure 4-2a, the total ion current (solid line), and ion currents for m/z 44 (dashed line) and m/z 98 (dotted line) are plotted versus the cellulose-NiAl$_2$O$_4$ sample temperature in the 200-300°C range. The total ion current and m/z 44 ion current began to increase about 220°C and continued to rise to about 300°C. The total ion current and the m/z 44 ion current increased at about the same rate until the sample temperature reached about 260°C. Between 260°C and 300°C, the total ion current almost tripled whereas that for m/z 44 barely doubled. An ion at m/z 98 became noticeable in mass spectra when the sample reached 240°C. The intensity of the m/z 98 ion increased with sample temperature but was always much less than that for m/z 44. In Figure 4-2b, the total ion current (solid line) and m/z 44 ion current (dashed line) are plotted versus cellulose-1%Pt/Al$_2$O$_3$ sample temperature in the 200-300°C range. Both the total ion current and m/z 44 ion current increased with the sample temperature. Both curves exhibited similar shapes. No ions at m/z values larger than 44 were detected during the thermal decomposition of the cellulose-1%Pt/Al$_2$O$_3$.

Volatile products generated from cellulose thermal decomposition were monitored by TA-MS at the start of the decomposition only. The presence of m/z 44 ion (and m/z 28, which was present but not profiled) is characteristic of carbon dioxide. The similarity of the TIC and m/z 44 profiles for the cellulose-1%Pt/Al$_2$O$_3$ sample suggests that CO$_2$ was by far the main product of decomposition. The intensity of m/z 44 and the similarity of the shapes of the TIC and m/z 44 profiles below 260°C for the cellulose NiAl$_2$O$_4$ sample suggest that carbon dioxide was a major product of the low temperature thermal decomposition of this sample. The presence of the ion at m/z 98 during cellulose-NiAl$_2$O$_4$ sample decomposition and the differences between the TIC and m/z 44 profiles above 260°C confirm that carbon dioxide was not the only volatile product. Recent studies[22,24] using mass spectrometry to analyze cellulose decomposition

133

products have reported that m/z 98 is one of the most abundant ions detected. Evans and coworkers[23] have assigned m/z 98 to anhydrosugars such as levoglucosan formed during uncatalyzed cellulose thermal decomposition. The formation of this non-catalytic product suggests that some cellulose was not in contact with $NiAl_2O_4$ catalytic sites. This may have been due to poor mixing of the cellulose-catalyst blend prior to thermal analysis. It may also suggest that access to $NiAl_2O_4$ catalytic sites is difficult or that $NiAl_2O_4$ has fewer sites than $1\%Pt/Al_2O_3$.

TA-MS results revealed that the low temperature weight loss observed during cellulose thermal decomposition in an inert atmosphere when it was mixed with $NiAl_2O_4$ and $1\%Pt/Al_2O_3$ (Figure 4-1) corresponded solely to cellulose degradation and that the major product was carbon dioxide. The presence of either $NiAl_2O_4$ or $1\%Pt/Al_2O_3$ lowered the temperature at which cellulose decomposed. This indicates that both substances catalyzed cellulose decomposition. Furthermore, the major product of this decomposition was carbon dioxide, which is a product of complete oxidation. Platinum on alumina is a known oxidation catalyst. As a result, one can assume that both $NiAl_2O_4$ and $1\%Pt/Al_2O_3$ catalyze the thermal decomposition of cellulose by favoring an oxidation mechanism involving the oxygen present in cellulose (~50% wt.). The first step would likely be a weakening of the carbon-oxygen bond in cellulose due to the interactions between the nickel in nickel aluminate and oxygen from cellulose as shown in the following arrangement:

134
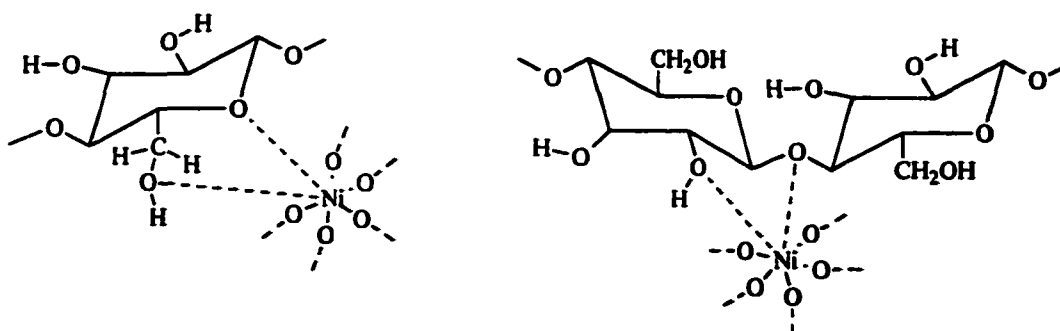
In nickel aluminate, Ni^{2+} ions occupy octahedral sites surrounded by O^{2-} ions in a cubic spinel structure.[38] At the catalyst surface, oxygen deficiencies can result in electrophilic attack on cellulose oxygen atoms. Attack on oxygen atoms that are part of the 6-membered ring or that form the 1,4-β-linkages would result in the most significant cellulose chain rupture.

The results from cellulose thermal decomposition in the presence of nickel aluminate suggests that nickel aluminate may have oxidation catalyst properties. The ability to selectively remove oxygen from cellulose as carbon dioxide might be a useful means of creating a high C/H ratio residue. This residue may be used as a solid fuel (i.e. charcoal), or as pigment (i.e. carbon black).

III. n-BUTANE OXIDATION

The potential of nickel aluminate as an oxidation catalyst was evaluated by comparing its activity for the complete oxidation of n-butane to that of 1% platinum on alumina by using the new fixed bed catalytic microreactor-GC/MS system.

$$n\text{-Butane} + Oxygen \longrightarrow Carbon\ Dioxide + Water$$

$$n\text{-}C_4H_{10} + 13/2\ O_2 \longrightarrow 4\ CO_2 + 5\ H_2O$$
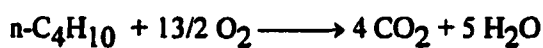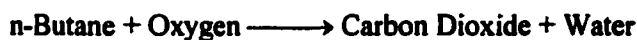
A mixture of 10mL/min dry air from Airgas (Radnor, PA) and 0.1mL/min n-butane from Airgas (Radnor, PA) entered the reactor through the reactant inlet and passed through 100mg of catalyst previously calcined in-situ in 10mL/min air for 2 hours at 600°C. After calcination, the catalyst temperature was ramped at 4°C/min from 100°C to a temperature at which all n-butane was converted to carbon dioxide. Reactor effluent (15µL) was automatically injected every 4°C (1 min) into a 10 meter AT™-1 capillary gas chromatographic column maintained at ambient temperature. The thermocouple located inside the gas chromatograph

oven read 29°C due to the proximity of heated components (interface and reactor system ovens). An 8-port valve equipped with two sample loops was used. Therefore, each valve rotation resulted in one GC/MS injection. Injections were made after 2°C sample temperature increases (30 seconds). Helium was used for the GC carrier gas (2mL/min) and for the make-up gas (25mL/min). After separation, the GC flow was split in the 100°C interface by opening the reactor-GC/MS splitter valve so that the mass spectrometer ion source pressure reached 1×10^{-6} Torr. To maximize scan rates, no signal averaging was employed, resulting in about 8 scans per second for the mass range 28,35-78 amu.

Figure 4-3 shows 250 successive gas chromatograms obtained during n-butane oxidation by $NiAl_2O_4$ plotted versus catalyst temperature (x-axis) over the 100-600°C range. The y-axis denotes the mass spectrometer total ion current (for the 35-78 amu mass range only). This data set contains more than 65,000 mass spectra. As the catalyst temperature increased, the n-butane peak diminished and a peak corresponding to carbon dioxide grew. The n-butane and carbon dioxide peak heights are about equal, denoting about 50% conversion, when the $NiAl_2O_4$ catalyst temperature reached 475°C. Figure 4-4a shows TIC chromatograms obtained at catalyst temperatures of 473°C and 475°C. The x-axis denotes retention time. Two peaks, eluting within about 6 seconds, resulted from each injection. The first peak corresponded to carbon dioxide, with the mass spectrum conatining the characteristic m/z 44 ion. The second peak was n-butane, having a mass spectral base peak at m/z 43. Figures 4-4b and 4-4c depict the same chromatograms except that ion currents at m/z 43 and m/z 44 are plotted rather than the total ion current. Figure 4-4a clearly shows that the two TIC peaks were not baseline resolved. This is due to the tailing of the carbon dioxide peak (Fig. 4-4c). Because of the incomplete resolution, TIC chromatographic peaks were not used for peak area integrations. Instead, n-butane concentration variations in the reactor effluent were determined by integrating m/z 43 selected ion chromatographic peaks (Fig. 4-4b). The n-butane mass spectrum contains a small peak at

136
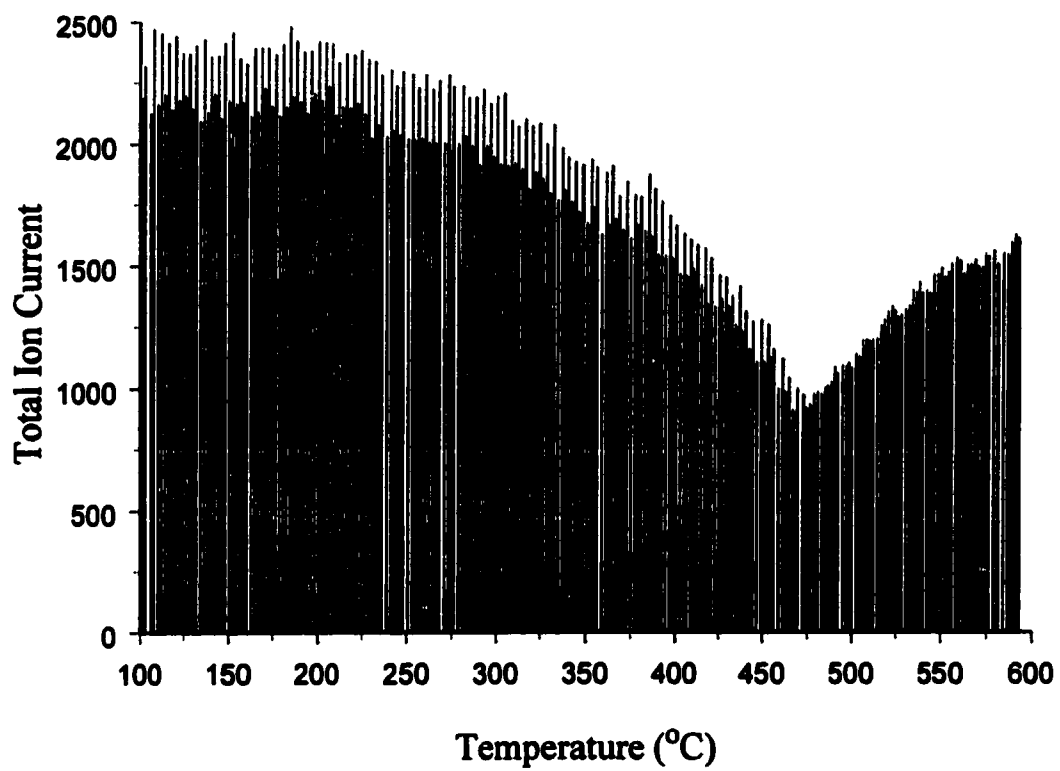
Figure 4-3 : Effect of Catalyst Temperature on n-Butane Oxidation by NiAl₂O₄

137
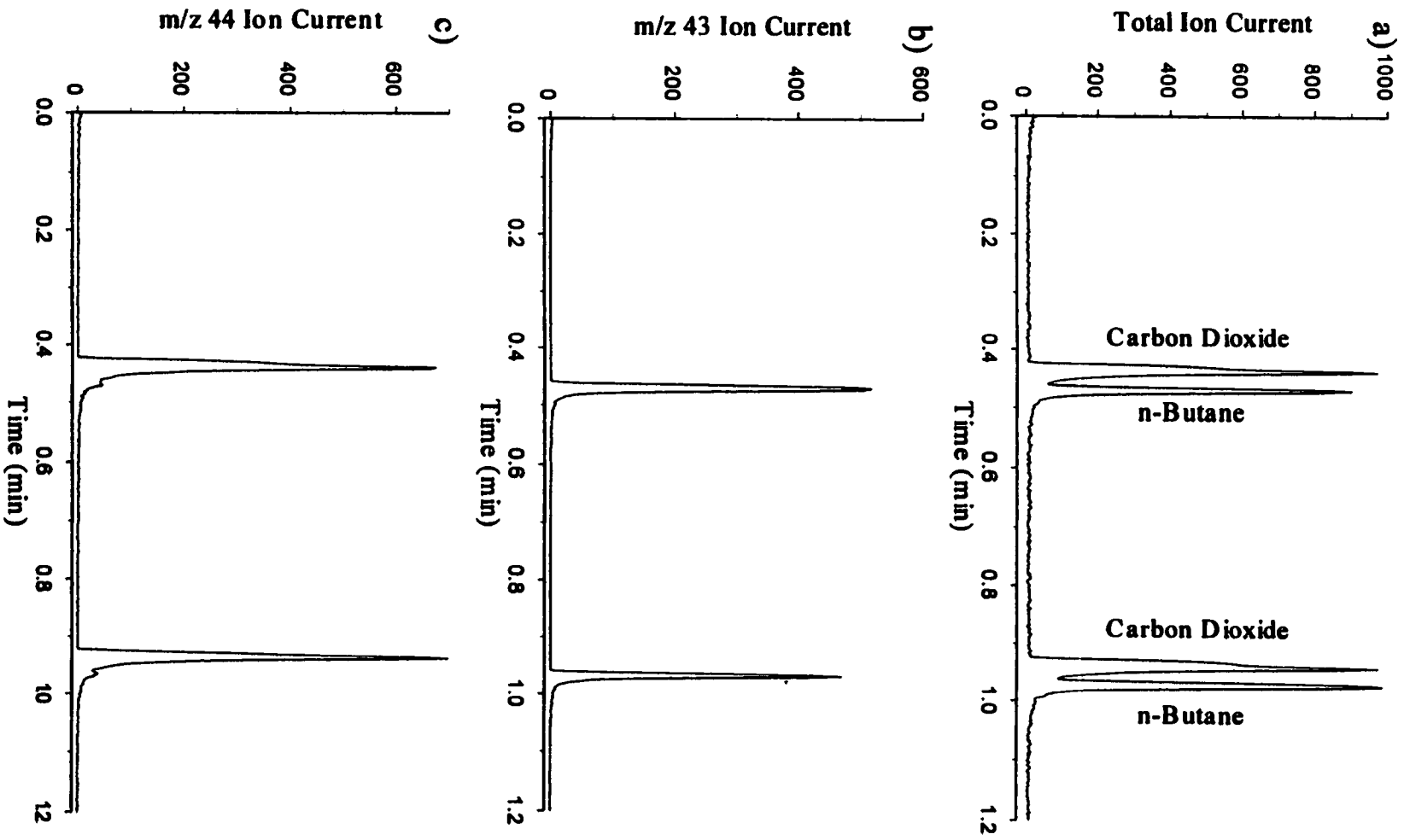
Figure 4-4 : n-Butane Oxidation - Chromatogram for NiAl$_2$O$_4$ at 473°C and 475°C

138

m/z 44. The n-butane contribution to the m/z 44 selected ion chromatographic peaks is a small peak on the tailing side of the carbon dioxide peak (Figure 4-4c). As a result, m/z 44 chromatographic peaks could not be directly integrated to monitor carbon dioxide formation. The n-butane contribution was removed by subtracting one eighth of the m/z 43 signal (the contribution from n-butane only) from the m/z 44 signal, as shown in equation 1.

$$\text{Carbon Dioxide Signal} = \text{Signal}_{m/z\,44} - (1/8 \times \text{Signal}_{m/z\,43}) \qquad (1)$$

Figure 4-5 shows the resulting integrated peak areas representative of a) n-butane (m/z 43) and b) carbon dioxide (corrected m/z 44) plotted versus catalyst temperature in the 100-600°C range. The n-butane peak area (Fig. 4-5a) was constant at about 6,500 counts from 100°C to about 250°C, at which temperature it began to decrease because n-butane was converted to carbon dioxide. The n-butane peak area continued to decrease with increasing catalyst temperature up to 580°C, at which n-butane was barely detectable. A small amount of carbon dioxide in the mass spectrum background was responsible for a small chromatographic peak with an area of about 200 counts from 100°C to 300°C (Fig. 4-5b). The carbon dioxide peak area began to increase above 300°C and continued to increase up to 600°C.

The n-butane oxidation experiment was repeated with the 1%Pt/Al$_2$O$_3$ catalyst and with the sample tube filled with quartz wool instead of catalyst. The experiment with quartz wool was designed to determine the temperature range at which uncatalyzed n-butane thermal oxidation occurred. The quartz wool was placed inside the sample tube to compensate for catalyst sample effects on linear flow and pressure inside the reactor. Integrated peak areas representing n-butane and carbon dioxide for the three measurements were normalized by using equation 2. Normalized areas ranged from 0 to 100.

$$\text{Normalized Areas} = \frac{\text{Area} - \text{Area}_{min}}{\text{Area}_{max}} \times 100 \qquad (2)$$
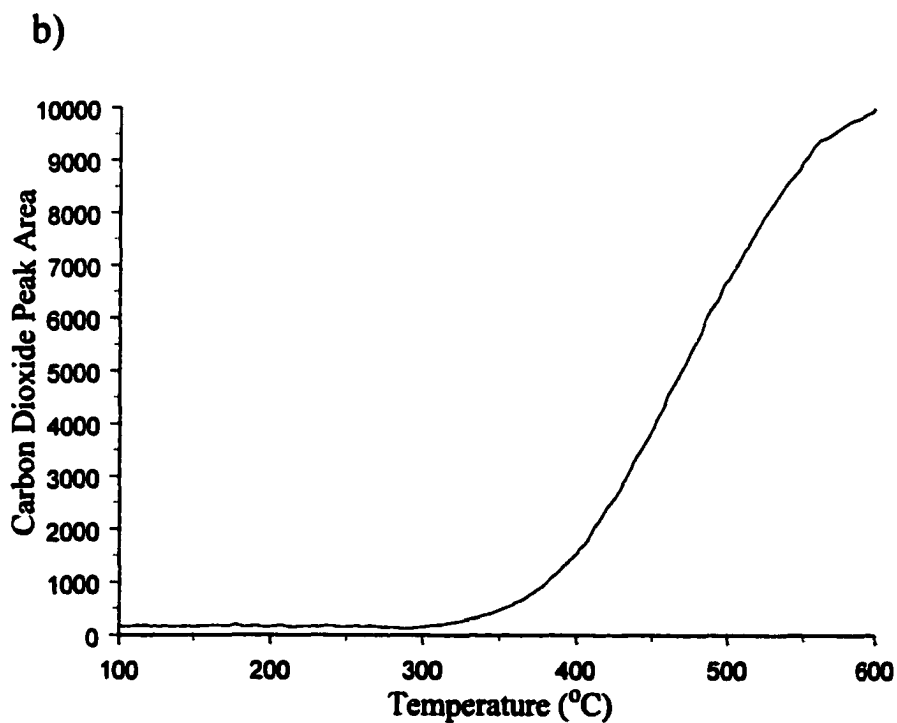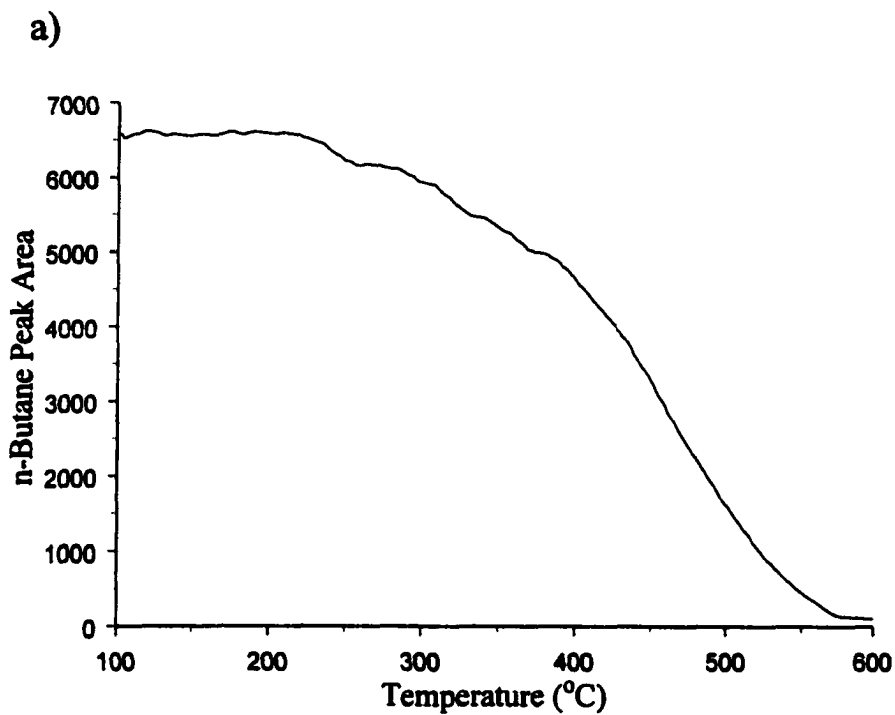
Figure 4-5 : n-Butane Oxidation by $NiAl_2O_4$ - Chromatographic Peak Areas Representative of
a) n-butane (m/z 43) and b) carbon dioxide (corrected m/z 44)

Figure 4-6 shows the results of n-butane oxidation by a) NiAl$_2$O$_4$, b) 1%Pt/Al$_2$O$_3$ and c) from thermal oxidation. In these three figures, n-butane (solid line) and carbon dioxide (dashed line) normalized peak areas are plotted versus the reactor furnace temperature. For comparison, all three graphs were plotted for the same temperature range (i.e. from 100°C to 850°C). Figure 4-6a shows the effect of the catalyst temperature on the NiAl$_2$O$_4$ activity for n-butane oxidation. n-Butane oxidation by NiAl$_2$O$_4$ began at about 250°C and was complete by 600°C. The point at which both lines crossed represents 50% conversion and occurred at about 450°C. Figure 4-6b shows the temperature dependant n-butane oxidation activity for the 1%Pt/Al$_2$O$_3$ catalyst. n-Butane oxidation by 1%Pt/Al$_2$O$_3$ began at about 120°C, reached 50% conversion just below 200°C, and was complete by 250°C. Uncatalyzed n-butane oxidation is illustrated in Figure 4-6c. n-Butane oxidation began when the temperature rose above 500°C. n-Butane conversion to carbon dioxide reached about 50% when the reactor temperature was near 675°C. n-Butane was completely oxidized when the temperature reached 820°C.

Figure 4-6 clearly shows that NiAl$_2$O$_4$ catalyzed the oxidation of n-butane, because it lowered the reaction temperature by about 225°C (for 50% conversion) compared to uncatalyzed oxidation. However, the NiAl$_2$O$_4$ activity for n-butane oxidation was not as good as that of the 1%Pt/Al$_2$O$_3$ catalyst. These results suggest that nickel aluminate is an oxidation catalyst, but not as good as platinum on alumina.

Using the same experimental conditions, kinetic studies similar to those described in Chapter 3 for n-hexane cracking were used to determine activation energies for n-butane oxidation by NiAl$_2$O$_4$ and 1%Pt/Al$_2$O$_3$. n-Butane conversions determined from isothermal oxidations in the 320-420°C range for NiAl$_2$O$_4$ and in the 110-170°C range for 1%Pt/Al$_2$O$_3$ were used to generate Arrhenius plots. Conversion was calculated at each temperature (T) by using equation 3:
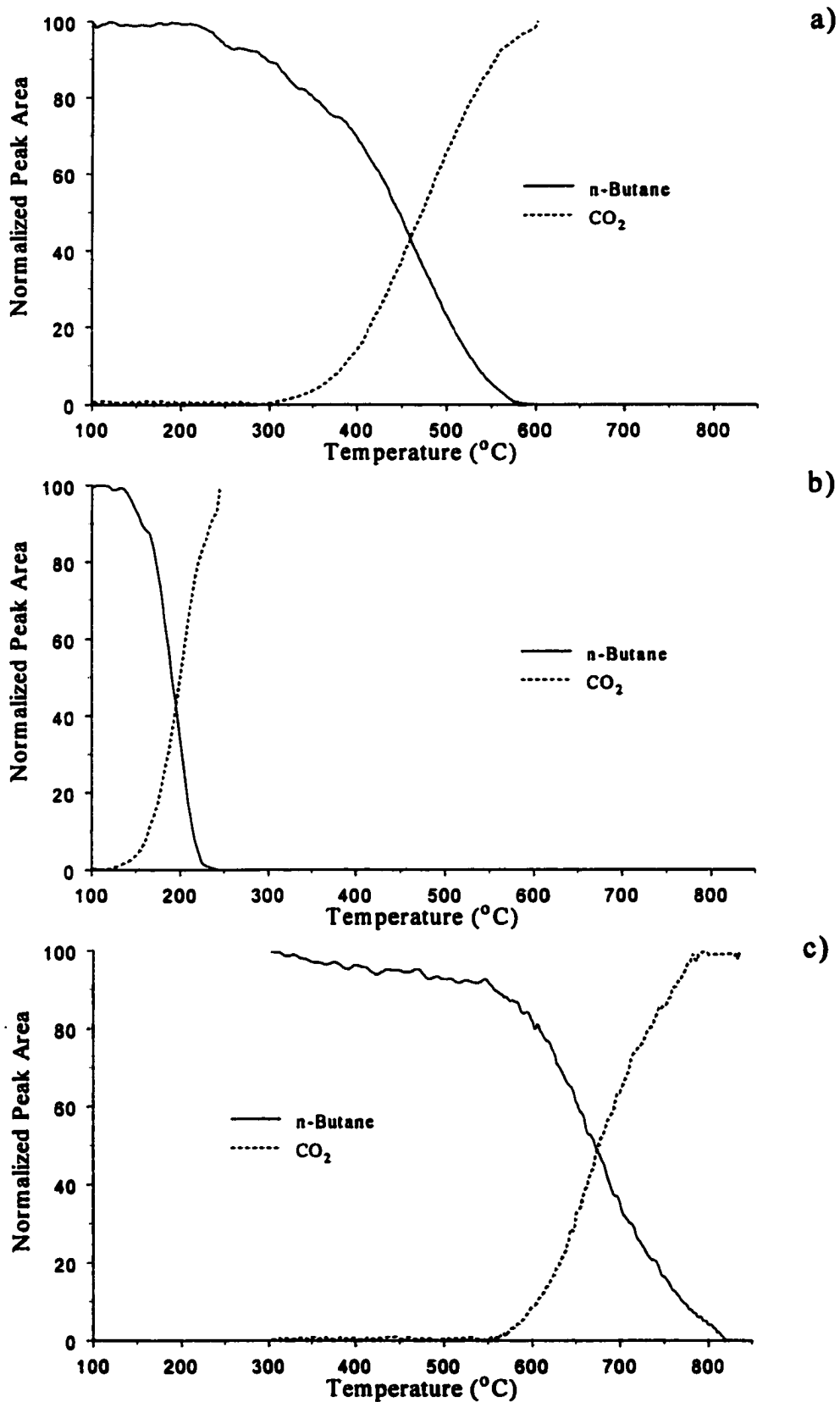
Figure 4-6 : n-Butane Oxidation by a) $NiAl_2O_4$, b) $1\%Pt/Al_2O_4$, and c) No Catalyst

142

$$\text{Conversion}_T = \left(\frac{\sum_{n=1}^{n=5} \text{Area}_{m/z\ 43\ Bypass} - \sum_{n=1}^{n=5} \text{Area}Z_{m/z\ 43\ T}}{\sum_{n=1}^{n=5} \text{Area}_{m/z\ 43\ Bypass}} \right) \quad (3)$$

where $\text{Area}_{m/z\ 43\ Bypass}$ corresponds to the n-butane peak area derived from m/z 43 selected ion chromatograms when the microreactor manual valve was in the bypass mode and $\text{Area}_{m/z43\ T}$ represents the n-butane peak areas derived from m/z 43 selected ion chromatograms when the microreactor manual valve was in the reactor mode and the reactor furnace was at temperature T. All peak areas were averages of five injections.

The Arrhenius plots shown in Figure 4-7 were generated by plotting the natural logarithm of conversion versus the reciprocal absolute temperature. Both plots yielded straight lines, from which activation energies were calculated. Peak area reproducibility resulted in a ±2kJ/mol uncertainty on the activation energy values. n-Butane oxidation occurred at higher temperature for $NiAl_2O_4$ than for $1\%Pt/Al_2O_3$. However, the activation energy found for n-butane oxidation by $NiAl_2O_4$ (20kJ/mol) was significantly lower than that of $1\%Pt/Al_2O_3$ (36kJ/mol). This may be explained by the fact that the pre-exponential factor was much lower for $NiAl_2O_4$. Because the natural logarithm of conversion instead of rate constant was used to generate the Arrhenius plots, the y-intercept is not equal to the pre-exponential factor, A, in the Arrhenius equation. However, the intercepts provide relative information regarding the pre-exponential factor. The intercept for the line obtained from the n-butane oxidation by $1\%Pt/Al_2O_3$ was 9.3 whereas that from oxidation by $NiAl_2O_4$ was only 2.8. These values correspond to relative pre-exponential factors of 10509 and 15.5 respectively. This suggests that although $NiAl_2O_4$ sites may be more effective for oxidation (lower activation energy), it is more difficult for reactants to get to the sites or to get into the proper orientation at the sites.
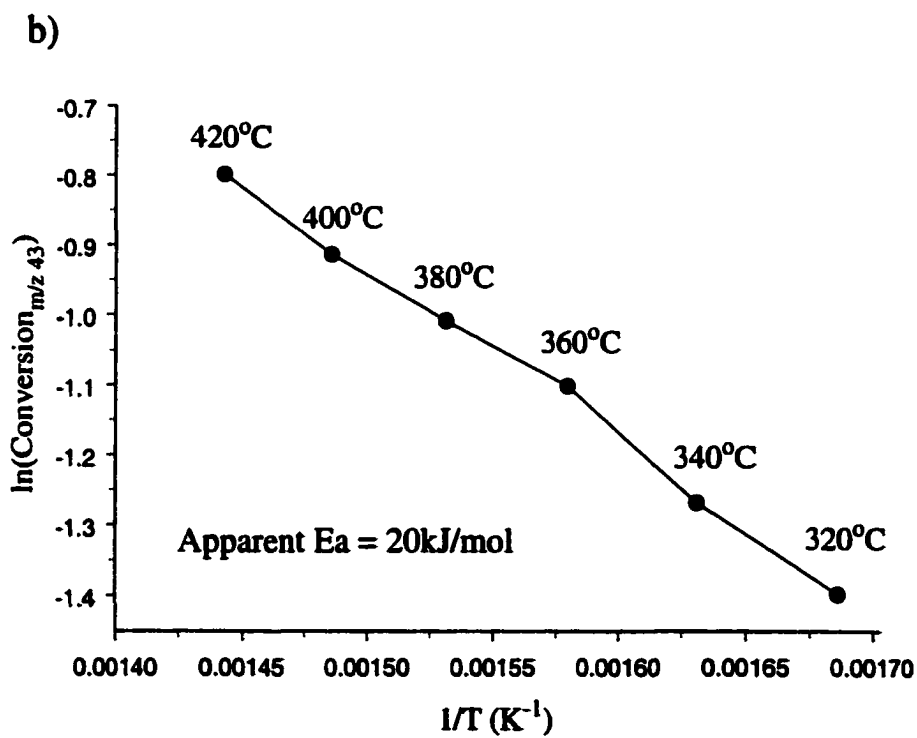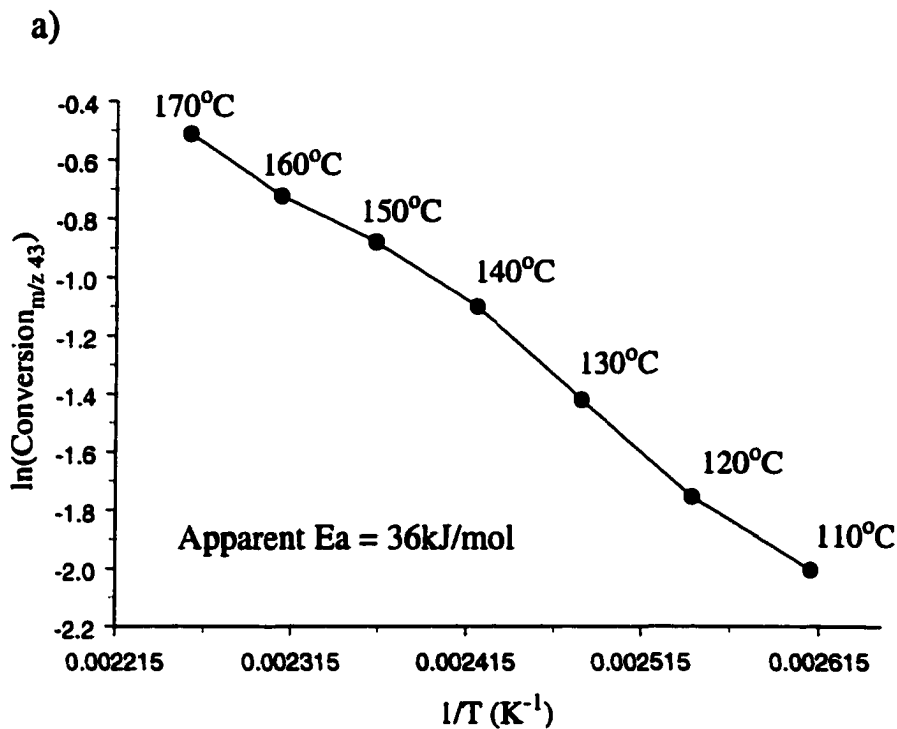
Figure 4-7 : Arrhenius Plots for the Oxidation of n-Butane by
a) 1% Pt/Al$_2$O$_3$ and b) NiAl$_2$O$_4$

IV. CONCLUSION

Results from this study have shown that nickel aluminate is an oxidation catalyst. It lowered the temperature of cellulose thermal decomposition in an inert atmosphere and for n-butane oxidation. However, nickel aluminate does not appear to be as good an oxidation catalyst as platinum on alumina because the temperature shift is much less.

The lower activation energy obtained for n-butane oxidation by nickel aluminate may indicate that individual nickel aluminate sites are more effective than those of platinum on alumina. However, this higher efficiency is effectively offset by a low probability for the reaction to occur. The data presented here is insufficient for a prediction of the structure of the active sites in nickel aluminate or the mechanism of oxidation. Future studies such as surface analysis or volatile product analysis from thermal decomposition of smaller sugars (glucose, saccharose, etc.) when mixed with nickel aluminate might provide information regarding the mechanism of oxidation by nickel aluminate.

V.   REFERENCES

1.   A.V. Bridgwater, and J.M. Double, *A strategic Assessment of Liquid Fuels from Biomass*, in *Research in Thermo-Chemical Biomass Conversion*, A.V. Bridgwater, and A.V. Kuester, Elsevier Science Publishers: Amsterdam, The Netherlands, 1988

2.   J. Arauzo, D. Radlein, J. Piskorz, and D.S. Scott, *Energy Fuels*, 8 (1994) 1192-1196 "A New Catalyst for the Catalytic Gasification of Biomass"

3.   S. Balthazor, N. Hesse, and R.L. White, Unpublished results

4. G.J. Hutchings, S.H. Taylor, and I.D. Hudson, *Designing Heterogeneous Oxidation Catalysts*, in *Science and Technology in Catalysis 1998*, H. Hattori and K. Otsuka, Studies in Surface Science and Catalysis, Kodansha Ltd: Tokyo, Japan and Elsevier Science Publishers: Amsterdam, The Netherlands, Vol. 121, 1999

5. G.I. Golodets, *Heterogeneous Catalytic Reactions Involving Molecular Oxygen*, Studies in Surface Science and Catalysis, Elsevier Science Publisher: Amsterdam: The Netherlands, Vol. 15, 1983

6. T.J. Truex, R.A. Searles, and D.C. Sun, *Plat. Met. Rev.*, **36** (1992) 2-11

    "Catalyst for Nitrogen Oxides Control under Lean Burn Conditions"

7. K.C. Taylor, *Catal. Rev. -Sci. Eng.*, **35** (1993) 457-481

    "Nitric Oxide Catalysis in Automotive Exhaust Sustems"

8. M. Shelef, *Chem. Rev.*, **95** (1995) 209-225

    "Selective Catalytic Reduction of NO_x with N-Free Reductants"

9. N. Takahashi, H. Shinjoh, T. Iijima, T. Suzuki, K. Yamazaki, K. Yokota, H. Suzuki, N. Miyoshi, S.-I. Matsumoto, T. Tanizawa, T. Tanaka, S.-S. Tateishi, and K. Kasahara, *Catal. Today*, **27** (1996) 63-69

    "The New Concept 3-Way Catalyst for Automotive Lean-Burn Engine"

10. A. Fritz, and V. Pitchon, *Appl. Catal. B*, **13** (1997) 1-25

    "The Current State of Research on Automotive Lean NO_x Catalysis"

11. F. Shafizadeh, *Adv. Carbohydr. Res.*, **16** (1971) 273-279

    "Chemical Composition and Thermal Analysis of Cottonwood"

12. Y. Tsuchiya, and K. Sumi, *J. Appl. Polym. Sci.*, **14** (1970) 2003-2013

    "Thermal Decomposition Products of Cellulose"

13. C. Flaque, and S. Montserrat, *J. Appl. Polym. Sci.*, **74** (1999) 201-209

    "Thermal Degradation of Celluloses and their Vinylic Copolymers by Thermogravimetric Analysis"

14. M. Gronli, M.J. Antal Jr., and G. Varhegyi, *Ind. Eng. Chem. Res.*, **38** (1999) 2238-2244

"A Round-Robin Study of Cellulose Pyrolysis Kinetics by Thermogravimetry"

15. X.-G. Li, *J. Appl. Polym. Sci.*, **71** (1999). 573-578

"High-Resolution Thermogravimetry of Cellulose Esters"

16. M.-R. Huang, and X.-G. Li, *J. Appl. Polym. Sci.*, **68** (1998) 293-304

"Thermal Degradation of Cellulose and Cellulose Esters"

17. M.E. Calahorra, M. Cortazar, J.I. Eguiazabal, and G.M. Guzman, *J. Appl. Polym. Sci.*, **37** (1989) 3305-14

"Thermogravimetric Analysis of Cellulose: Effect of the Molecular Weight on Thermal Decomposition"

18. F. Shafizadeh, and A.G.W. Bradbury, *J. Appl. Polym. Sci.*, **23** (1979) 1431-1442

"Thermal Degradation of Cellulose in Air and Nitrogen at Low Temperatures"

19. C. Fairbridge, R.A. Ross, and S.P. Sood, *J. Appl. Polym. Sci.*, **22** (1978) 497-510

"A Kinetic and Surface Study of the Thermal Decomposition of Cellulose Powder in Inert and oxidizing atmospheres"

20. G. Varhegyi, E. Jakab, F. Till, and T. Szekely, *Energy Fuels*, **3** (1989) 755-60

"Thermogravimetric-Mass Spectrometric Characterization of the Thermal Decomposition of Sunflower Stem"

21. G. Varhegyi, M.J. Antal Jr., T. Szekely, F. Till, and E. Jakab, *Energy Fuels*, **2** (1988) 267-272

"Simultaneous Thermogravimetric-Mass Spectrometric Studies of the Thermal Decomposition of Biopolymers. 1. Avicel Cellulose in the Presence and Absence of Catalysts"

22. R.J. Evans, D. Wang, F.A. Agblevor, H.L. Chum, and S.D. Baldwin, *Carbohydr. Res.*, **281** (1996) 219-235

"Mass Spectrometric Studies of Thermal Decomposition of Carbohydrates using ^{13}C-labeled Cellulose and Glucose"

23. R.J. Evans, and T.A. Milne, *Energy Fuels*, **1** (1987) 123-137

147

24.   M. Statheropoulos, and S.A. Kyriakou, *Anal. Chim. Acta*, **409** (2000) 203-214

        "Quantitative Thermogravimetric-Mass Spectrometric Analysis for Monitoring the Effects of Fire

        Retardants on Cellulose Pyrolysis"

25.   X.-G. Li, M.-R. Huang, and H. Bai, *J. Appl. Polym. Sci.*, **73** (1999) 2927-2936

        "Thermal Decomposition of Cellulose Ethers"

26.   B.-I. Park, J.W. Bozzelli, M.R. Booty, M.J. Bernhard, K. Mesuere, C.A. Pettigrew, J.-C. Shi,

        and S.L. Simonich, *Environ. Sci. Technol.*, **33** (1999) 2584-2592

        "Polymer Pyrolysis and Oxidation Studies in a Continuous Feed and Flow Reactor: Cellulose

        and Polystyrene"

27.   M.J. Antal Jr., G. Varhegyi, and E. Jakab, *Ind. Eng. Chem. Res.*, **37** (1998) 1267-1275

        "Cellulose Pyrolysis Kinetics: Revisited"

28.   M.J. Antal Jr., and G. Varhegyi, *Energy Fuels*, **11** (1997) 1309-1310

        "Impact of Systematic Errors on the Determination of Cellulose Pyrolysis Kinetics"

29.   E. Jakab, K. Liu, and H.L.C. Meuzelaar, *Ind. Eng. Chem. Res.*, **36** (1997) 2087-2095

        "Thermal Decomposition of Wood and Cellulose in the Presence of Solvent Vapors"

30.   J.G. Reynolds, and A. K. Burnham, *Energy Fuels*, **11** (1997) 88-97

        "Pyrolysis Decomposition Kinetics of Cellulose-Based Materials by Constant Heating Rate

        Micropyrolysis"

31.   P. Yang, and S. Pingyu; *J. Appl. Polym. Sci.*, **60** (1996) 1137-1146

        "Thermal Analysis of Different Cellulosic Fabrics"

32.   I. Milosavljevic, V. Oja, and E.M. Suuberg, *Ind. Eng. Chem. Res.*, **35** (1996) 653-62

        "Thermal Effects in Cellulose Pyrolysis: Relationship to Char Formation Processes"

33.   I. Milosavljevic, and E.M. Suuberg, *Ind. Eng. Chem. Res.*, **34** (1995) 1081-1091

        "Cellulose Thermal Decomposition Kinetics: Global Mass Loss Kinetics"

34.   M.J. Antal Jr., and G. Varhegyi, *Ind. Eng. Chem. Res.*, **34** (1995) 703-717

        "Cellulose Pyrolysis Kinetics: The Current State of Knowledge"

148

35. N. Nishioka, M. Yamaoka, H. Haneda, K. Kawakami, and M. Uno, *Macromolecules*, **26** (1993) 4694-4699

"Thermal Decomposition of Cellulose/Synthetic Polymer Blends Containing Grafted Products. 1. Cellulose/Poly(Methyl Methacrylate) Blends"

36. G. Varhegyi, M.J. Antal Jr., T. Szekely, and P. Szabo, *Energy Fuels*, **3** (1989) 329-35

"Kinetics of the Thermal Decomposition of Cellulose, Hemicellulose, and Sugarcane Bagasse"

37. D.F. Arseneau, *Can. J. Chem.*, **49** (1971) 632-638

"Competitive Reactions in the Thermal Decomposition of Cellulose"

38. V.E. Henrich and P.A. Cox, *The Surface Science of Metal Oxides*, Camgridge University Press: Cambridge, England, 1994

APPENDIX A

TEMPERATURE CONTROLLER WIRING

A.1. MICROREACTOR SYSTEM
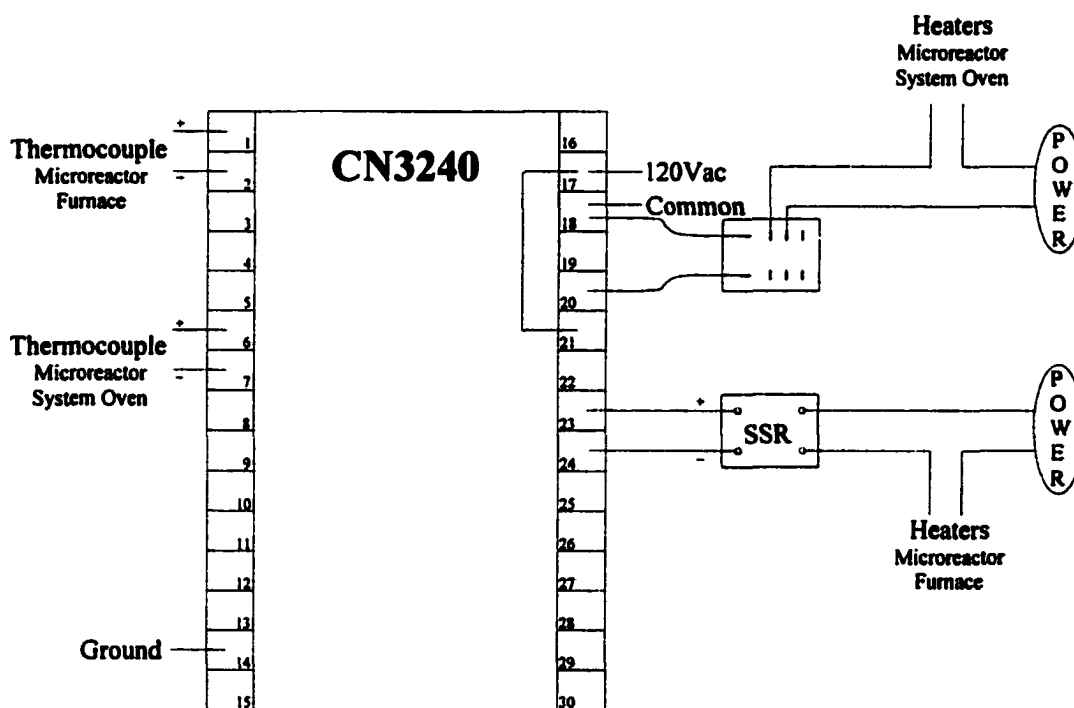
An Omega CN3240 dual input temperature controller was used to control the microreactor

system oven and furnace temperatures. The 120V ac power line was connected to terminals 17

(high), 18 (common) and 14 (ground). The microreactor furnace power was controlled by a solid

state relay (Omega SSR240DC10) connected to terminals 23 (+) and 24 (-). The tube furnace

"control" thermocouple was a type K fine wire thermocouple (Omega CHAL-010) and was

connected to terminals 1 (+) and 2 (-).

Power to the microreactor system oven strip heaters was controlled by a mechanical relay (Grainger K10P-11A15-120) connected to terminals 18 (-) and 20 (+). The microreactor system oven thermocouple was a type K glass braid insulated thermocouple (Omega 5TC-GG-K-24-36) connected to terminals 6 (+) and 7 (-).

A.2. REACTOR FURNACE
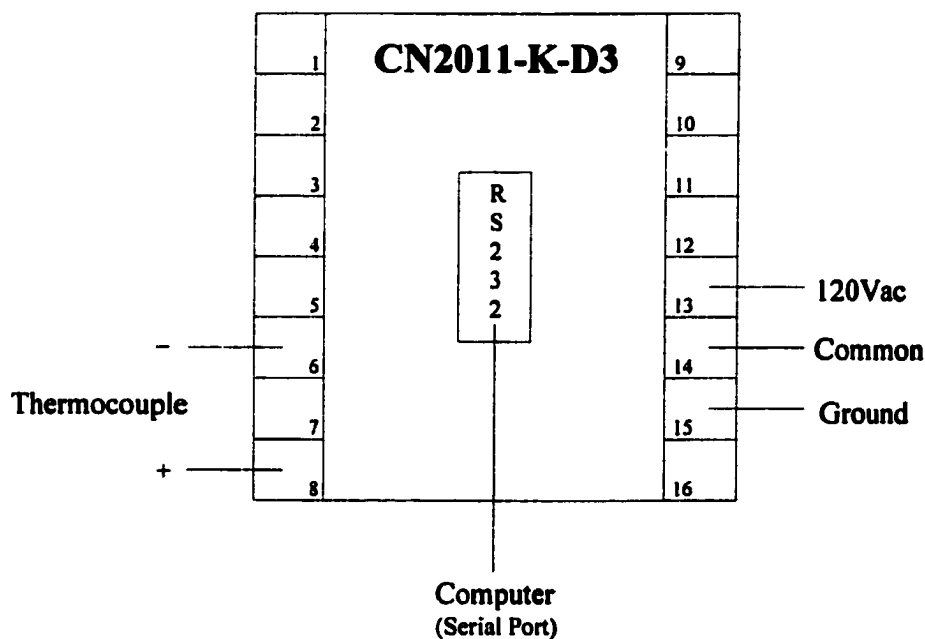
An Omega CN2011-K-D3 temperature controller was used to read the catalyst sample temperature. This temperature controller was wired for 120V ac operation. The ac power line was connected to terminals 13 (high), 14 (common) and 15 (ground). The tube furnace "measurement" thermocouple was a type K fine wire thermocouple (Omega CHAL-010) and was connected to terminals 6 (-) and 8 (+) of the temperature controller. The temperature controller was equipped with an RS232 port so that sample temperatures could be stored by a computer. The computer employed to read temperatures was also connected to the gas

chromatograph temperature controller, and was used to start GC oven temperature ramps and to engage the automatic valve actuator for GC injections.

A.3. GAS CHROMATOGRAPH
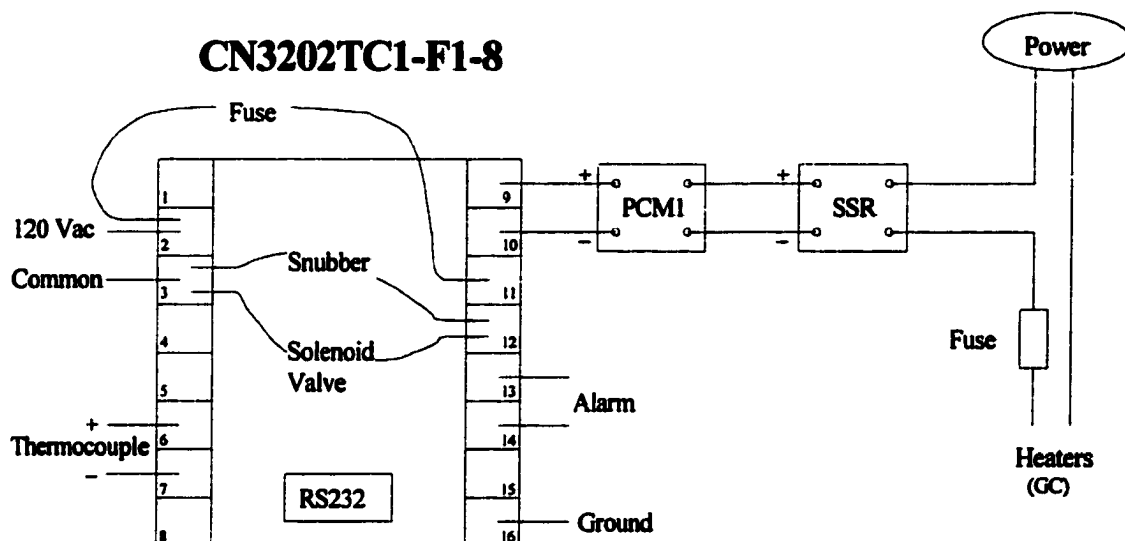
CN3202TC1-F1-8

An Omega CN3202TC1-F1-8 heat/cool temperature controller was used to control the gas chromatograph oven temperature. It varied the GC oven heating element current and energized the liquid nitrogen valve to maintain temperature setpoints. The 120V ac power line was connected to terminals 2 (high), 3 (low) and 16 (ground). Power to the GC oven nichrome wire heaters was controlled by a solid state relay (Omega SSR240DC25) and a pulse converter module (Omega PCM1) connected to terminals 9 (+) and 10 (-). The pulse converter module was mounted on the solid state relay terminals. The pulse converter module transformed the ON/OFF solid state relay to a proportional power regulator and was used with a 4-20mA ouput from the temperature controller. The 4-20mA control output was protected with a 1A fuse. The GC oven thermocouple was a type K fine wire thermocouple (Omega CHAL-010) connected to terminals 6 (+) and 7 (-). The liquid nitrogen delivering solenoid valve was connected to rear

152

terminals 3 and 12. When the internal switch between terminals 11 and 12 was closed, the valve was energized by the jumper connecting terminals 2 and 11. A 1A fuse protected the solenoid valve. A snubber circuit was placed across the solenoid to neutralize its inductance. The alarm switch, terminals 13 and 14, was used to trigger the six-port valve sequence programmer to intitiate GC/MS injections.

A.4. GC/MS INTERFACE
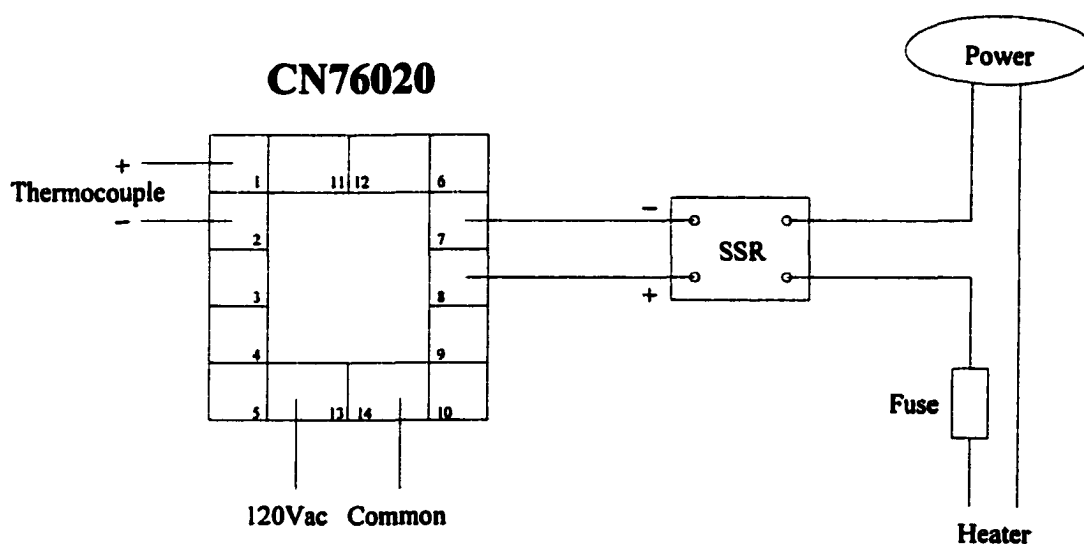
An Omega CN76020 temperature controller was used to maintain the GC/MS interface oven temperature. The 120V ac power line was connected to rear terminals 13 (high) and 14 (common). Power to the interface strip heaters was controlled by a solid state relay (Omega SSR240DC10) connected to terminals 7 (-) and 8 (+). A 1A fuse protected the relay. The temperature sensor was a type K glass braid insulated thermocouple (Omega 5TC-GG-K-24-36) that was located in the interface and connected to terminals 1 (+) and 2 (-).

APPENDIX B

DATA ACQUISITION/TREATMENT PROGRAMS

Five programs (ADC.BAS, TIC.EXE, TIC1.EXE, MS-INT.EXE, and MSINT.EXE) are described here. The first one is written in QBASIC, all the other are written in C++. These programs were initially written by Dr. Robert L. White, University of Oklahoma, Norman Oklahoma. I modified some of the C++ programs to manipulate FID and mass spectrometric TIC data. Comments describing program features are in *italics*.

B.1. "ADC.BAS"

The ADC.BAS QBASIC program records digitized FID signals and integrates chromatographic peaks (e.g. when the FID value>0). If the "zero" on the HP 5890 Serie II gas chromatograph is not properly adjusted, the FID signal can subsequently be integrated by using a threshold value to define peaks (by a program similar to "ms-int.exe" described in a subsequent section).

The amplifier - analog / digital converter was connected to the parallel port of an IBM compatible computer. The ADC.BAS program uses printer codes (e.g. paper out) to express numerical values. Strings of 12 bits were collected (one bit at a time) and then transformed into a number. This data collection method was fast enough that signal averaging was needed to reduce the digitization rate. The digitization rate depended on the computer processing speed. Consequently, the signal averaging parameter was adjusted for each computer employed.

The ADC.BAS program saves two data files. The "chromatogram" file contains the FID chromatographic data (time, signal), and the "integration" file contains the FID chromatographic peak areas (time, area). The program uses a loop to save FID signals and calculate the FID peak areas. In this loop, the program uses two successive data points, each defined by a time and a signal value ("time" and "sig" for the current data point ; "prevtime" and "prevsig" for the previous data point). A second loop saves the FID peak area and time only if the area is larger than a threshold. At the end, the current data point becomes the previous data point.

B.2. "TIC.EXE"

The TIC.EXE C++ program adds catalyst temperature information to a mass spectrometer TIC data file generated during a reactor-MS experiment. A similar program was used to add temperature data to an FID data file.

The "TIC.EXE" program reads the furnace temperature file (furnfile.tfu) to get time in seconds, "furn_t_*" and temperature in °C, "temp_*". The asterisk can represent either "low" or "high", because two sets of variables are used by the program. As long as the TIC data time "tic_time" (initially set to 0) is less than "furn_t_high", the program reads the TIC data file (ticfile.tic) for time in minutes, "tic_time" and TIC signal, "val". The program then calculates the heating rate "slope" between the two temperature data points and interpolates the catalyst temperature "temp" for each TIC data point. Finally, the time in minutes "tic_time", calculated temperature in °C, "temp", and the TIC signal, "val", are saved in a new data file (outfile.ti). The program also uses an integer variable, "count", to end the program when the end of file for the temperature or TIC data files are reached.

B.3. "TIC1.EXE"

The TIC1.EXE C++ program adds catalyst temperature information and injection marks to a repetitive injection TIC data file generated during a reactor-GC/MS experiment. A similar program was used to add temperature data and injection marks to FID data files.

The "TIC1.EXE" program reads the furnace temperature file (furnfile.tfu) to obtain time in seconds, "furn_t_*", temperature in °C, "temp_*", and injection marks "mark_*". The asterisk can represent either "low" or "high", because two sets of variables are used by the program. Because the furnace heating ramp is not linear over an entire experiment, heating rates between two successive injections are calculated (i.e. slope between the points). Then, the program reads the TIC data file (ticfile.tic) for time in minutes, "tic_min", and TIC signal, "val". Calculated heating rates are used with the TIC file times to interpolate catalyst temperatures, "temp" for each TIC data file signal. Finally, time in minutes, "tic_min", calculated temperature in °C, "temp", TIC signal, "val", and injection marks, "mark_high" are saved in a new data file (outfile.ti). The program also uses an integer variable, "count", to end the program when end of file for either temperature or TIC data files is encountered.

B.4. "MS-INT.EXE"

The MS-INT.EXE C++ program integrates TIC peaks by using a threshold to define a baseline. This program uses TIC data files that contain temperature data and injection mark. Another program (not shown here) was used to integrate TIC peaks before addition of temperature information and injection marks. Variations of both programs were used to integrate FID peaks.

The "MS-INT.EXE" program reads the processed data file (tifile.ti) for time in minutes, "time", temperature in °C, "temp", TIC signal, "signal" and injection marks, "mark". The

chromatographic peak area, "area", is initially set to zero. Two variables, "s_time" and "s_temp", hold the chromatographic peak start time and corresponding furnace temperature. The program compares the TIC signal to a threshold value, "thres", previously set by the operator. As long as the TIC signal is larger that the thershold value, the area is increased by the TIC signal value. When the TIC signal drops below the threshold value and if the chromatographic area is considered significant (i.e. the area value must be larger than 100), the initial chromatographic peak retention time "s_time", the corresponding furnace temperature, "s_temp", and the chromatographic peak area, "area" are saved in a new data file (outfile). The program also uses an integer variable, "count", to end the program when TIC data file end-of-file is reached.

B.5. "MSINT.EXE"

The MSINT.EXE C++ program integrates TIC chromatographic peaks by using the injection time (from the furnace temperature data file) and a specified retention time range to define peak locations. A similar program was used to integrate repetitive injection FID peaks.

The retention time range to integrate is defined in the "MSINT.EXE" program by two times in minute "tstart" and "tend" set by the operator. The chromatographic peak area, "sum", is initially set to zero. The program reads the furnace temperature data file (furn.tfu) to retrieve time in seconds, "itime", temperature in °C, "temp", and injection marks, "mark". The program finds an injection mark and converts its corresponding time into "mtime" (time in minutes). Then, the program reads the initial TIC data file (msfile.tic) for time in minutes, "time", and TIC signal, "val". As long as the TIC data file "time" is less than the sum of the furnace temperature data file "mtime" and "tstart", the program jumps to the next TIC data. When "time" is finally greater than the sum of "mtime" and "tstart" and as long as "time" is less than the sum of the

furnace temperature data file "mtime" and "tend", the program increases the "sum" by the TIC

signal, "val". Finally, the program saves the injection time, "mtime", the corresponding furnace

temperature in °C, "temp", and the chromatographic peak area, "sum", in a new data file

(outfile). The program also uses an integer variable, "count", to end the program when the TIC

data file end is reached.

ADC.BAS

```
DIM BIT%(11)                                        set a string of 12 characters
INPUT "CHROMATOGRAM FILENAME:", OUTFILE$            operator selects the chromatogram filename
OPEN OUTFILE$ FOR OUTPUT AS #1                      define chromatogram file as "output #1"
INPUT "INTEGRATION FILENAME:", OUTINT$             operator selects the integration filename
OPEN OUTINT$ FOR OUTPUT AS #2                       define integration file as "output #2"

NAVE% = 500                                         set signal average variable "nave" to 500
AREA! = 0                                           set peak area variable "area" to 0
TIMEAREA! = 0                                       set timearea variable to 0
START& = TIMER                                      set start variable to the internal clock value
PREVSIG! = 0                                        set prevsig variable to 0
PREVTIME! = 0                                       set prevtime variable to 0
PRINT "0, 0"                                        print first point (0,0) to screen
PRINT #1, "0, 0"                                    print first point (0,0) in chromatogram file

WHILE INKEY$ <> "e"                                 WHILE loop will run until "e" is pressed

        SIG! = 0                                    set the sig variable to 0
        FOR j% = 1 TO NAVE%                         FOR loop collecs for variable nave times
                OUT &H378, 1
                OUT &H378, 0

                FOR i% = 0 TO 11                    FOR loop receives the string of 12 characters
                        OUT &H378, 2                                          one by one
                        OUT &H378, 0
                        IF (INP(&H379) AND &H20) THEN IF loop sets each character to 0 or 1
                                BIT%(i%) = 1
                        ELSE
                                BIT%(i%) = 0
                        END IF                      end of IF loop
                NEXT i%                             end of FOR loop

                NUM% = BIT%(11) + BIT%(10) * 2 + BIT%(9) * 4 + BIT%(8) * 8 + BIT%(7) * 16 +
                BIT%(6) * 32 + BIT%(5) * 64 + BIT%(4) * 128 + BIT%(3) * 256 + BIT%(2) * 512 +
                BIT%(1) * 1024 + BIT%(0) * 2048     transform the string of 12 bits into a number
                SIG! = SIG! + NUM%                  add number to variable sig
                TIME! = (TIMER - START&) / 60       set time variable in minute
        NEXT j%                                     end of FOR loop

        SIG! = INT(SIG! / NAVE%)                    set variable sig to its average over nave times

        IF (PREVSIG! = 0) AND (SIG! <> 0) THEN      IF loop prints chromatographic peaks value
                                                    to screen and in chromatogram file
                PRINT USING "###.###, ######"; PREVTIME!; PREVSIG!
                PRINT USING "###.###, ######"; TIME!; SIG!
                PRINT #1, USING "###.###, ######"; PREVTIME!; PREVSIG!
                PRINT #1, USING "###.###, ######"; TIME!; SIG!
                TIMEAREA! = TIME!
                AREA! = SIG!

        ELSEIF (PREVSIG! <> 0) THEN
                PRINT USING "###.###, ######"; TIME!; SIG!
                PRINT #1, USING "###.###, ######"; TIME!; SIG!
```

159

```
                    AREA! = AREA! + SIG!

        END IF                                          end of IF loop

        IF (PREVSIG! <> 0) AND (SIG! = 0) AND (AREA! > 50) THEN
                                                        IF loop prints peaks area in integration file
                    PRINT #2, USING "###.###, ########"; TIMEAREA!; AREA!
        END IF                                          end of IF loop

        PREVSIG! = SIG!                                 set prevsig variable to sig variable
        PREVTIME! = TIME!                               set prevtime variable to time variable

WEND                                                    end of WHILE loop

CLOSE #1                                                close chromatogram file
CLOSE #2                                                close integration file
```

TIC.EXE

```
#include <stdio.h>
#include <math.h>

char root[25], furnfile[25], ticfile[25], outfile[25];

main()
{
int count;                                            variable use to find end of file
float furn_t_low, furn_t_high, temp_low, temp_high;   variables from temperature data file
float tic_time, val;                                  variables from TIC data file
float mtime_low, mtime_high, slope, temp;             variables used in calculations
FILE *furn, *tic, *out, *fopen();

printf("Repetitive Injection Rootname: ");            ask for file rootnamename
scanf("%s", root);                                    read file rootname (enter by operator)
strcpy(furnfile, root);                               copy the file rootname in "furnfile"
strcpy(ticfile, root);                                copy the file rootname in "ticfile"
strcpy(outfile, root);                                copy the file rootname in "outfile"
strcat(furnflle, ".tfu");                             add extension ".tfu" to "furnfile"
strcat(ticfile, ".tic");                              add extension ".tic" to "ticfile"
strcat(outfile, ".ti");                               add extension ".ti" to "outfile"

out = fopen(outfile, "wt");                            open "outfile" to write text
furn = fopen(furnfile, "rt");                          open "furnfile" to read text
tic = fopen(ticfile, "rt");                            open "ticfile" to read text

tic_time = 0;                                          set variable tic_time to 0
fscanf(furn, "%f, %f, %f\n", &furn_t_low, &temp_low); reads first furnace temperature data
while ((count = fscanf(furn, "%f, %f\n", &furn_t_high, &temp_high)) >= 1)
                                                       WHILE loop will run until end of furnace
                                                                          temperature file
        {
        while(tic_time < (furn_t_high/60))            WHILE loop selects TIC data points to treat
                {
                count = fscanf(tic, "%f, %f\n", &tic_time, &val);
                if (count != 2)                        IF loop indicates end of data file "*.tic" file
                        {
                        printf("ERROR, count incorrect");
                        exit(0);
                        }
                mtime_high = (furn_t_high / 60);       transform time from second to minute
                mtime_low = (furn_t_low / 60);         transform time from second to minute
                if (furn_t_low != furn_t_high)         IF loop calculate slope and TIC data points
                        {                                                  temperature
                        slope =(temp_high - temp_low)/(mtime_high - mtime_low);
                        temp = ((tic_time - mtime_low) * slope + temp_low);
                        fprintf(out, "%f, %.2f, %.0f\n", tic_time, temp, val);
                        }
                }
        furn_t_low = furn_t_high;                      set high time variable to low
        temp_low = temp_high;                          set high temperature variable to low
        }
return;
}
```

161

TIC1.EXE

```c
#include <stdio.h>
#include <math.h>

char root[25], furnfile[25], ticfile[25], outfile[25];

main()
{
int count;                                              variable use to find end of file
float furn_t_low, furn_t_high, temp_low, temp_high, mark_low, mark_high;
                                                        variables from temperature data file
float tic_time, val;                                    variables from TIC data file
float mtime_low, mtime_high, slope, temp;               variables used in calculations
FILE *furn, *tic, *out, *fopen();


printf("Repetitive Injection Rootname: ");              ask for file rootnamename
scanf("%s", root);                                      read file rootname (enter by operator)
strcpy(furnfile, root);                                 copy the file rootname in "furnfile"
strcpy(ticfile, root);                                  copy the file rootname in "ticfile"
strcpy(outfile, root);                                  copy the file rootname in "outfile"
strcat(furnfile, ".tfu");                               add extension ".tfu" to "furnfile"
strcat(ticfile, ".tic");                                add extension ".tic" to "ticfile"
strcat(outfile, ".ti");                                 add extension ".ti" to "outfile"


out = fopen(outfile, "wt");                             open "outfile" to write text
furn = fopen(furnfile, "rt");                           open "furnfile" to read text
tic = fopen(ticfile, "rt");                             open "ticfile" to read text


fscanf(furn, "%f, %f, %f\n", &furn_t_low, &temp_low, &mark_low);
                                                        read furnace temperature file
fscanf(tic, "%f, %f\n", &tic_time, &val);
                                                        read TIC data file
fprintf(out, "%f, %.2f, %.0f, %.0f\n", tic_time, temp_low, val, mark_low);
                                                        save starting point (first injection)
while ((count = fscanf(furn, "%f, %f, %f\n", &furn_t_high, &temp_high, &mark_high)) >= 2)
                                                        WHILE loop will run until end of furnace
    {                                                                  temperature file
    if(count == 3)
        {
        while(tic_time < furn_t_high/60)
            {
            count = fscanf(tic, "%f, %f\n", &tic_time, &val);
            if (count != 2)                             IF loop indicates end of TIC data file
                {
                printf("ERROR, count incorrect");
                exit(0);
                }
            mtime_high = (furn_t_high / 60);            transform time from second to minute
            mtime_low = (furn_t_low / 60);              transform time from second to minute
            if (furn_t_low != furn_t_high)              IF loop calculates heating rate, temperature
                {                                                         and save data points
                slope =(temp_high - temp_low)/(mtime_high - mtime_low);
                temp = ((tic_time - mtime_low) * slope + temp_low);
                fprintf(out, "%f, %.2f, %.0f\n", tic_time, temp, val);
```

162

```
                              }
                    }
          fscanf(tic, "%f, %f\n", &tic_time, &val);     read next injection TIC data
          fprintf(out, "%f, %.2f, %.0f, %.0f\n", tic_time, temp, val, mark_high);
                                                         save next injection data point
          furn_t_low = furn_t_high;                      set high time variable to low
          temp_low = temp_high;                          set high temperature variable to low
          }
     }
return;
}
```

MS-INT.EXE

```c
#include <stdio.h>
#include <math.h>

char tifile [25], outfile[25];

main()
{
int count;                                variable use to find end of file
int thres;                                variable use to define base of peak
float time, temp, signal, mark;           variables from initial data file "*.ti file"
float s_time, s_temp, area;               variables used in calculation
FILE *ti, *out, *fopen();

printf("Input .ti Rootname: ");           ask for file rootname
scanf("%s", tifile);                       read file rootname (enter by operator)
strcat(tifile, ".ti");                     add extension ".ti" to "ticfile"

printf("Specify Threshold Value: ");       ask for integration threshold value
scanf("%d", &thres);                       read threshold value (enter by operator)

printf("Specify Filename for Integration Results: ");   ask for output integration filename
scanf("%s", outfile);                      read output filename (enter by operator)

out = fopen(outfile, "wt");                open "outfile" to write text
ti = fopen(tifile, "rt");                  open "tifile" to read text

while((count = fscanf(ti, "%f, %f, %f, %f\n", &time, &temp, &signal, &mark)) > 2)
                                           WHILE loop will run until end of initial
        {                                             data file "*.ti file"
        area = 0;                          set variable area to 0
        s_time = time;                     set s_time variable to time
        s_temp = temp;                     set s_temp variable to temp
        while(signal > (float) thres)      WHILE loop to calculate peak area
                {
                count = (fscanf(ti, "%f, %f, %f, %f\n", &time, &temp, &signal, &mark));
                if(count<3)                IF loop indicates end of data file "*.ti" file
                        {
                        printf("ERROR, count incorrect");
                        exit(0);
                        }
                area += signal;            add signal to area
                }
        if(area >= 100)                    IF loop neglects small peaks (area<100)
                fprintf(out, "%3.2f, %3.2f, %.0f\n", s_time, s_temp, area);
        }
return;
}
}
```

164

MSINT.EXE

```
#include <stdio.h>
#include <math.h>

char root[25], furnfile[25], msfile[25], outfile[25];

main()
```

`{`	
`int count;`	*variable use to find end of file*
`int itime, temp, mark;`	*variables from temperature data file*
`int val;`	*variable from TIC data file*
`float time;`	*variable from TIC data file*
`float tstart, tend, mtime, sum;`	*variables used in calculation*
`FILE *furn, *ms, *out, *fopen();`	
`printf("Repetitive Injection Rootname: ");`	*ask for file rootname*
`scanf("%s", root`	*read file rootname (enter by operator)*
`strcpy(furnfile, root);`	*copy the file rootname in "furnfile"*
`strcpy(msfile, root);`	*copy the file rootname in "msfile"*
`strcat(furnfile, ".tfu");`	*add extension ".tfu" to "furnfile"*
`strcat(msfile, ".tic");`	*add extension ".tic" to "msfile"*

```
printf("Input start and end times (min) for integration (start, end): ");
```
	ask for retention time range to integrate
`scanf("%f, %f", &tstart, &tend);`	*read time range (enter by operator)*

`printf("Specify Filename for Integration Results: ");`	*ask for output integration filename*
`scanf("%s", outfile);`	*read output filename (enter by operator)*

`out = fopen(outfile, "wt");`	*open "outfile" to write text*
`furn = fopen(furnfile, "rt");`	*open "furnfile" to read text*
`ms = fopen(msfile, "rt");`	*open "msfile" to read text*

`time=0;`	*set variable time to 0*
`while ((count = fscanf(furn, "%d, %d, %d\n", &itime, &temp, &mark)) >= 2)`	
	WHILE loop will run until end of temperature data file ".tfu file"*
`{`	
`if(count == 3)`	*IF loop find injection mark*
`{`	
`sum = 0;`	*set variable sum to 0*
`mtime = (float) itime/60;`	*save injection time in minute*
`while(time < (mtime + tstart))`	*WHILE loop skips top beginning of*
`{`	*retention time range to integrate*
`count = fscanf(ms, "%f, %d\n", &time, &val);`	
`if(count != 2)`	*IF loop indicates end of data file "*.tic" file*
`{`	
`printf("ERROR, count incorrect");`	
`exit(0);`	
`}`	
`}`	
`while(time < (mtime + tend))`	*WHILE loop integrates retention time range*
`{`	
`count = fscanf(ms, "%f, %d\n", &time, &val);`	

```
                    if(count != 2)              IF loop indicates end of data file "*.tic" file
                        {
                        printf("ERROR, count incorrect");
                        exit(0);
                        }
                    sum += (float) val;         add val to sum
                    }
            if(count == 2)                      IF loop saves integrated value
                fprintf(out, "%f, %d, %f\n", mtime, temp, sum);
            }
        }
    return;
}
```

APPENDIX C

Validation of the Use of Conversion for Kinetic Studies

The rate of a chemical reaction can be expressed as a function of reactant and product concentrations as shown by equation 1:

$$\text{Rate} = k\,[\text{Reactant}]^x[\text{Product}]^y \tag{1}$$

where k is the reaction rate constant, and x and y are coefficients that depend on the reaction mechanism and the order of the reaction. Under steady-state catalytic reactor conditions, reactant and product concentrations are constant and the reaction rate is directly proportional to the rate constant (regardless of reaction order):

$$\text{Rate } \alpha\, k \tag{2}$$

The rate of a catalytic reaction is proportional to conversion, X, (defined as the fraction of reactant converted to products) and the proportionality constant includes the amount of catalyst used, W, and the reactant flow space velocity, F, as shown by equation 3:

$$\text{Rate } \alpha\, \frac{W}{F}X \tag{3}$$

Note that equation 3 is only valid at low conversion conditions, for which reactant and products concentrations are nearly constant throughout the catalyst bed. Combining equations 2 and 3 gives:

$$k\, \alpha\, \text{Rate } \alpha\, \frac{W}{F}X \tag{4}$$

Equation 4 clearly indicates that under low conversion steady-state conditions, the rate constant for a reaction is directly proportional to conversion.

The rate constant for a reaction is temperature dependent, as first shown by Arrhenius :

$$k = A \exp\left(-\frac{E_a}{RT}\right)$$ (5)

where k is the rate constant, A is the pre-exponential factor (also called frequency factor), E_a is the activation energy in Joules per mole, R is the gas constant with the value 8.314 J mol^{-1} K^{-1}, and T is the temperature in Kelvin. Activation energies are often used to characterize catalyst effectiveness for a specific reaction. The activation energy can be determined from the slope, $-E_a/R$, of the straight line obtained by plotting the natural logarithm of the rate constant against the reciprocal absolute temperature :

$$\ln k = -\frac{E_a}{R} \times \frac{1}{T} + \ln A$$ (6)

Because conversion and rate constant are directly proportional, X can be substituted for k in equation 6:

$$\ln X = -\frac{E_a}{R} \times \frac{1}{T} + \ln A'$$ (7)

Thus, activation energy can be obtained from the slope, $-E_a/R$, of the straight line obtained by plotting the natural logarithm of conversion versus the reciprocal absolute temperature. The proportionality constant between conversion and rate constant does not affect the slope (i.e. E_a), but is included in the intercept, (ln A').